PHASE DIAGRAMS AND APPLICATIONS OF AMPHIPHILIC BLOCK COPOLYMERS IN AQUEOUS SOLUTIONS

Inauguraldissertation

zur

Erlangung der Würde eines Doktors der Philosophie

vorgelegt der

Philosophisch-Naturwissenschaftlichen Fakultät

der Universität Basel

von

Jörg Braun

aus

Deutschland

Basel, 2011

Genehmigt von der Philosophisch-Naturwissenschaftlichen Fakultät auf Antrag von

Prof. Dr. Wolfgang Meier

und

Prof. Dr. Corinne Vebert

Basel, den 29. März 2011

Prof. Dr. Martin Spiess

Dekan

Für meine Eltern, Albert und Elisabeth Braun

„Ich habe nicht nachgedacht, ich habe experimentiert. "

Abstract

Conventional amphiphilic block copolymers are macromolecules consisting of at least a hydrophilic segment covalently attached to a hydrophobic segment. They are unique and versatile building blocks in supramolecular polymer chemistry, both for the generation of highly organized, self-assembled structures and for the structural control of material interfaces. In the absence of solvents, the phase-behavior of block-copolymers is sparingly described. In aqueous solutions block copolymers self-assemble into nanoscopic objects. These structures are gaining more and more attention for technical formulations. Self-assembly is simply induced by dissolving dry powder of amphiphilic copolymers in water. This self-assembly process, however, cannot be described solely based on bulk phase behavior and very few experimental phase diagrams of block copolymer/water mixtures have been reported. In order to control, predict and eventually achieve a comprehensive understanding of this process and in particular the formation of vesicles, worm/rod-like micelles and spherical micelles it is important to systematically investigate the phase behavior of block copolymers across the whole water concentration range. We therefore undertook investigations of the self-assembly of two block copolymers. Preliminary encapsulation studies reveal their potential for applications relevant for drug delivery.

The concentration profile of the identified amphiphilic block-copolymers diluted in aqueous solution was examined across the whole concentration range with four poly(ethylene oxide)-*block*-poly(γ-methyl-ε-caprolactone) (PEO-*b*-PMCL) block copolymers keeping the hydrophilic block length constant but varying the hydrophobic lengths. Bulk polymers did not display any ordered morphology. With increasing water concentrations the polymers underwent transitions from lamellar phases to packed vesicles and eventually all polymers self-assembled into vesicles in dilute aqueous solutions. At high concentration the largest polymer organized further into an inverse hexagonal phase prior to self-assembly into a lamellar phase. The smallest block-copolymer also self-aggregated into rod-like micelles and exhibited a hexagonal phase between the packing of the rod-like micelles/vesicles and the lamellar phase.

The concentration profile of phases assembled by amphiphilic block-copolymers diluted in aqueous solution was examined as well across the whole concentration range with three poly(isobutylene)-block-poly(ethylene oxide) block copolymers having the same hydrophobic block length but varying in their hydrophilic lengths. In contrast to PEO-*b*-PMCL these

polymers self-aggregated depending on the hydrophilic length into micelles, worm-like micelles and for the shortest polymer into vesicles. Thus, increasing the polymer concentration lead to a different phase behavior. The largest polymer which solely formed micelles, underwent transitions from packed micelles with a few packed worm-like micelles to a hexagonal phase and finally into a lamellar phase, in contrary to the middle length polymer, which self-aggregated into worm-like micelles. The best to our knowledge, it is the first time that an experimental phase diagram is built such that it displays the formation of worm/rod-like micelles. With the composition studied in here, the worms, with increasing polymer concentration, pack and undergo afterwards into a hexagonal and finally a lamellar phase has been observed. For the shortest polymer the phase behavior was similar to that of vesicles self-assembled by PEO-*b*-PMCL. In contrast, the pure polymer formed an inverse hexagonal phase.

It was eventually shown that PEO_{23}-$PMCl_{32}$ can be used to encapsulate both small and large molecules. By adjusting the pH towards acidic conditions the responsiveness of the vesicles could be triggered to release the encapsulated material.

Table of contents

PHASE DIAGRAMS AND APPLICATIONS OF AMPHIPHILIC
BLOCK COPOLYMERS IN AQUEOUS SOLUTIONS

1. Introduction

Polymers, with their extraordinary range of properties, play an essential role in everyday life[1] and can be found everywhere. For instance drinks are conditioned in bottles made of poly(ethylene terephthalate) (PET), which is one of the most widely used synthetic polymer. Scientists, however, are fascinated by Nature. It is thus essential to first have a look into Nature's library of polymers before having a look on the polymers synthesized in a laboratory. A variety of natural polymers exist. For instance wood and accordingly paper are mainly composed of cellulose, which belongs to the family of polysaccharides. Foods like bread, corn and potatoes are composed of starch which belongs to the same polysaccharide family. Aside from these examples a lot more natural polymeric materials (such as shellac, amber, and natural rubber) have been identified and used for centuries. In addition to polymers that are surrounding us, polymers can be found in the human body as well. Here, one prominent example is deoxyribonucleic acid (DNA).[2, 3] It is a polymer that contains the genetic information used in the development and functioning of all known living organisms and it is one of the three major macromolecules that are essential for all known forms of life. The other two macromolecules are ribonucleic acid (RNA)[4] and proteins. Inspired by those natural polymers, much work has been done with the ambition to synthetically mimic these polymers, understand their mechanism of action and even create new macromolecules. All started almost 200 years ago (1811), when Henri Braconnot did his pioneering work on derivatives of cellulose compounds, which is probably the earliest breakthrough in polymer science.[5] 100 years later (1907) the first completely synthetic polymer was synthesized by Leo Baekeland (Bakelit).[6] Since then a very large list of synthetic polymers has been generated which includes synthetic rubber, bakelite, neoprene, nylon, poly(vinyl chloride), poly(styrene), poly(ethylene), poly(propylene), poly(acrylonitrile), silicone, and many more. Thus, we are surrounded by and partially composed of polymers. Interestingly, when the public speaks about polymers, it mostly refers to plastics. The main difference, however, between plastics and polymers is that plastics are one form of aggregated polymers whereas polymers are very large single molecules. This difference can also be emphasized by simply analyzing the roots of these two words: plastic comes from the word *plastikos* and means shapeable and *polymer* is derived from two Greek words as well: *πολύ(poly)* and *μέρος (meros)*. Both words combined mean "many parts". Accordingly, polymers are more than just

INTRODUCTION

plastics, and their role ranges from familiar synthetic plastics and elastomers to natural biopolymers. [7-9]

Despite of the features macromolecules have on their own, it is also essential to analyze and understand their intermolecular behavior. This field is called supramolecular polymer chemistry. Thus, it refers to the area beyond single polymers and focuses on the chemical systems made up of a discrete number of assembled polymers. While traditional polymer chemistry focuses on covalent bonds, supramolecular polymer chemistry examines the weaker and reversible non-covalent interactions between molecules (van der Waals, electrostatic forces or hydrogen bonding). But in order to achieve microstructural features, the polymer architecture on its own has to be considered at first.

1.1. Block copolymers

The simplest polymer architecture is a linear chain of one repeating monomer – a single backbone with no branches – also referred to as homopolymers[10] (figure 1.1a). Due to statistical reasons, termination reactions, etc. - intrinsic to the synthesis and length of the macromolecules – polymers in the same reaction flask have not exactly the same molar mass. There is always a size distribution around an average value described by a molecular weight distributions (M_W/M_N), where M_W and M_N represent the weight and number-average molecular weights, respectively. When polymers are composed out of a main chain with one or more substituent side chains or branches they are referred to as for example star polymers[11-14], comb polymers[14, 15], brush polymers[14, 16-18], hyperbranched polymers[13, 19], and dendrimers[13, 19-22] (Figure 1.1).
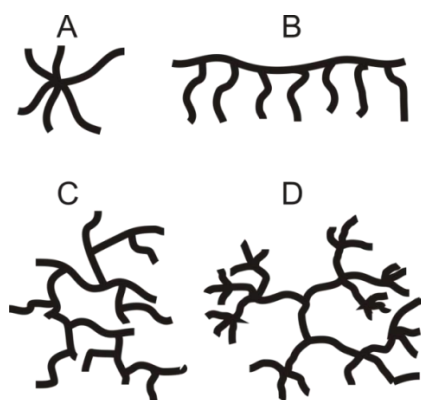
Figure 1.1. Schematic representation of a a) star, b) comb, c) branched polymer and d) dendrimer.

As soon as these polymers and linear polymers are consisting of more than one repeating monomer they are referred as copolymers. Depending on how the monomers are arranged along the macromolecule different classes of copolymers are generated. The most characterized and simplest configurations of copolymers are linear copolymers. Possible linear copolymer configurations build up by just two different monomers can be divided into the following types (Figure 1.2 b-e): Alternating copolymers (existing out of regular alternating A and B monomers), periodic copolymers (composed of A and B units arranged in a repeating sequence (e.g. (A-B-B-A-A-B-A-A)$_n$)), statistical copolymers (copolymers in which the sequence of monomers follows a statistical rule) and block copolymers.

A-A-A-A-A-A-A-A-A-A-A-A   a

A-B-A-B-A-B-A-B-A-B-A-B   b

A-A-A-B-B-A-B-A-B-B-B-A   c

(A-B-B-A-A-B-A-A)$_n$ d

A-A-A-A-A-B-B-B-B-B-B-B   e
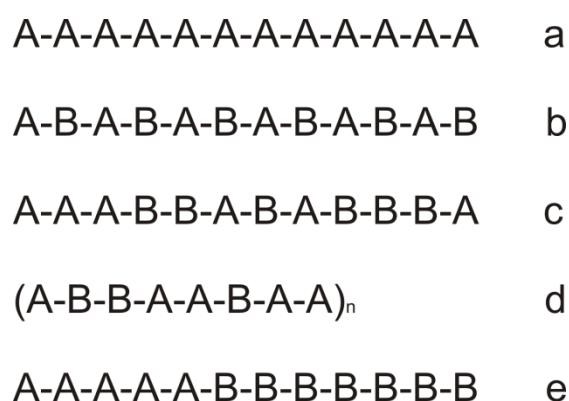
Figure 1.2. Schematic representation of a) homopolymer existing out of one repeating monomer A, and copolymers existing out of two distinct monomers A and B: b) alternating, c) statistical, d) periodic and e) block copolymers.

The latter copolymer (block copolymer) is composed of at least two (Figure 1.2e) or more homopolymer subunits linked by covalent bonds. A more "realistic snapshot" of block copolymers is shown in Figure 1.3. Here, two block copolymers are shown, which are mainly investigated in supramolecular chemistry.[23-26] An *AB* block copolymer consisting of two chemically different blocks, and an *ABA* block copolymer also consisting of two chemically different blocks, but block *A* is repeated twice. Here, *A* represents the homopolymer existing out of monomers A and *B* the second homopolymer covalently attached to block *A* and composed out of monomers B, respectively. Accordingly, block copolymers are macromolecules composed of sequences, or blocks, of chemically distinct repeating units. In this work the focus was on amphiphilic block copolymers consisting of two chemically incompatible blocks, a hydrophobic and a hydrophilic block. Both blocks are composed of hydrophobic and hydrophilic monomers, respectively.

AB

ABA
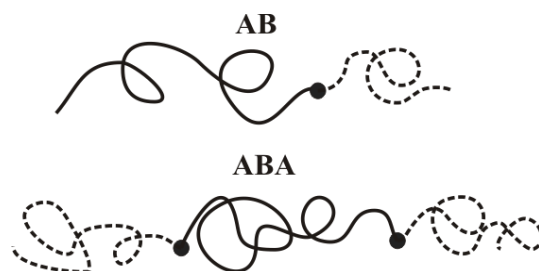
Figure 1.3. Schematic representation of block copolymers mainly used in supramolecular chemistry. *A* represents a hydrophilic and *B* a hydrophobic block.[27]

These amphiphilic block copolymers are unique and versatile building blocks in supramolecular polymer chemistry, both for the generation of highly organized, self-assembled structures at the nanometer scale and for the structural control of material interfaces.[28]

In order to understand and control self-assembled block copolymer nanostructures in detail fundamental studies remain to be done starting with the phase behavior of block copolymers in bulk.

1.2 Phase behavior of bulk block copolymers

In the absence of solvents, the phase-behavior of block copolymers can be described in terms of the strength of the interactions between the blocks (χ), the total number of statistical segments (N), the volume fraction of one of the blocks (f), and the differences in the conformational properties of the polymer chains (ε).[29, 30] On the one hand, the two chemically different blocks are covalently attached (short range interaction); consequently they cannot move away from each other. On the other hand, since the blocks are chemically incompatible, they try to avoid each other (long-range interaction). Subsequently, they start to self-organize into thermodynamically preferred structures. A simple case is shown in Figure 1.4 A. Here, the two chemically incompatible polymer blocks are represented by boxes (*A* and *B*) representing domains. The distances between two *A* and two *B* blocks is called d-spacing and represents the periodic length of the structure, which covers a range from 10 nm to 1 cm, hence seven orders of magnitude. When the formation of ordered structures is anticipated, as a result of an appropriate pair of forces, the question arises as to what kind of superlattice will be organized and of which periodicity. The *A* and *B* domains are separated from each other by an interface (dashed line in Figure 1.4 B). Lamellar domains – planar interfaces between

4

block *A* and *B* – are formed preferably because of the stretched shape of an *A/B* pair. Accordingly, the periodic length *d* of the superlattice depends on the size of the *A* and *B* domains.
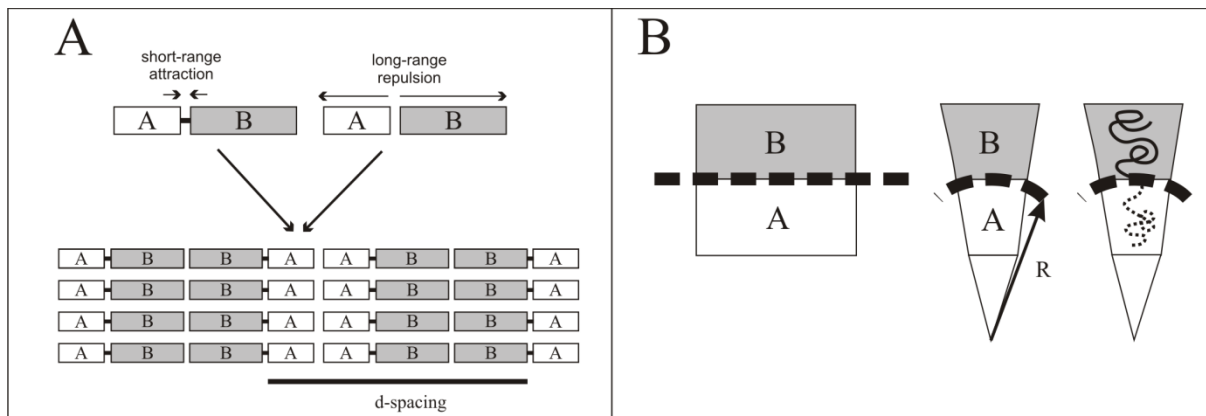
Figure 1.4 a) Schematic illustration of short-range repulsive and long-range attractive forces leading to an ordered structure by self-organization. *d*-spacing is the periodic length of the structure.[27] b) Local geometry and the curvature of domains and interfaces. The superlattice structure depends on the volume fraction $f = V_A/V_B$ of the domains and on the curvature radius *R* of the interface. For a planar interface $R = \infty$. The application of this model to block copolymers is shown at the right hand side.[27]

When the *A* domain is smaller than the *B* domain, curved interfaces will be formed. The bend can be characterized by the curvature radius *R* (Figure 1.4 B). The topology of the domains of the superlattice is not readily apparent from curved interfaces. The kind of superlattice depends on the volume fraction $f = V_A/V_B$ of the domains and on the radius of curvature *R* of the interface. Not only the classical superlattices (spheres *S*, hexagonally packed cylinders *C*, and lamellae) result from these considerations, but so do sophisticated minimal surfaces such as gyroid *G*, perforated lamellae *PL*, or double-diamond *D* surfaces. Figure 1.5 shows schematically the interdependence of these surfaces with the area-averaged mean curvature *H* as a function of the *A*-block volume fraction *f*.
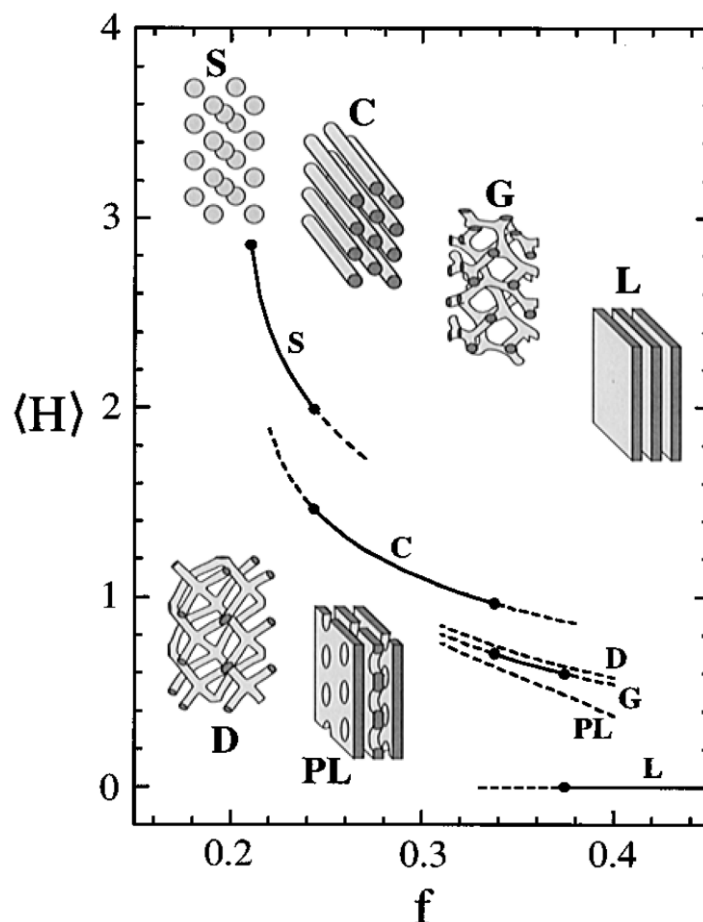
Figure 1.5. Area-averaged mean curvature H as a function of the A-block volume fraction f for each of the structures shown schematically calculated using the self-consistent mean field theory. The stable and metastable states are shown by solid and dashed lines, respectively, and transitions are denoted by dots. As the molecules become asymmetric, structures with more curvature are preferred. S: spheres, C: hexagonally packed cylinders, G: gyroid, L: lamellae, D: double-diamond structure, PL: perforated lamellae.[31]

The free energy of a superlattice can be calculated by means of self-consistent mean field theory.[32, 33] The superlattice with the lowest energy conforms to the equilibrium structure, the stability range of which can be represented in a phase diagram (Figure 1.6 A). Here, the theoretical lowest energy-containing structures are displayed interdependent with the interactions between the blocks (χ) multiplied by the total number of statistical segments (N) as a function of the volume fraction of the hydrophilic block (f). Hajduk *et al.* investigated the phase behavior of bulk poly(ethylene)-*block*-poly(ethylene oxide) (PEE-*b*-PEO)[34] and they showed (Figure 1.6 B) that their experimental observations were in good agreement with the theory.

6
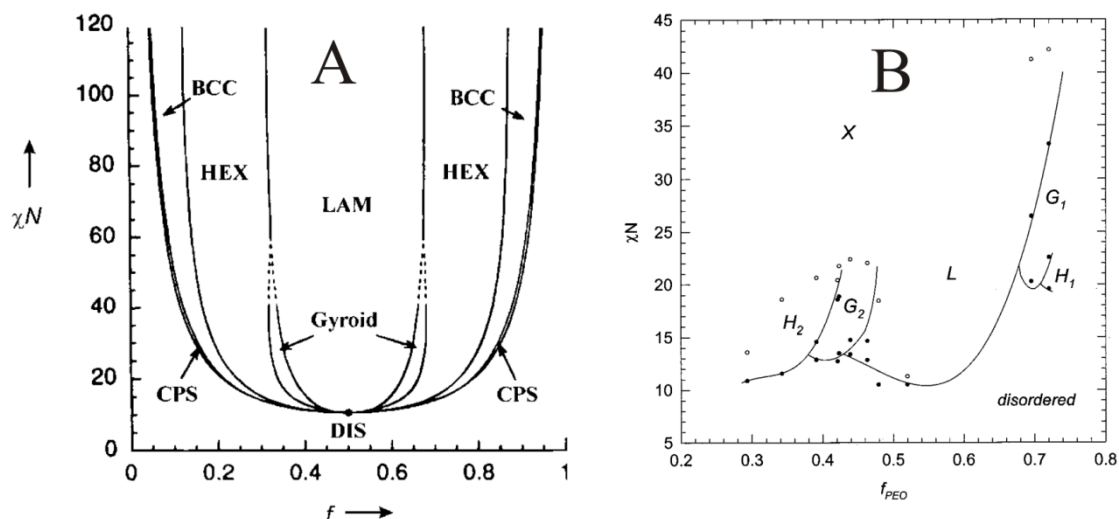
Figure 1.6. Phase diagrams for bulk block-copolymers. Interactions between the blocks (χ) multiplied by the total number of statistical segments (N) as a function of the volume fraction of the hydrophilic block (f). a) Phase diagram obtained from self-consistent mean field theory.[32, 33] b) Phase diagram obtained from experimental measurements of PEE-*b*-PEO.[34] *LAM* and *L*: lamellae, *HEX, H_1, H_2*: hexagonal phase, *G_1, G_2*: bicontinuous gyroid, *CPS*: closed packed spheres, *X*: semicrystalline lamellae, and *DIS*: disordered phase.

1.3 Phase behavior of block copolymers in solution

One of the scientist tasks is to achieve a comprehensive understanding prior to, at last mimic nature. In this regard a major task is to improve for instance the delivery of drugs in the human body in order to decrease their side effects.[35] Most of the "nanoscopic reaction machines" are in aqueous media. Therefore it is not sufficient to characterize the behavior of block copolymers in bulk but also in water. In the following subchapters the various morphologies of self-assembled block copolymers are investigated subsequent to dispersion in water.

1.3.1. Isotropic regime

The self-assembly process of block copolymers diluted in aqueous solution, however, cannot be described solely by the abovementioned parameters. In solution, the interaction between the polymer and the solvent also plays a critical role in determining the thermodynamically preferred structure. [36, 37] This interaction, in turn, depends on the polymer concentration, the volume ratio of the two different segments, and the chemical composition of the hydrophilic

and hydrophobic blocks. In solution block-copolymers self-assemble into nanoscopic structures. Typical self-assembled morphologies of block copolymers in solution are micelles, rods, and vesicles, among others (Figure 1.7).[38-46]
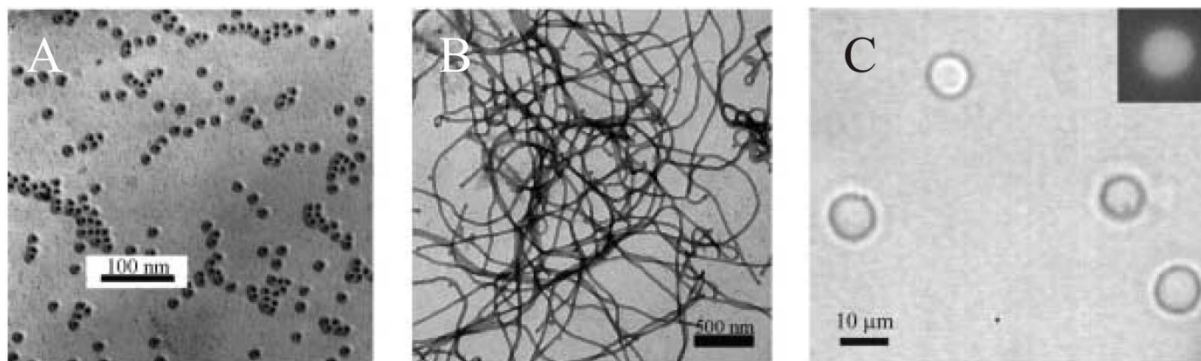
Figure 1.7. TEM pictures of self-assembled structures of block-copolymers a) micelles[47], b) worm-like micelles[27] and c) vesicles[48].

Micelles are a simple and well-known morphology self-assembled from amphiphilic block copolymers. They are not formed only in polar solvent; they can also be found in organic solvents (inverse micelles).[49-51] In polar solvents the corona is hydrophilic and the core is composed of the hydrophobic polymers, whereas in apolar solvents it is accordingly *vice versa*. The size of the micelle depends on the length of the polymers. Experimental results can be described by a power law[39] (equation 1), in which the aggregation number Z (the number of block copolymers in a micelle), correlates with the degree of polymerization of the insoluble block N_A, the degree of polymerization of the soluble block N_B, and the enthalpy of mixing of the soluble and insoluble block Z_0.

$$Z = Z^0 N_A^\alpha N_B^\beta$$

(eq. 1.1)

For most of the polymers, $\beta = 0.8$ and equation 1.1 describe the formation of micelle by diblock,[39, 52] triblock,[52] graft,[53] and heteroarm star copolymers.[54, 55] Micelles can be used as drug[56-58] and gene[59-61] carriers. They can also be used for surface modification in order to promote specific characteristics, e.g. wetting, dispersibility and stabilization of solid pigment particles in a liquid or in a solid phase as well as improved biocompatibility.[62, 63] Micelles are therefore used in many industrial and pharmaceutical applications.[64-66]

Micelles tend toward elongated structures when the packing parameter of the amphiphilic molecule, $p = v/Al$, increases towards $p = 1/2$, where p is the volume of the hydrophobic part of the block-copolymer, A is the surface area occupied by the surfactant head group and l is the extended length of the hydrophobic portion. Micelles are considered rod-like if the length of the micelle is short compared to its persistence length, and worm-like when the overall length, or contour length, is much greater than its persistence length.[46] The persistence length is defined as the length over which correlations in the direction of the tangent are lost. Consequently the persistence length defines the stiffness of a polymer. In contrast to micelles[67-70], the interaction of particles with cells and within animals has not been studied extensively, and the effects of shape have received little attention. It was found that worm-like micelles - also known as filomicelles - persisted in the circulation up to one week after intravenous injection.[71] This is about ten times longer than their spherical counterparts. Under fluid flow conditions, spheres are taken up by cells more readily than elongated micelles (worm/rod-like micelles) because the latter are extended by the flow.[72, 73] Moreover, worm/rod-like micelles appear surprisingly useful in their ability to reptate through the blood stream and permeate tumor tissues to target anticancer drugs.[71, 74, 75] Indeed, when compared to spherical micelles composed of the same copolymer, worm-like micelles increased the maximum tolerated dose of Paclitaxel® (tax) – an anti-cancer drug –, allowing higher doses to be administered.[75] Filomicelles might therefore be expected to minimize the accumulation of cytotoxic drugs such as tax in healthy organs. Despite of their use as drug delivery agents, worms made from low molecular weight surfactants have served as templates for inorganic frameworks[76] and as additives in oil recovery fluids.[77]

The self-assembly process of block copolymers leading to vesicle formation has been considered to be a vesiculation.[78] A bilayer is formed, which then close-up to form a vesicle. Classically, the shape of self-assembled structures is determined by the size of the hydrophobic blocks, at a constant hydrophilic block length. This further influences the curvature of the hydrophilic-hydrophobic interface. The interface is described by two parameters[78, 79], the mean curvature H and the Gaussian curvature, K_G, defined by the two radii of curvature, R_1 and R_2:

$$H = \frac{1}{2}\left(\frac{1}{R_1} + \frac{1}{R_2}\right)$$

(eq. 1.2)

$$K_G = \frac{1}{R_1 R_2}$$

(eq. 1.3)

INTRODUCTION

The interfacial curvature is related to the surfactant packing parameter as follows[80]:

$$\frac{v}{al} = 1 - Hl + \frac{K_G l^2}{3}$$
(eq. 1.4)

where v is the hydrophobic volume of the amphiphile, a is the interfacial area of the hydrophobic volume and l is the chain length of the hydrophobic segment.[81] The packing parameter $p=v/al$ determines the geometry of the aggregates. Hence, when $p < ⅓$, spherical micelles are formed, and when $⅓ <p < ½$, cylindrical micelles are observed (*cf.* above), whereby $½ <p < 1$ corresponds to the formation of vesicles.[82] If $p = 1$, planar bilayers are formed, and finally for $p > 1$, inverted structures are expected. These trends are well established for small surfactants and lipids and are generally valid also for amphiphilic block copolymers. But with block copolymer based systems the packing parameter will only provide an estimation of the morphologies expected in the system, as the actual situation depends on the complex balance among several forces.[83] In any case, it is more convenient to use the volume or weight fraction f of the hydrophobic block ($0 <f < 1$) to describe the shape of amphiphilic block copolymers. In fact, decreasing the lengths of the hydrophilic blocks at constant hydrophobic block lengths causes a transition from spherical to wormlike micelles and finally to vesicular structures.[84, 85] The latter of those morphologies – vesicles – are of most interest. In contrast to vesicles formed out of lipids (liposomes) the hydrophobic blocks of block copolymers is much longer (leading to greater van der Waals energies) and they entangle in the vesicle membrane. Therefore polymeric vesicles are more stable than lipid-based vesicles[84, 86] and can also be used to encapsulate water soluble guest molecules in their inner pool, e.g. drugs. Thus, they can be used as drug delivery devices.[87-91] Further applications of polymer vesicles are nanoreactors, supramolecular biomaterials, lab-on-a-chip components, and building components in microfluidic and bioprocessing applications.[92-97]

1.3.2. Lyotropic regime

Commercial formulations are often made by simply dissolving dry amphiphilic copolymers in water. A simplistic view is that amphiphiles spontaneously self-assemble into their thermodynamically/kinetically preferred structure (cf. chapter before). But the molecular processes involved in these formations are much more complex. For instance the vesicle formation can be theoretically described by water diffusion into the bulk polymer, swelling of hydrophilic domains and eventually the swollen lamella sheets start to detach, that finally bend and close to form vesicles. Thus, the polymer traverses the whole concentration range

10

from the bulk to diluted aqueous solutions upon dissolving in water. In order to control, predict and understand micelle, worm/rod-like and vesicle formation, it is thus important to systematically investigate the phase behavior of block copolymers as a function of their concentration in water across the whole concentration range. And in order to establish proper rules on the phases a block copolymer has to overcome in order to form micelles, worm/rod-like micelles or vesicles a broad variety of polymers has to be studied.

Only a few experimental binary phase diagrams of block copolymer/water mixtures have been reported.[34, 98-103] However, they do not describe any phase behavior of worm-, or rod-like micelles forming block copolymers. One example describes poly(oxyethylene)-*block*-poly(oxybutylene) (EB) phase behavior. When this polymer is capable of forming micelles it was shown that for concentrations between 23 and 38 wt% at low temperatures the EB block copolymers form body-centered cubic (bcc) or face-centered cubic (fcc) structures. At higher temperature a hexagonally packed rod structure was observed.[100-102] However, not the whole concentration regime was investigated. In contrast, when the polymer is self-assembling into vesicles at low polymer concentrations, the polymer undergo transitions from vesicles to packed/interconnected vesicles, then to a sponge phase and subsequently to a lamellar phase. For the polymer with higher molecular weight, the morphology changed further into a hexagonal phase and finally into a disordered phase.[98, 99] In another report[34] the phase behavior of PEE-*b*-PEO was investigated depending on the weight ratio between the two segments. Mainly lamellar and hexagonal phases were observed. But no closer look on the isotropic regime was carried out.

1.4. *"Living polymers"*

Before phase diagrams of block copolymers can be arranged it is crucial to synthesize well-defined block copolymers, which ensure correct interpretation of phase diagrams. But before the state-of-the-art polymerization techniques are shortly introduced, a short historical background is given on anionic polymerization which was the first example of "living polymers" chemistry.

1.4.1. *Short historical background on anionic polymerization*

As early as 1910, interests in anionic polymerization aroused curiosity through several reports stating that a viscous material could be generated from dienes in the presence of alkali

metals.[104-107] In 1929, Karl Ziegler put forth a proposition for the addition of sodium or lithium metals to dienes and suggested a mechanism for anionic polymerization.[108] Ziegler *et al.* suggested that two atoms of sodium add to the unsaturated double bonds of dienes, forming two carbon–sodium linkages. They proposed a mechanism through propagation via the insertion of monomers into the carbon–sodium linkage.[109-111] It was believed that the carbon-sodium linkage was a covalent bond, since it was not understood clearly at that time to be different.[112-114] Schlenk *et al.*, however, proposed an alternative mechanism involving a radical intermediate for the formation of viscous materials composed of dienes in the presence of sodium.[115, 116]

In 1914, Schlenk and Thal[106, 107] undertook studies on the interactions of alkali metals with aromatic hydrocarbons, which later became the foundation for radical anion chemistry. Schlenk *et al.*[116] and Scott *et al.*[117] showed that the reaction of aromatic hydrocarbons with metallic sodium forms a colored 1:1 complex in a polar solvent such as in ether. This complex was later identified as a negatively charged aromatic radical anion associated with the sodium counterion.[118, 119] Such a complex is formed via an electron transfer from metal to aromatic hydrocarbon, assisted by solvation of a polar solvent. In 1936, Scott and coworkers used complexes of aromatic hydrocarbons with sodium to initiate the anionic polymerization of α-olefins.[117, 120] Although several reports concerning the anionic polymerization of vinyl monomers were published in the late 1940s[121-123], it was Michael Szwarc who first demonstrated the anionic polymerization of styrene using sodium naphthalenide in tetrahydrofuran (THF).[124, 125] He suggested that the initiation of polymerization occurs via electron transfer from the sodium naphthalenide radical anion to the styrene monomer. A new species, a styryl radical anion, forms upon addition of an electron from the sodium naphthalenide (Figure 1.8).
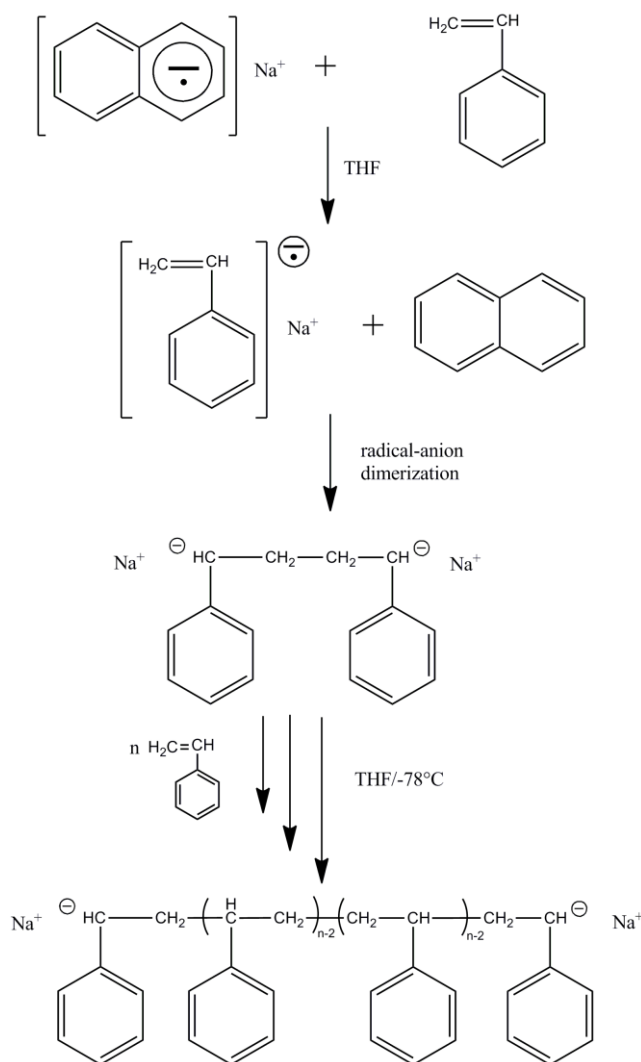
Figure 1.8. Anionic polymerization of styrene using sodium naphthalenide as the initiator and THF as the solvent.[126]

Different formal anion mechanisms were proposed to explain how the styryl anion is formed. But Szwarc *et al.* was able to prove, using spectroscopic and kinetic measurements, the formation of a radical anion through an electron transfer process and subsequent rapid dimerization, yielding dimeric-dicarbanion. This anion starts the propagation of styrene.[124, 125] The propagating benzyl anion is bright red. The color of the reaction mixture remains after the incorporation of all the monomers. This indicated that the chain ends remain active. The resumption of propagation was demonstrated when another portion of fresh styrene was added. A special reactor was designed to prove the transfer and termination-free nature of the polymerization.[127] Michael Szwarc characterized this route of the polymerization as "living polymerization" and called the polymers "living polymers".[125] Here, the term 'living' refers to

13

the ability of the chain-ends of these polymers to retain their reactivity for a sufficient time, enabling continued propagation. Detailed kinetic measurements confirmed that such polymerizations are indeed free from termination and transfer reactions.[124, 125]

Although accounts of several reports on the anionic polymerization of vinyl monomers were available in the literature previous to this observation, Szwarc's first report on living anionic polymerization of styrene free of termination and transfer reactions in THF marks the beginning of lively research activities in this field.[121-125] Accordingly, other polymer research fields have also emerged. Besides sodium, catalysts based on other metals[128-132], such as tin[129, 133, 134] and aluminium[133, 135, 136] are currently widely used, respectively as tinoctoate and aluminium alkoxides. As an example, the mechanism[133] of aluminium-mediated ring opening polymerization (ROP) of ε-caprolactone is shown in figure 1.9.
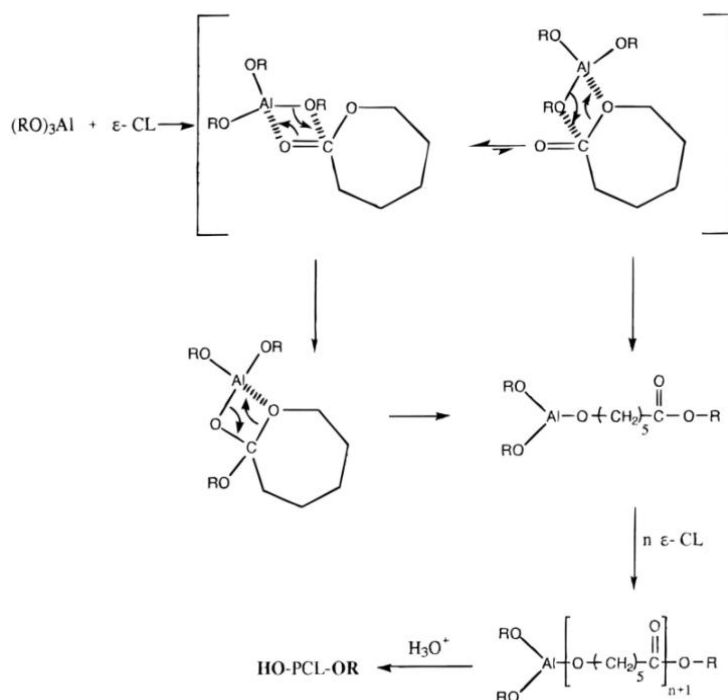
Figure 1.9. ROP mechanism of poly(ε-caprolactone).[133]

1.4.2. Anionic and other "living" polymerization techniques

The emergence of "living polymers" enabled the sequential addition of monomers to various carbanion-terminated linear polymer chains. Consequently, molecular weight distributions (M_W/M_N) of "living" polymerization are very close to 1.[137] Nowadays, it is however possible to synthesize polymers of various architectures and functionalities.[138, 139-144] On the one hand,

14

new monomers have become accessible for controlled polymerization, which has given rise to the preparation of new classes of amphiphilic or functional polymers and, on the other hand, new polymerization techniques have been developed.[140, 145] In this respect the "living" polymerization is of special interest, since lower reactivity of the living chain ends enables polymerization to be accomplished with less technical issues such as using inert gas, high vacuum, rigorous exclusion of air and humidity.[140] Therefore, these polymerization routes are of considerable interest from a technical and scale-up-process point of view. Those "living" polymerizations can be divided into "living" cationic[146-150], radical[145, 151-161] and anionic polymerizations[140, 162-166]. Table XXX shows subcategories of these polymerizations.

Table 1.1. Common living polymerization techniques.

Reactive group	Polymerization technique
Cationic	Cationic polymerization
	Ring opening (ROP)
Radical	Nitroxide polymerization
	Organometals
	ATRP[a]
	RAFT[b]
Anionic	Anionic polymerization
	GTP[c]
	Ring opening (ROP)

[a] Atom-Transfer Radical Polymerization, [b] Reversible Addition Fragmentation,[c] Chain Transfer Polymerization, Group Transfer Polymerization.

2. Scope of the thesis

The state of the art in chapter 1.3 reports on specific block copolymer systems, but a much broader variety of block copolymers will need to be studied in order to achieve a comprehensive understanding to formulate proper rules necessary for the theoretical treatment of nanostructured systems. In this thesis the phase evolutions of poly(ethylene oxide)-*block*-poly(γ-methyl-ε-caprolactone) (PEO-*b*-PMCL) and poly(isobutylene)-*block*-poly(ethylene oxide) (PIB-*b*-PEO) from pure polymer to dilute aqueous solutions were investigated. These block copolymers are of special interest for potential applications, because the hydrophilic PEO is tolerated by living organisms and exhibits very low adsorption affinity for proteins.[167] Moreover, the hydrophobic and fluid PMCL is biodegradable[168] whereas PIB is bio- and hemocompatible.[169-171] Thus, supramolecular structures formed by block copolymers of these polymers are both biocompatible and biodegradable. PIB is a commercially important polymer that finds a large number of applications exploiting its thermal stability, good flexibility at ambient temperature, and impermeability to gases.[172, 173] The glass transition temperatures T_g of PIB, PMCL and PEO are below -50 °C.[174-176] A Tg below room temperature ensures that the formed structures, e.g. membranes of vesicles, are flexible and fluid, thus mimicking the properties of biological lipid membranes. The aqueous core of vesicles is a reservoir for encapsulation of various hydrophilic compounds, rendering them ideal for medical,[177] pharmaceutical,[178] and nutritional applications.[179] Valuable work on PEO-*b*-PMCL and PIB-*b*-PEO block-copolymers was carried out.[180-183] However, the morphologies, in particular for the vesicular system, have not been studied in detail and the phase transitions from bulk polymer to diluted systems has not been investigated. Moreover PEO-*b*-PMCL block-copolymers consisted of a large hydrophobic block, which resulted in decreased solubility in water. In order to mimic biological systems, vesicles that feature a comparably thin membrane (8 − 15 nm) are desirable; otherwise, the membranes are too hydrophobic to further allow, for example, insertion of membrane proteins.[42] Furthermore, the amphiphiles must be able to form vesicles on a relatively short time scale, due to the often short life times of biological macromolecules such as enzymes. Therefore, block copolymers with a relatively low molecular weight and low Tg are desirable. Taking these requirements into consideration, polymers with molecular weights below 10 000 g/mol were investigated.

The theoretical background of the synthesis and self-assembly process of block copolymers sat, it is essential to systematically investigate the phase behavior of distinct block copolymers to establish their phase diagrams. Moreover, such investigations will help to further understand the process of vesicle and worm/rod-like micelles and micelle formation which, in turn, will help to control this process. In this regard the first and the second subchapters of the "results and discussion" part will describe the phase behavior of PEO-*b*-PMCL and PIB-*b*-PEO, respectively. The synthesis of the block-copolymers is discussed first. Next, the evolution of the various morphologies in the lyotropic regime, starting from the pure polymer down to low polymer concentrations is characterized through small-angle X-ray scattering (SAXS). At low polymer concentrations, SAXS measurements were combined with transmission electron microscopy (TEM) and light scattering (DLS and SLS) in order to determine the process of self-assembly of these block copolymers. Based on these data, phase diagrams are presented that will show how the hydrophobic to hydrophilic ratio influences the phase transitions and the characteristics of the supramolecular self-assembled aggregates in the isotropic regime.

The last subchapter shows preliminary results regarding encapsulation with vesicle forming PEO-*b*-PMCL.

3. Materials and Methods (and some short theoretical backgrounds)

All chemicals and solvents were purchased from Sigma-Aldrich (Schnelldorf, Germany) in the highest available purity and used without further purification unless otherwise stated.

3.1. Synthesis of the block copolymers

3.1.1. Synthesis of poly(ethylene oxide)-block-poly(γ-methyl-ε-caprolactone)

PEO-*b*-PMCL diblock copolymers were synthesized from a common MeO-PEO-OH by the aluminium-mediated ring-opening polymerization of methyl-ε-caprolactone (MCL) according to a previously published protocol.[180] The monomer γ-methyl-ε-caprolactone (MCL) was synthesized via a Bayer-Villiger reaction using 1.4 eq. of *m*-chloroperbenzoic acid (mCPBA) and 1 eq. of 4-methyl-cyclohexanone in dichloromethane, as described elsewhere.[15] First, in order to remove traces of water from MeO-PEO-OH, an azeotropic mixture formed by adding toluene was vacuum distilled to yield residual, pure polymer. Prior to synthesis, THF was dried by reflux over a Na/K-alloy with the addition of small amounts of benzophenone used as colorimetric indicator. First the macroinitiator MeO-PEO-OH (1.00 g, 1.00 mmol) was activated by reacting it with 2 equivalents of triethylaluminium in the presence of pyridine (0.5 mL) in 10 mL THF. To start the polymerization, MCL was added directly to the solution. After 20 min the reaction was terminated by adding 10 mL of 0.5 % sulfuric acid in a 1:1 vol.-% mixture of water and methanol. The block-copolymer was purified by precipitation in petrolether and dried over magnesium sulfate. The polydispersity index M_w/M_n, ratio of the apparent weight-average and apparent number-average molecular weights, and the composition were determined by gel permeation chromatography (GPC) on a ViscotekTDAmax with a PLgel 5 µm mixed *c* column, using THF as solvent and polystyrene (PS) standards. ^{1}H-NMR spectra were recorded on a Bruker DPX-400 NMR spectrometer in CDCl$_3$ (99.8% D, 0.1% TMS) at room temperature. The signals were referenced to tetramethylsilane (TMS) at $\delta = 0.00$ ppm. The spectrometer was operated at 400 MHz. Number-average molar masses (M_n) of the PMCL block were calculated based on the integrals of the peaks corresponding to the methyl group compared to the integrals of the ethylene oxide groups. The yield was ≥ 80 %.

3.1.2. Synthesis of poly(isobutylene)-block-poly(ethylene oxide)

ω-hydroxy-poly(isobutylene) (PIB-OH) was synthesized by quasi-living cationic polymerization as follows: The polymerization of isobutylene was initiated with 2-chloro-2,4,4-trimethylpentane in conjunction with $TiCl_4$ in the presence of a nucleophile[184], and the polymerization was quenched with allyltrimethylsilane[185, 186], leading to allyl-terminated PIB. Hydroboration of the terminal double bonds with 9-borabicyclo[3.3.1]nonane (0.5 M in THF) and subsequent oxidative cleavage of the carbon-boron bonds with alkaline H_2O_2 resulted in PIB-OH[187, 188]. In order to remove cyclooctane-1,5-diol, a by-product formed during the treatment with 9-BBN, the crude product was dissolved in hexane and precipitated three times by the drop-by-drop addition of methanol under vigorous stirring. Finally, the polymer was redissolved in hexane, precipitated into acetone, filtered, and dried in vacuum. Thin-layer chromatography (TLC) and ^{1}HNMR analyses showed that the product was free from contaminants and exhibited 100 % end-functionality[185, 186]. According to vapor-pressure osmometry and GPC using PS standards, the number-average molecular weight M_n of the sample was 4450 g mol^{-1} (corresponding to 79 isobutylene repeating units), and M_w/M_n was 1.1.

The block-copolymer PIB-*b*-PEO was synthesized according to a procedure described elsewhere[189]. Briefly, to a 5 wt% solution of PIB-OH in THF was added 1.0 equivalents of the phosphazene base t-BuP$_4$ (1 M solution in hexane) via a syringe and stirred at room temperature for 1 hour. Then, ethylene oxide was added via a syringe into the reactor. The reaction mixture was stirred at that temperature for a few minutes, then slowly heated to 40 °C and stirred for 6 days under a dry argon atmosphere. After quenching the polymerization with acetic acid, the reaction solution was washed with the strongly acidic cation exchanger DOWEX Marathon to remove traces of protonated t-BuP$_4$, filtered and concentrated. The M_w/M_n and the composition were determined by GPC and ^{1}H-NMR. M_n was calculated from the integrals of the peaks corresponding to the poly(isobutylene) groups compared with those of the ethylene oxide peaks. The yield of block copolymers $\geq$ 70 %.

3.2. Preparation of solutions

3.2.1. Solutions used for phase behavior studies

Polymer solutions at concentrations below 1 wt% were stirred for at least four weeks in doubly-distilled water at room temperature in order to reach the thermodynamically preferred

structures. Prior to measurement, the solutions were extruded 10-times through 1 μm -, 10-times through 400 nm -, and 10-times through 200 nm Nuclepore Track-Etch filters (Whatman, Schleicher &Schuell) with a barrel extruder (Lipex extruder, Northern lipids Inc.). Solutions with polymer concentrations above 1 wt% were shaken continuously for at least two weeks at room temperature. For this purpose, homemade Teflon capsules containing ceramic grinding balls were used and continuously shaken with a peptide shaker (Bioblock Scientific, Agitest).

3.2.1. Solutions used for encapsulation studies of PEO_{23}-b-$PMCL_{32}$ vesicles.

Both Enhanced Cyan Fluorescent Protein (ECFP) and fluorescein encapsulation experiments were performed in phosphate buffer solutions (PBS) containing 137 mM sodium chloride (NaCl), 2.7 mM potassium chloride (KCl), 0.37 mM potassium dihydrogenphosphate (KH_2PO_4) and 2.1 mM of disodium hydrogenphosphate (Na_2HPO_4) and were adjusted between pH 3.8 and 7.5 with 2M hydrochloric acid (HCl). Prior to measurements all buffer solutions were autoclaved at 121 C° and degassed.

Encapsulation of fluorescein: The starting concentration of fluorescein was 25 μM. The vesicles were prepared by solvent displacement: The polymer was dissolved in approximately 50-60 mL of THF and then the fluorescein solution was added drop wise under constant stirring. The final polymer concentration is 10 mg/mL. The whole setup was left for about 3-4 days. The resulting solution was then dialyzed against PBS to remove the excess dye, extruded 10 times through 0.4 mm Nuclepore Track-Etch filters (Whatman, Schleicher &Schuell) manually and purified by size exclusion chromatography (SEC) on a Sepharose 2B stationary phase. The purified vesicles were then exposed to various pH conditions (3.8-7.5) and the fluorescein release was followed by measuring the fluorescence of the dye at 480 nm excitation wavelength and 515 nm emission wavelength.

Encapsulation of ECFP: The starting concentration of ECFP was 0.3 mg/mL (~11mmol). The vesicles were prepared by bulk swelling. The polymer was added to an ECFP solution at a 10 mg/mL concentration and left under stirring for three days at 4 °C. The resulting solution was extruded 10 times through 0.4 mm Nuclepore Track-Etch filters (Whatman, Schleicher &Schuell) manually and purified by SEC on a Sepharose 2B stationary phase. The release of ECFP was monitored by fluoresence correlation spectroscopy (FCS).

3.3. Static and dynamic light scattering

Light scattering (LS) is a powerful technique to characterize the structure modes of formation and interaction of supramolecular systems. Studying the scattering of light by structures with sizes in the sub-micrometer range allows the determination of critical characteristics such as shape or internal structure.

In the static light scattering (SLS) mode, the absolute value of the intensity of the scattered light is monitored, whereas instantaneous variations in intensity are recorded by dynamic light scattering (DLS). A combination of these two light scattering modes yields complementary thermodynamic and hydrodynamic information such as the molecular weight, size and shape of the system under investigation.[190] The detailed theory behind LS is reported in several excellent publications [190-192]. Briefly, electro-magnetic waves − or photons − interact with the local electron cloud of the analyte. This interaction results in an energy transfer from the electro-magnetic wave to the electrons, inducing fluctuations, depending on the polarizability of the analyte. Since any accelerated particle emits light, the electrons reemit photons. This process, extending from the interaction between the incident photon to the reemission of light is called LS, and the analysis of the characteristics of the scattered light yields information about the system under investigation.

3.3.1. Theoretical background of dynamic light scattering

When a particle assumes Brownian motion and irradiates, two frequencies in addition to the frequency that would normally be scattered and which are of equal intensity are generated and detected, inducing a positive and a negative Doppler shift proportional to the particle velocity. The interference between the non-shifted wave (photon reemission) and the two waves due to Brownian motion yields infinitesimal variations in intensity. Detection of these infinitesimal variations in intensity is the basic principle of DLS, which is therefore particularly suited to the study of properties of solutions. The scattered intensity is acquired as a function of time and is then self-correlated. This yields the relaxation time due to the Brownian motion and leads to the characterization of the particle size through hydrodynamic models of the diffusion coefficients. In DLS experiments, a time correlation function decaying in time is measured. From this, the cooperative translatory diffusion coefficient D_m at a concentration c can be determined.

$$Dm = D_0(1 + k_d c)$$

(eq. 3.1)

where D_m is a z-averaged cooperative translational diffusion coefficient and k_d the diffusion virial coefficient. The extrapolation to zero concentration yields a diffusion coefficient D_0, which allows the calculation of the hydrodynamic radius R_h via the Stokes-Einstein equation[8]

3.3.2. Theoretical background of static light scattering

The scattered intensity by dilute solutions is usually described by the virial expansion

$$\frac{Kc}{R(q)} = \frac{1}{M_w P(q)} + 2A_2 c + 3A_3 c + \cdots$$

(eq. 3.2)

with the scattering vector $q = \left(\frac{4\pi}{\lambda}\right)_{n0} \sin\left(\frac{\theta}{2}\right)$ where M_w is the weight-average molecular weight, $P(q)$ the particle scattering factor, and A_i the ith virial coefficient. The time-averaged scattered light intensity is expressed by $\frac{Kc}{R(q)}$, with an optical contrast factor $K = \left[\frac{4\pi^2 n_0^2}{\lambda^4 N_A}\right]\left(\frac{dn}{dc}\right)^2$. n_0 is the refractive index of the solvent, c the concentration of the polymer solution, $R(q)$ the Rayleigh ratio of the solution corrected for the contribution of the pure solvent, and dn/dc the refractive index increment. At small angles, the particle scattering factor can be expanded in a Taylor series, yielding

$$P(q) = 1 - \frac{1}{3}R_g^2 q^2$$

(eq. 3.3)

with R_g is the radius of gyration. Inserting eq 3.3 in 3.2 gives

$$\frac{Kc}{R(q)} = \frac{1}{M_w}\left(1 + \frac{1}{3}R_g^2 q^2\right) + 2A_2 c + 3A_3 c + \cdots$$

(eq. 3.4)

Measurements at several finite angles and concentrations can be extrapolated in a Zimm, Berry or Guinier plot[193] and permit the determination of single particle properties such as M_w, R_G, and A_2. A Berry plot was used since this plot includes the interaction between large aggregates.

3.3.3. Setup and limitations of light scattering

The intensity of the scattered light monitored over the course of a LS measurement depends on both the concentration and angle of detection.
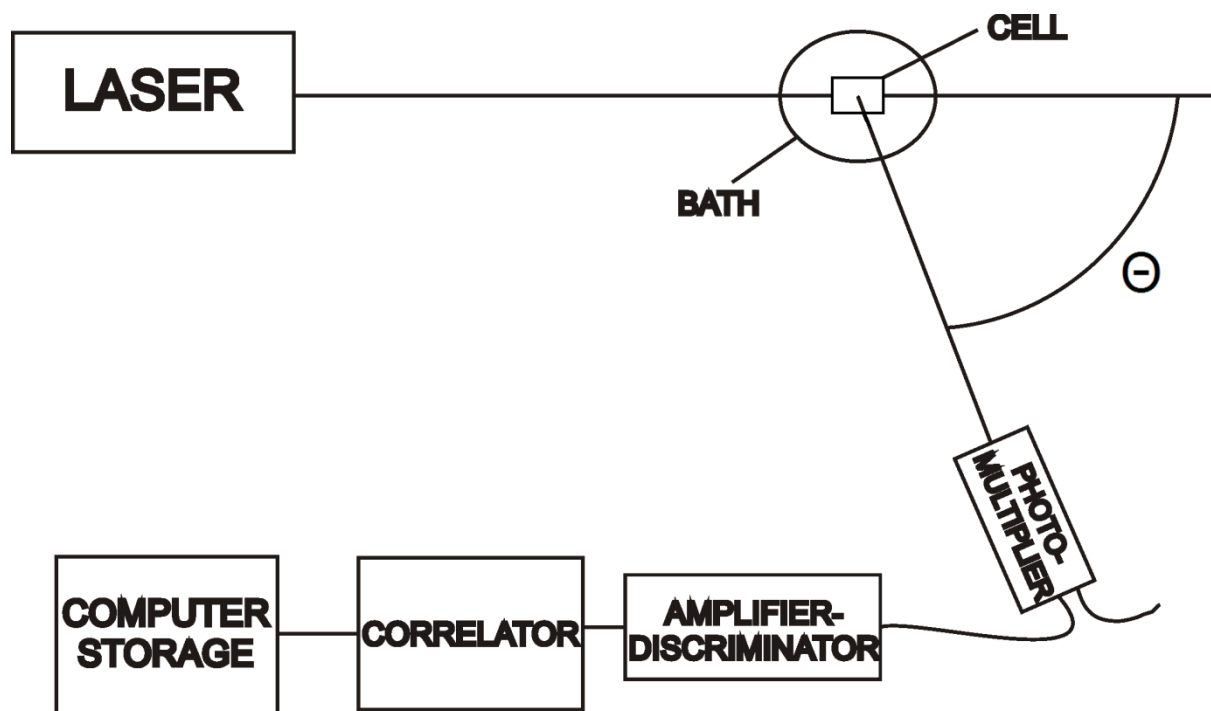
Figure 3.1: Schematic representation of a typical light scattering setup.

Therefore, for example, to accurately quantify the size of a particle, rather than merely observing relative changes that depend on the composition of the surrounding medium, measurements must be carried out at several concentrations and angles. Small particle sizes below the laser wavelength / 20, in nm, however, can be represented as single scattering centers; here, the intensity of scattered light does not exhibit angular dependence. The shape of the particle is assumed to be spherical, and hydrodynamic models of the diffusion coefficient yield the equivalent hydrodynamic size of a sphere of the particle under investigation. The most common model uses the Stokes-Einstein equation, which assumes no intermolecular interactions between small, spherical particles. Concentration-dependent measurements therefore enable extrapolation to infinite dilution for accurate size quantification by LS.

However, few macromolecules are of a size that matches this criterion. When particles cannot be described as point scattering centers, the scattered light from two different parts along the same molecule interfere constructively or destructively, leading to an angle dependence of the intensity of scattered light. As in cases of shape anisotropy, for which the autocorrelation function must be corrected, the determination of the size of the molecules is hampered by LS angle-dependent measurements.

3.3.4. Experimental setup of light scattering

The static and dynamic light scattering experiments were performed using a commercial goniometer (ALV/CGS-8F, ALVLangen) equipped with a He:Ne linear polarized laser (JDS Uniphase, wavelength = 632.8 nm) at scattering angles between 40° and 150° in 5° increments. An ALV-7000 correlator was used to calculate the photon intensity autocorrelation function. The samples were centrifuged for 5 min prior to measurement in order to avoid the presence of dust particles in the solution. Measurements were performed in quartz cells (dimensions 10x75 mm). These cells were mounted in a thermostated optical matching vat with a temperature accuracy of T = 0.02 K. The experiments were performed at T = 293.00 K. Toluene was used as the calibration standard. Solutions with concentrations below 0.1 wt% were analyzed. The weight-average molecular weight (M_w), average radius of gyration (R_g) and the second virial coefficient (A_2) were obtained from the SLS data using Berry analysis.[16] In the case of DLS, second order cumulant analysis of the data was performed.[194] The angle-dependent apparent diffusion coefficient (D_{app}) was extrapolated to zero concentration and zero momentum transfer (q^2) and converted to the hydrodynamic radius (R_H) using the Stokes-Einstein equation.[195] The refractive index increment dn/dc was obtained at the corresponding temperature and wavelength of the light scattering set-up by using a commercial ALV-DR-1 differential refractometer.

3.4. Transmission electron microscopy

The first TEM was built by Max Knoll and Ernst Ruska in 1931[196-199], with resolving power greater than that of light in 1933 and the first commercial TEM in 1939.

TEM is a microscopy technique whereby a beam of electrons is transmitted through an ultra-thin specimen, interacting with the specimen as it passes through. An image is formed from the interaction of the electrons transmitted through the specimen; the image is magnified and focused onto an imaging device to be detected by a sensor such as a charge-coupled device camera.

At smaller magnifications TEM image contrast is due to absorption of electrons in the material, due to the thickness and composition of the material. At higher magnifications complex wave interactions modulate the intensity of the image, requiring expert analysis of the observed images. Alternate modes of use allow for the TEM to observe modulations in

24

chemical identity, crystal orientation, electronic structure and sample induced electron phase shift as well as the regular absorption based imaging.

3.4.1. Experimental setup of transmission electron microscopy

Samples were prepared by negative staining of a drop of polymer solution with a 2% uranyl acetate. They were deposited on a carbon-coated copper grid and examined with a Philips EM400 at an acceleration voltage of 80 kV.

3.5. Small angle X-ray scattering

SAX analysis is a technique for studying structural features of colloidal size (0.1 - 100 nm). Any scattering is characterized by a reciprocity law giving an inverse relation between scattering angle and morphology. Colloidal dimensions from a few to thousands of Å are enormously large compared to X-ray wavelength (most frequently Cu based X-ray sources are used having a wavelength λ of 1.54 Å). This makes the angular range of observable scattering correspondingly small. X-rays are primarily scattered by electrons. Due to that SAXS is only observed when electron density inhomogeneities in the colloidal size range exist in the sample. And we only consider coherent scattering (the scattered waves have a constant relative phase), since incoherent scattering is negligibly weak at small angles. Thus, the scattering process is that electrons resonate with the frequency of the X-rays passing through the samples and emit secondary waves which interfere with each other. A small example is given below: Figure 3.2a schematizes scattering by a spherical particle.
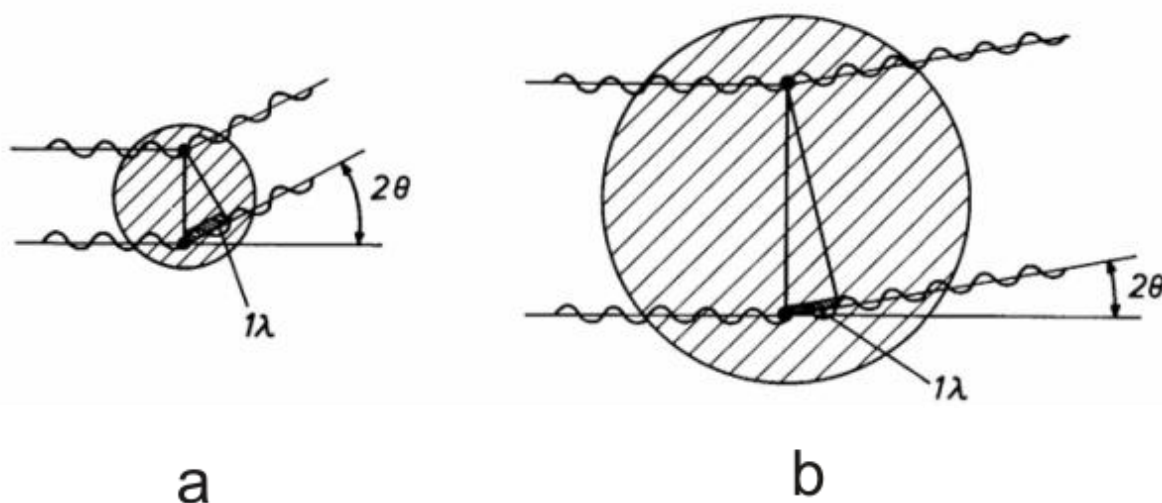
Figure 3.2. Illustrative SAXS by a small (a) and a large sphere (b).

MATERIALS AND METHODS

The waves scattered by the two indicated points at an angle 2θ have a path difference of 1λ. 2θ is the angle between the incident X-ray and the scattered wave. If the scattering by all points (electrons) is taken into account (large detection angle), the superposition of waves with all possible phases will essentially lead to no scattering in the direction of 2θ as a result of destructive interferences. At smaller detection angles, the phase difference becomes smaller and the waves will interfere constructively. The scattering maximum is therefore observed in the direction of zero angle, at which all waves are exactly in phase.
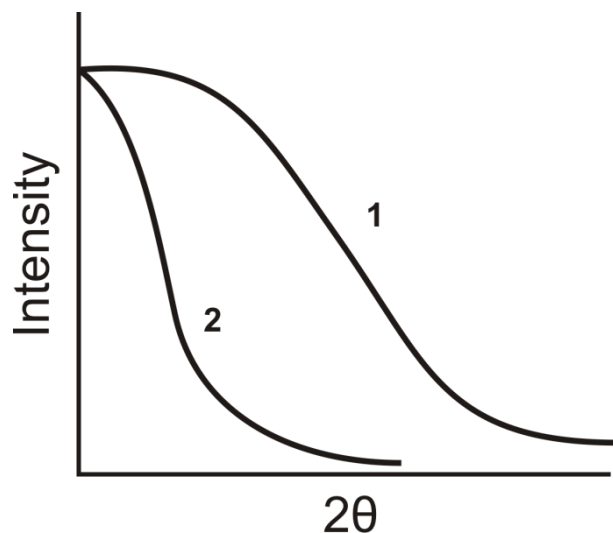
Figure 3.3. SAXS patterns by a large (curve 2) and a small sphere (curve 1).

The observed scattering curve will be qualitatively like curve 1 in Figure 3.3. Applying the above scheme to a much larger sphere (using the same wavelength λ) a path differences of 1 λ will already occur at smaller scattering angles (Figure 3.2b) resulting in a narrower scattering curve (curve 2, Figure 3.3). Finally for particles that are huge compared to the wavelength, SAXS occurs. This leads depending on the structure to different SAXS patterns.

3.5.1. Experimental setup of Small angle X-ray scattering

A Bruker AXS Nanostar setup, including an Incoatec Cu-IμS microfocused X-ray source ($\lambda = 0.154$ nm) with Montel multilayer optics at a generator power of 40W (45kV, 630μA) and a virtually noise-free, real-time Våntec 2D-detector with photon counting ability, was used to perform X-ray measurements in the range of scattering vectors from $0.1 - 3$ nm^{-1}. All 2D images of the samples loaded in quartz capillaries (diameter 1.5 mm) were taken at ambient temperatures with exposure times of 8 h per sample and azimuthally-averaged using Fit2D software to produce 1D intensity profiles.

3.6. Fluorescence detection

Florescence is used in many aspects of daily life, some of the popular examples are neon tubes[200] as well as fluorescent dyes.[201, 202]

Fluorescence is the characteristic property of certain molecules called fluorochromes, fluorophores or fluorescent dyes. It is best described by a model of electronic energy levels of a molecule as illustrated by the so-called Jablonski diagram (cf. Figure 3.4). In the first stage an electron is excited by a photon from an external photon source (laser) from the ground state S_0 into an excited electronic singlet state $S_1`$. This level is quickly converted to the so-called relaxed singlet exited state S_1 (exited-state lifetime). After this relaxation, which has in general a relaxation time between 0.1 to 10 ns, fluorescent emission occurs. The molecule emits spontaneously a photon and relaxes back to the ground state S_0, resulting in fluorescence.
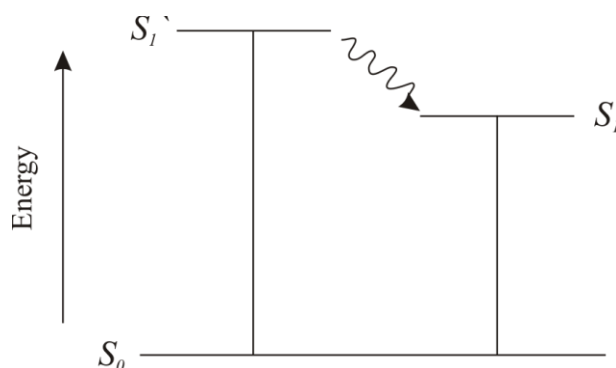
Figure 3.4. Jablonski diagram, an electronic state diagram.

3.6.1. Fluorescence correlation spectroscopy

The concept and experimental realization of FCS was developed in the 1970s by Magde, Elson and Webb, based on the technique of DLS.[203] FCS is an experimental technique that monitors the motion of fluorescently labeled molecules in a tiny, optically defined observation volume. It is a noninvasive technique that allows probing the dynamics and interactions of labeled molecules in vitro and in vivo. The key principle of FCS is the analysis of spontaneous fluctuations of a laser-induced fluorescence signal. The fluorescent photons come from an ensemble of identical independent emitters at thermal equilibrium. By examining samples at low concentrations, the relaxation of spontaneous fluctuations in the fluorescence signal originating from the motion of fluorophores in and out of the observation volume are monitored. Statistical analysis of time correlations of thermodynamic

27

concentration fluctuations reveal the underlying dynamics within a sample. The second order autocorrelation function of these intensity variations yields thermodynamic and kinetic parameters of the system, such as the diffusion coefficient and concentration. These parameters can be extracted from the recorded autocorrelation curve by analysis with an appropriate mathematical model depending on the number of various particles inside.[204]

3.6.1.1. Experimental setup of Fluorescence correlation spectroscopy

FCS measurements were performed at room temperature in special chambered quartz glass holders (Lab-Tek; 8-well, NUNC A/S), on a Zeiss LSM 510-META/Confcor2 laser-scanning microscope equipped with an Argon-laser (488 nm) and a water-immersion objective (Zeiss C/Apochromat 40X, NA 1.2), with pinhole adjusted to 70 μm. Spectra were recorded over 30 s, and each measurement was repeated 10 times. Excitation power of the Ar-laser was $P_L =15$ mW, and the transmission at 488 nm was of 20%. Diffusion times for free ECFP were determined and fixed in the fitting procedure. The results were presented as a mean value of three independent measurements.

The fluorescence signal was measured in real time and the autocorrelation function was calculated by a software correlator (LSM 510 META - ConfoCor 2 System).

By means of an iterative least-square method, the values calculated by the algorithm are compared repeatedly to the experimentally generated autocorrelation curve and approximated until the difference between the two curves is minimized.

3.6.2. Fluorescence spectroscopy

Fluorescein kinetics in solution or upon encapsulation in vesicles were investigated with a PerkinElmer LS55 fluorescence spectrometer (Waltham, Massachusetts, USA) at ambient temperature. The fluorophore was excited at 480 nm and the emitted light was detected at 530 nm.

4. Results and Discussion

4.1. *Phase behavior of vesicle forming poly(ethylene oxide)-block-poly(γ-methyl-ε-caprolactone)*[103]

4.1.1. Synthesis of poly(ethylene oxide)-block-poly(γ-methyl-ε-caprolactone)

One of the most important tasks in polymer chemistry is to predict and control the polymer length over the course of the synthesis. The reaction, a living anionic polymerization, is known to yield well-defined homopolymers[10] and block-copolymers.[64] Block copolymers were synthesized by the aluminium-mediated ring-opening polymerization of γ-methyl-ε-caprolactone using a monofunctional PEO macroinitiator.

Preparation of the monomer. The monomer γ-methyl-ε-caprolactone (MCL) (3) was prepared by the Baeyer-Villiger oxidation of 4-methylcyclohexanone (1) using 1.4 equivalents of mCPBA (2).[176, 205] In a typical reaction, 4-methylcyclohexanone and mCPBA were dissolved in CH_2Cl_2 (~10 w/v % solution) and stirred vigorously at 25 °C for 24 h. Removal of the mCPBA byproduct was achieved by repeated filtration until no white precipitate was present when the solution was cooled to -78 °C. The mixture was then washed three times with saturated $NaHCO_3$ and once with brine before drying over $MgSO_4$. The solution was concentrated *in vacuo*. The crude product was stirred over calcium hydride prior to isolation by vacuum distillation. A clear solution was obtained. ^{1}H-NMR (CDCl3): δ 4.13-4.31 (m, 2H), 2.56-2.71 (m, 2H), 1.71-1.96 (m, 3H), 1.27-1.56 (m, 2H), 1.00 (d, 3H); 13C NMR (CDCl3): δ 176.0, 67.9, 37.1, 35.0, 33.0, 30.6, 22.0.
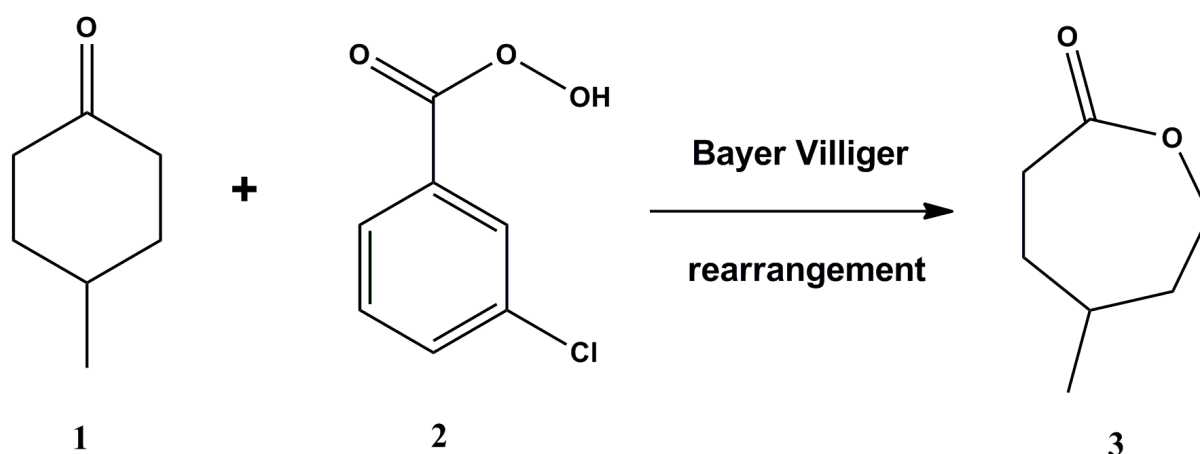
Figure 4.1.1. Baeyer villiger rearrangement of 4-methylcyclohexane (1) and mCPBA (2) to result in MCL (3).

RESULTS AND DISCUSSION

Preparation of diblock copolymers. In order to remove traces of water from MeO-PEO-OH (4), an azeotropic mixture formed by adding toluene was vacuum distilled to yield residual, pure polymer. Prior to synthesis, THF was dried by reflux over a Na/K-alloy with the addition of small amounts of benzophenone. THF, 1.1 equivalents of triethylaluminum (1M in heptane) with respect to polymer and 3 equivalents of pyridine with respect to aluminum were added to the flask under N_2. The flask was placed in an oil bath and reacted at 60 °C for 1 hour under a slight Ar flow. MCL (3) was added directly to the macroinitiator solution and the polymerization was carried out at 60 °C for approximately 20 min. Reactions were quenched with aqueous HCl (0.1 M in 50:50 methanol/water) and products precipitated in petrolether to remove unreacted MCL. Recovered copolymers were redissolved in CH_2Cl_2, dried over MgSO4, filtered. Purified diblocks (5) were then dried *in vacuo*. ^{1}H-NMR (CDCl3): 4.10 (m, 2H, -C(O)-O-C**H**2), 3.65 (s, 4H, -C**H**2-O-C**H**2-), 2.30 (m,3 2H, -C**H**2-C(O)-O), 1.75-1.35 (m, 5H, -C**H**2-CH(CH3)-CH2-,-CH2-C**H**(CH3)-CH2- and -CH2-CH(CH3)- C**H**2-), 0.90 (d, 3H, -CH2-CH(C**H**3)-CH2-).
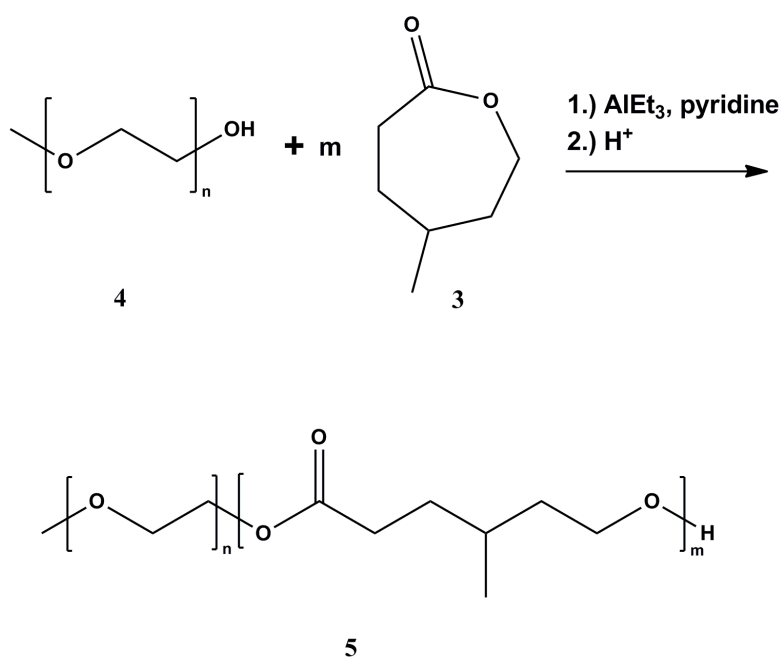
Figure 4.1.2. Aluminium-mediated ring-opening polymerization of MCL (3) using a monofunctional PEO macroinitiator (4) resulting in PEO-*b*-PMCL (5).

Table 4.1.1 shows the molecular characteristics of the synthesized polymers. Here, the first four polymers out of table 4.1.1 were studied more in detail. Except for PEO_{23}-$PMCL_{63}$, which self-assembles also into vesicles, the hydrophobic block is too large which leads to increased time for vesicle formation. For very long hydrophobic blocks ($N_{MCL} > 90$)

precipitation of the block copolymers even occurs. Figure 4.1.3 shows GPC elution curves of the polymers which were studied more in detail. And a ^{1}H-NMR example is also shown in Figure 4.1.3 on the right. (Figure 4.1.3 B).
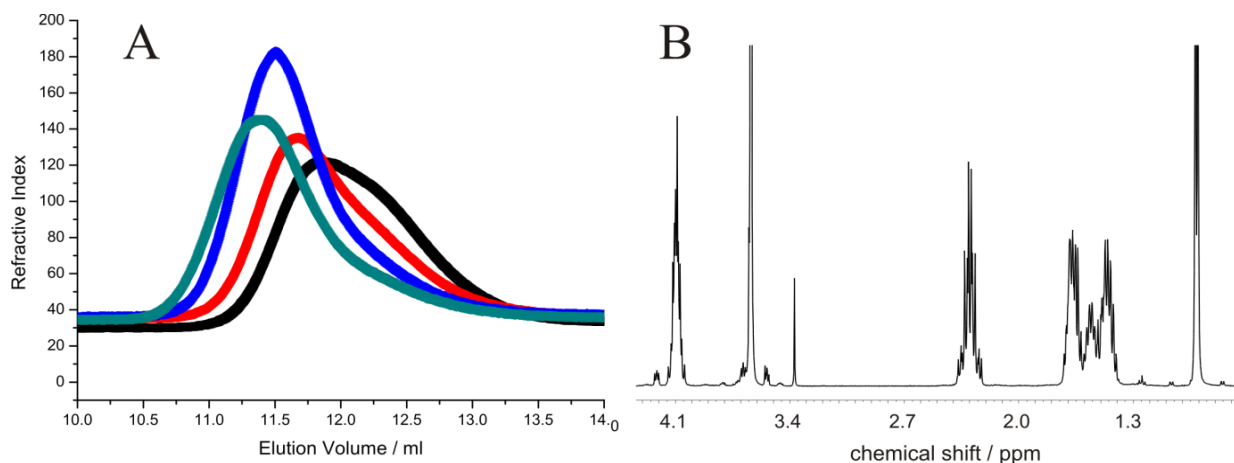
Figure 4.1.3..a) GPC elution chromatography of PEO_{23}-b-$PMCL_{25}$ (black), PEO_{23}-b-$PMCL_{32}$ (red), PEO_{23}-b-$PMCL_{44}$ (blue) and PEO_{23}-b-$PMCL_{54}$ (green). b) ^{1}H-NMR spectrum of PEO_{23}-b-$PMCL_{54}$ as an example.

According to ^{1}H-NMR spectroscopy (Table 4.1.1), the desired PMCL block lengths were obtained quite accurately. However, GPC measurements standardized with PS show slight deviations from the expected molecular masses. Since the molecular architecture of PS differs from that of the block-copolymers studied in here, the hydrodynamic radii of the polymers in THF are also different. This explains the deviation of the molecular masses measured by GPC compared to those obtained by NMR. As expected for an anionic polymerization, the polydispersity of all polymers was measured below 1.3.

RESULTS AND DISCUSSION

Table 4.1.1. Molecular characteristics of synthesized PEO-*b*-PMCL block copolymers.

Polymer	N_{MCL}(th.)[a]	N_{MCL}(NMR)[b]	M_n(NMR) (g/mol)[c]	M_n(GPC) (g/mol)[d]	M_w(GPC) (g/mol)[e]	PDI (M_w/M_n)[f]	w_{PMCL}[g]
PEO$_{23}$-*b*-PMCL$_{25}$	20	25	4200	5000	6400	1.28	0.76
PEO$_{23}$-*b*-PMCL$_{32}$	30	32	5100	5150	6300	1.22	0.8
PEO$_{23}$-*b*-PMCL$_{44}$	40	44	6600	5840	6780	1.16	0.85
PEO$_{23}$-*b*-PMCL$_{54}$	50	54	7900	6210	7510	1.20	0.87
PEO$_{23}$-*b*-PMCL$_{63}$	60	63	9000	7200	8100	1.18	0.88
PEO$_{23}$-*b*-PMCL$_{72}$	70	72	10200	8000	9900	1.24	0.90
PEO$_{23}$-*b*-PMCL$_{82}$	80	82	11500	8700	10800	1.24	0.91
PEO$_{23}$-*b*-PMCL$_{93}$	90	93	12900	9500	11900	1.25	0.92
PEO$_{23}$-*b*-PMCL$_{100}$	100	100	13800	10100	12900	1.27	0.93

[a] Targeted numbers of MCL monomers. [b] Number of monomer repeat units in the PMCL block as determined by ^{1}H-NMR spectroscopy. [c] Number-average molecular weight of block-copolymers as determined by ^{1}H-NMR spectroscopy. [d,e] Number- and weight average molecular weight of block-copolymers as determined by GPC with polystyrene as a standard. [f] Polydispersity index determined from GPC results. [g] Weight fraction of the PMCL block as determined by ^{1}H-NMR spectroscopy.

4.1.2. Lyotropic regime of poly(ethylene oxide)-block-poly(γ-methyl-ε-caprolactone) solutions

The synthesized polymers were allowed to self-assemble in water at various concentrations. It was possible to construct a phase diagram of the binary mixture of PEO-*b*-PMCL and water upon analysis of the evolution of the structures with concentration. In order to determine structures, two methods were considered: SAXS and TEM. SAXS is a fundamental tool in the study of macromolecules. The major advantage of this method lies in the possibility to obtain structural information on partially or completely disordered systems. Moreover, it can be used to analyze both concentrated and diluted samples. In contrast, TEM images are not useful to assess the morphology of highly concentrated polymer solutions, as the TEM grids become overloaded with polymer and the electron beam cannot pass through the material. Therefore, SAXS measurements were used to study the structures of the complete dilution series of PEO-*b*-PMCL block copolymers. Figure 4.1.4 shows the 1-D SAXS patterns of all block copolymers after self-assembly in water, starting from the pure polymer down to a 5 wt% polymer concentration in water.
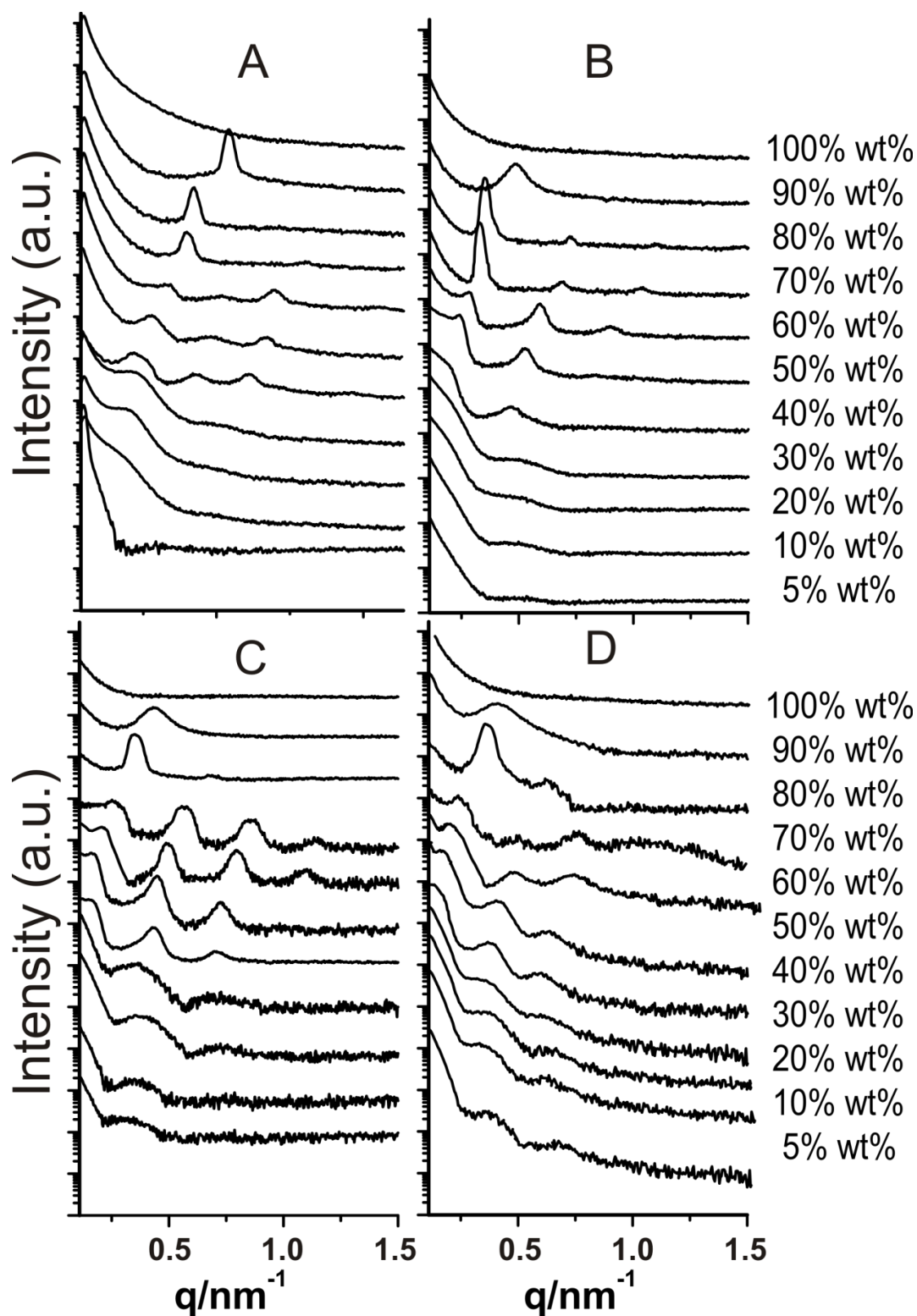
Figure 4.1.4. One-dimensional SAXS patterns for the dilution series of self-assembled block copolymers in water. a) PEO_{23}-b-$PMCL_{25}$, b) PEO_{23}-b-$PMCL_{32}$, c) PEO_{23}-b-$PMCL_{44}$ and d) PEO_{23}-b-$PMCL_{54}$. For clarity the SAXS patterns are shifted to higher intensities.

No Bragg peaks can be observed in any of the spectra of the pure polymers, indicating a disordered phase.[206] When small amounts of water are added to the polymers (90 wt% polymer) a form factor is observed in all polymer/water mixtures except for PEO_{23}-b-$PMCL_{25}$. This form factor presumably arises from a not well-ordered system which we assume to be a transition phase between the disordered and the following lamellar phase. In contrast PEO_{23}-b-$PMCL_{25}$ shows two superimposing patterns: a peak (0.54 ± 0.04 nm^{-1}) and a form factor. Since the next phase is a lamellar phase the peak is indicative for a lamellar phase and the form factor is indicative for a transition phase. Increasing the water concentration (80 wt% polymer) leads to the appearance of more than one peak in PEO_{23}-b-$PMCL_{32, 44 \text{ and } 54}$. For PEO_{23}-b-$PMCL_{32 \text{ and } 44}$, the second peak ($0.72 \pm 0.02$ and 0.68 ± 0.04 nm^{-1}, respectively) is shifted by a factor of two to a higher q than the first Bragg peak (0.36 ± 0.02 and 0.35 ± 0.03 nm^{-1}, respectively) indicating the presence of a lamellar phase. For PEO_{23}-b-$PMCL_{54}$, the second peak (0.63 ± 0.05 nm^{-1}) is shifted by $\sqrt{3}$ in relation to the first (0.36 ± 0.02 nm^{-1}), which is typical of a hexagonal phase. Here, the phase is predicted to be an inverse hexagonal (H_2) phase, a so-called "water in oil" phase[34] with cylinders of PEO in the PMCL matrix due to the very low mass fraction of water. The diameter of hexagonal rods of the inverse hexagonal phase can be calculated from the position of the first Bragg peak (q_1) in SAXS spectra according to $d_{H_2} = \dfrac{4\pi}{\sqrt{3}q_1}$. We found the spacing of those hexagonal rods to be 20.2 ± 1.0 nm. For PEO_{23}-b-$PMCL_{25}$, only one peak was observed. However, it is narrower than the peak at 90 wt%. Thus, the polymer-water mixture forms a transition-phase with some lamellar content.

At 70 wt% polymer, three polymer/water mixtures gave rise to SAXS patterns with more than two peaks, indicating well-ordered morphologies. The higher order Bragg peaks are shifted by factors 2;3; … relative to the main peak, providing proof of lamellar phases. PEO_{23}-b-$PMCL_{54}$ only reveals two peaks that are spaced by a factor of 3. The double shifted peak $2q_1$ has a low amplitude observed in this sample, presumably because the minimum of the form factor overlaps with the $2q_1$ peak of the lamellar peak and only a weak peak appears. From 60 wt% to 40 wt% polymer, the three polymers with larger PMCL blocks exhibited lamellar phases. In contrast, in the SAXS spectrum of PEO_{23}-b-$PMCL_{25}$ the second peak is shifted by a factor of $\sqrt{3}$. Moreover, the third peak has a higher intensity than the second, and the intensity of the second peak increased with increasing water concentration. For 40 wt% even two shoulder peaks near to the first and second peak are observed and for 40-60 wt% even weak peaks at position $3q_1$ can be observed. These facts indicate that a lamellar and a hexagonal

phase coexist in mixtures of this polymer in the intermediate concentration range. The occurrence of a hexagonal phase in addition to a lamellar phase was also reported in literature for poly(ethylene oxide)-*block*-poly(ethylethylene).[34] In contrast to the hexagonal phase that occurred for PEO_{23}-*b*-$PMCL_{54}$ at 80 wt% polymer, the water mass fraction is much higher; thus, we call the hexagonal phase formed by the smallest polymer an H_1 phase, i.e. an "oil in water" phase.[34]

The spacing *d* between layers in lamellar phases can be calculated by $d_L = \dfrac{2\pi}{q_1}$. Figure 4.1.5 summarizes the d-spacings, assuming, as a first approximation, that the first Bragg peak in the SAXS spectra of mixed, coexisiting phases arises solely from a lamellar phase.
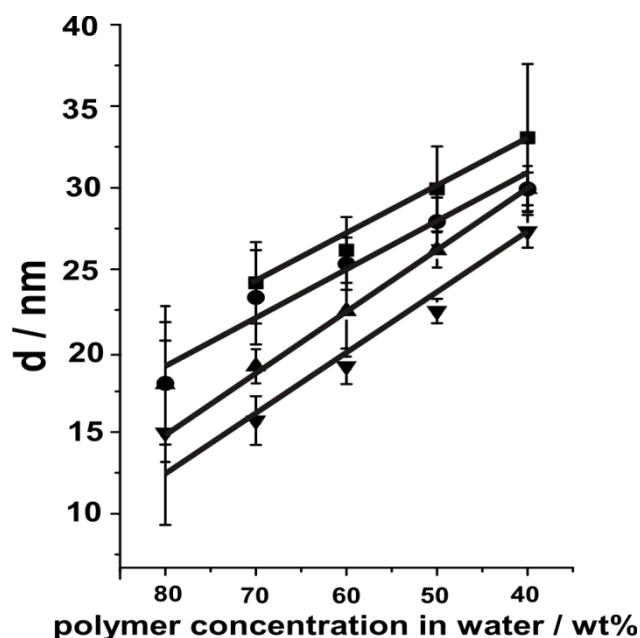
Figure 4.1.5. Lamellar d-spacing of PEO_{23}-*b*-$PMCL_{25}$ (▼), PEO_{23}-*b*-$PMCL_{32}$ (▲),PEO_{23}-*b*-$PMCL_{44}$ (●) and PEO_{23}-*b*-$PMCL_{54}$ (■). Continuous lines represent linear fitting of the data points.

For all polymer/water mixtures, the lamellar d-spacing increases with increasing water concentration. At low water content (70 wt% polymer) the d-spacing ranges from 15 ± 2 nm (PEO_{23}-*b*-$PMCL_{25}$) to 24 ± 3 nm (PEO_{23}-*b*-$PMCL_{54}$). The spacing increases linearly up to 28 ± 1 (PEO_{23}-*b*-$PMCL_{25}$) and 33 ± 5 nm (PEO_{23}-*b*-$PMCL_{54}$), respectively, at higher water content. This phenomenon is known as lamellar swelling – incorporation of water molecules into the interlamellar space – and is generally linear.[98] Not only can an increase in lamellar spacing be observed in Figure 4.1.5, but so can the influence of the hydrophobic part of the

36

block-copolymers on the inter-lamellar distance. At the same polymer concentration, a longer hydrophobic block results in greater d-spacing, for example at 60 wt% polymer the d-spacings are 19 ± 2 nm, 22 ± 3 nm, 25 ± 3 nm, and 26 ± 2 nm for PEO_{23}-b-$PMCL_{25}$ to PEO_{23}-b-$PMCL_{54}$. Lamellar d-spacing at distinct polymer concentrations was plotted interdependent with the number of PMCL units per block-copolymer (cf. Figure 4.1.6). In a first approximation, this data can be fitted by linear regression, resulting in similar slopes (0.28 ± 0.07 nm for 50 wt%, 0.27 ± 0.04 nm for 60 wt% and 0.3 ± 0.06 nm for 70 wt%, respectively) for all three polymers. Accordingly, since the length of the hydrophilic block is the same for all polymers – only the length of the hydrophobic block varies – we assume that the polymers are partially stretched. However, it should be noted that the data curves appear to converge towards constant values at high numbers of PMCL units, most likely due to partial-coil formations. Extrapolation of the curves in the figure 4.1.6 to zero MCL units reveals the PEO/water thickness at a given polymer concentration. Thus, the PEO/water (hydrophilic shell) thickness can be calculated be 15.8 ± 2.2 nm for 50 wt%, 12.5 ± 1.6 nm for 60 wt%, and 9 ± 2 nm for 70 wt%. Therefore the thickness of the lamellar layers depends on the length of the hydrophobic block.
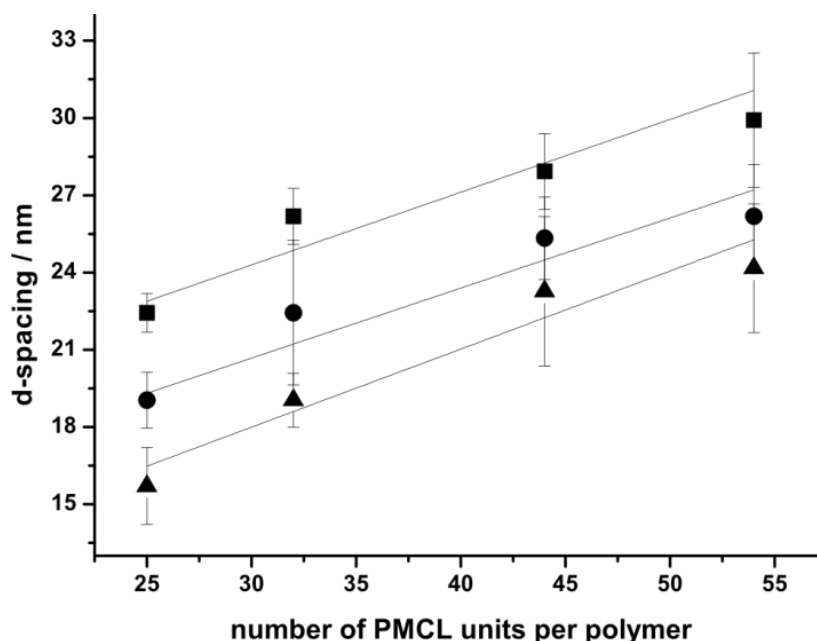
Figure 4.1.6. Lamellar d-spacing at distinct polymer concentrations (70 wt% (▲), 60 wt%(●) and 50 wt% (■)) interdependent with the number of PMCL units per block-copolymer.

A general observation is that the peak width in the lamellar regime becomes broader as the lengths of the hydrophobic blocks increase. Thus, the correlation length $\xi = \dfrac{2\pi}{\Delta q_1}$ in number of repeating lamellar layers can be calculated by the ratio of momentum transfer at the first peak (q_1) and the full width at half maximum (Δq_1), $\dfrac{q_1}{\Delta q_1}$. Figure 4.1.7 shows an example at 80 wt%. The smallest polymer has the most repeating layers, whereas the largest one has the fewest. Accordingly, the self-assembly of the smallest polymer is the most ordered.
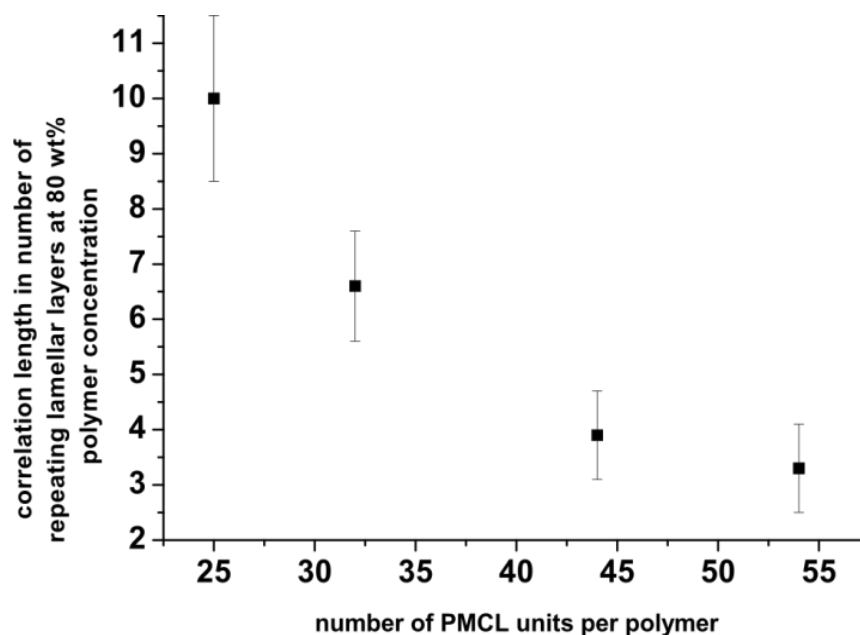
Figure 4.1.7. Number of repeating lamellae at 80 wt% of polymer plotted as a function of block-copolymer lengths.

At polymer concentrations of 30 wt% and lower, the well-defined, thin, repeating Bragg peaks vanish and broad form factors[22] appear. These form factors are typical of unilamellar and multilamellar aggregates.[98, 207] Furthermore, it is known that lamellae swell to a water concentration at which the repulsive interactions overcome the attractive interactions and the lamellar sheets start to unbind, resulting in peaks that broaden and shift their SAXS patterns[99], resulting in form factors. This indicates that more than one aggregate is present and that these phases are not well-ordered. Analyzing the distance between the minima of the form factors shows (except for PEO_{23}-b-$PMCL_{25}$) that, as the concentration of the polymer or the polymer length increase, the unilamellar and multilamellar aggregates become larger.

SAXS results at polymer concentrations $\leq$ 20 wt% were supported by TEM images in order to visualize the morphologies and to investigate the possible presence of two phases. At 20 wt% polymer, the three longer polymers (PEO$_{23}$-b-PMCL$_{54}$, PEO$_{23}$-b-PMCL$_{44}$, and PEO$_{23}$-b-PMCL$_{32}$) show lamellar layers (indicated by L in Figure 4.1.8) next to packed, deformed vesicles (indicated by P in Figure 4.1.8). The packed, deformed vesicles explain the appearance of form factors of multilamellar or unilamellar aggregates found with SAXS. For PEO$_{23}$-b-PMCL$_{25}$ a lamellar phase is also observed.
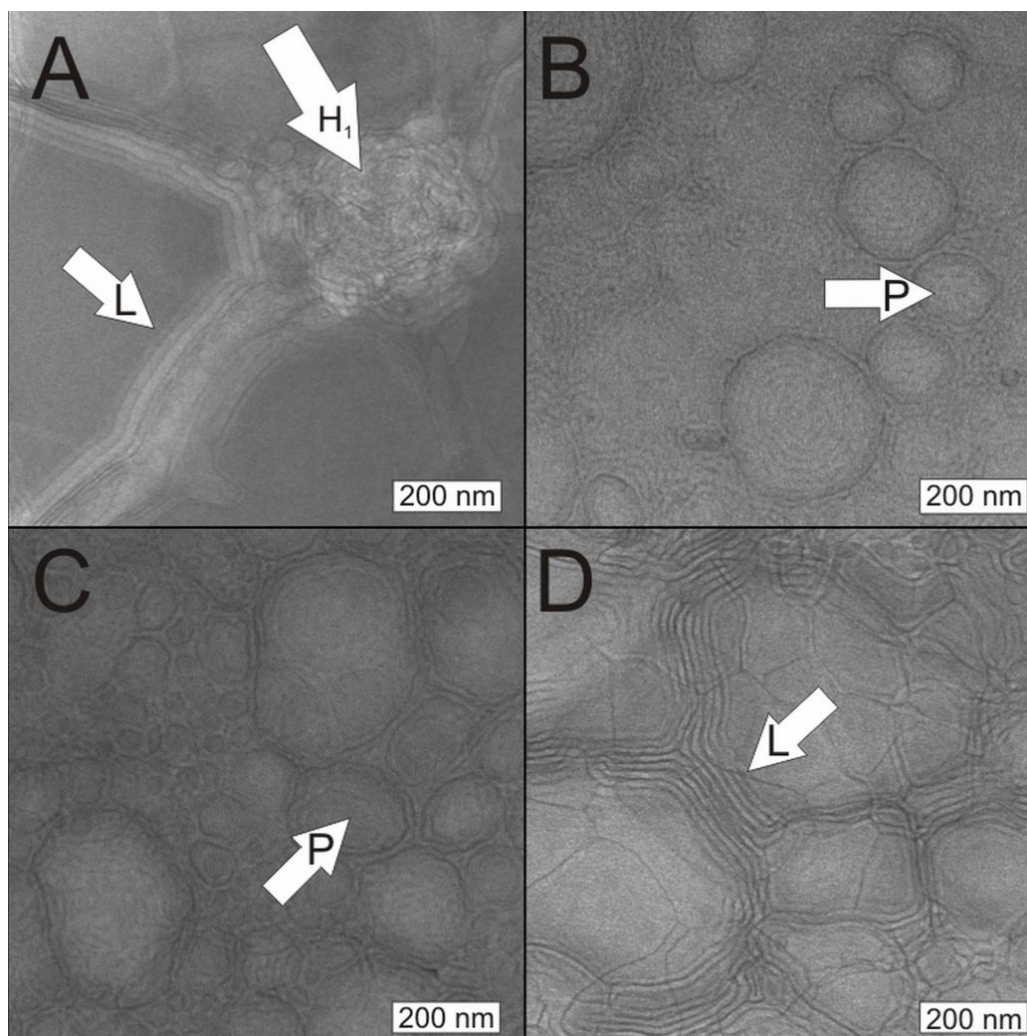
Figure 4.1.8. TEM images of 20 wt% solutions of a) PEO$_{23}$-b-PMCL$_{25}$, b) PEO$_{23}$-b-PMCL$_{32}$, c) PEO$_{23}$-b-PMCL$_{44}$ and d) PEO$_{23}$-b-PMCL$_{54}$. Arrows point to the different phases that exist at 20 wt%: hexagonal (H$_1$), lamellar (L) phase, and packed vesicles (P).

This phase presumably coexists next to another phase – based on the SAXS results at high PEO$_{23}$-b-PMCL$_{25}$ concentrations – a hexagonal H$_1$ phase (indicated by H$_1$ in Figure 4.1.8). At

10 wt% polymer concentration (Figure 4.1.9) some lamellae can be observed, but packed vesicles are dominant. In the case of PEO$_{23}$-b-PMCL$_{25}$ not only are packed vesicles present, but also packed rod-like micelles (Figure 4.1.9 A, indicated by an arrow). The dominant morphology in 5 wt% solutions of PEO$_{23}$-b-PMCL$_{54}$, PEO$_{23}$-b-PMCL$_{44}$ and PEO$_{23}$-b-PMCL$_{32}$ is packed vesicles (Figure 4.1.10). Packed vesicles have been previously observed for semi-dilute aqueous block copolymer solutions.[99] In the PEO$_{23}$-b-PMCL$_{25}$ solution, packed rod-like micelles and vesicles can again be observed.
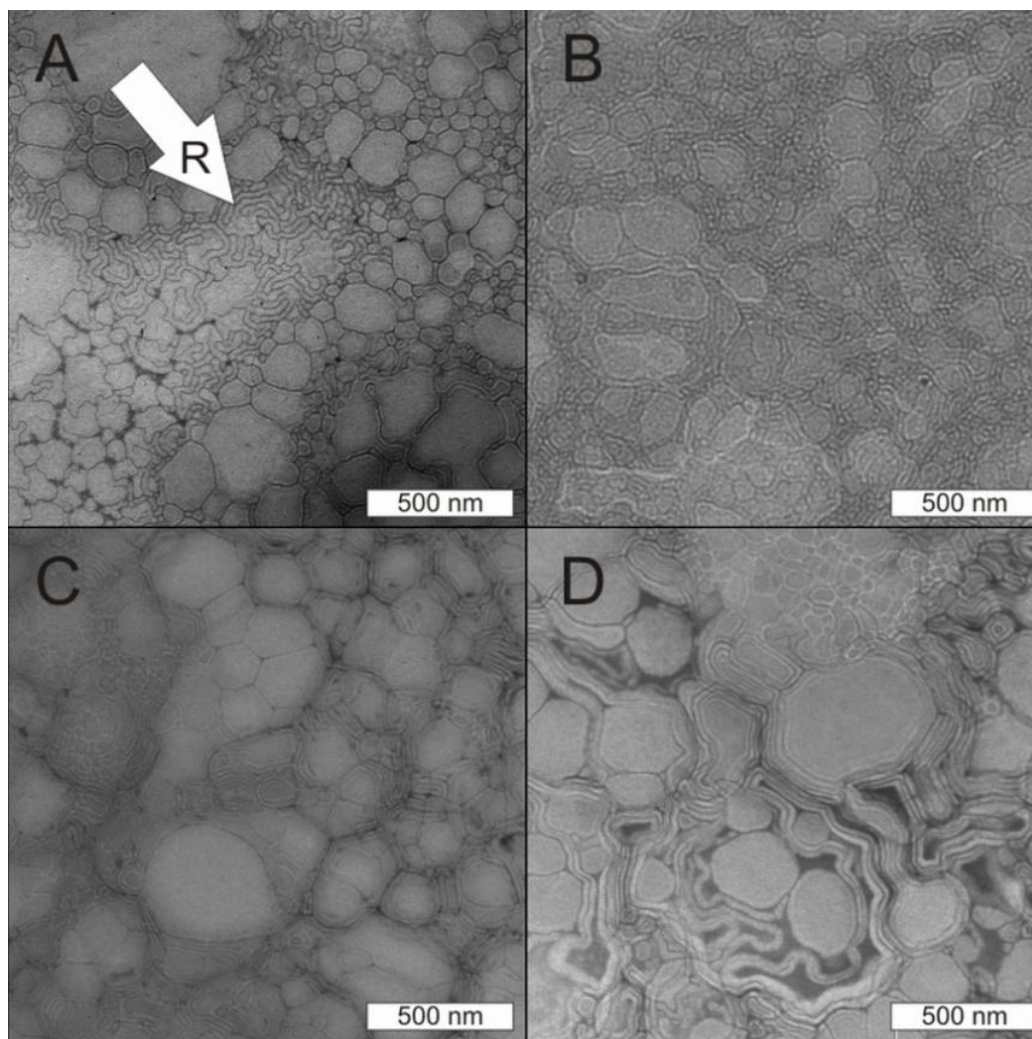
Figure 4.1.9. TEM images of 10 wt% solutions of a) PEO$_{23}$-b-PMCL$_{25}$, b) PEO$_{23}$-b-PMCL$_{32}$, c) PEO$_{23}$-b-PMCL$_{44}$ and d) PEO$_{23}$-b-PMCL$_{54}$. Arrows point to packed, rod-like micelles (R).
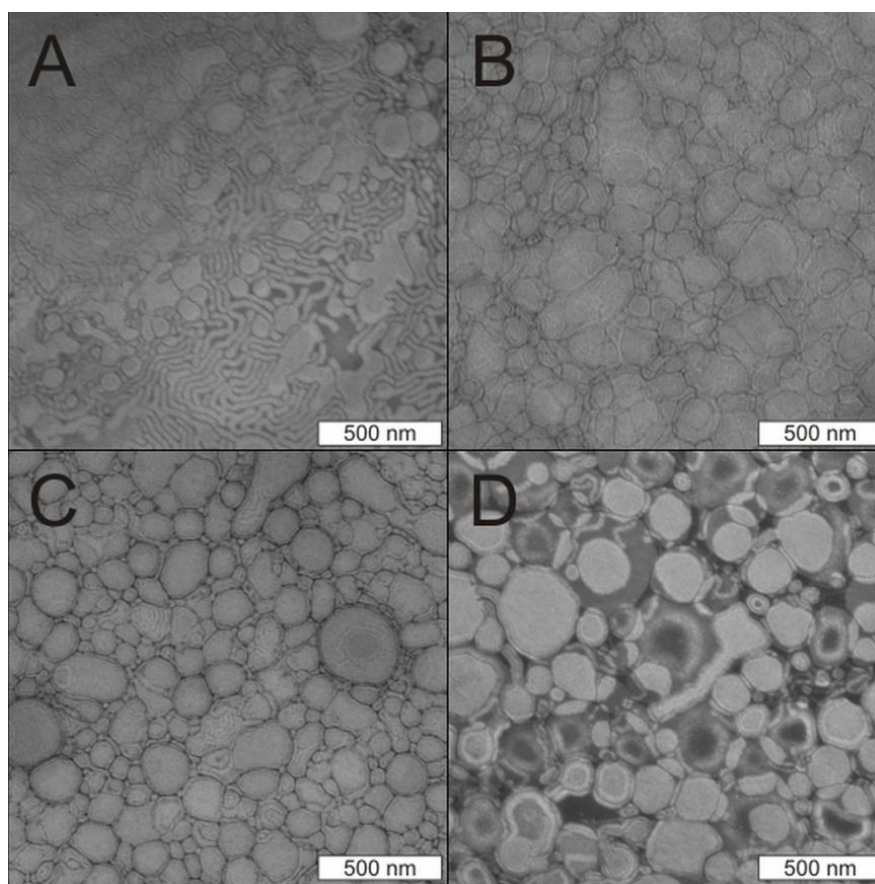
Figure 4.1.10. TEM images of 5 wt% solutions of a) PEO$_{23}$-*b*-PMCL$_{25}$, b) PEO$_{23}$-*b*-PMCL$_{32}$, c) PEO$_{23}$-*b*-PMCL$_{44}$ and d) PEO$_{23}$-*b*-PMCL$_{54}$.

4.1.3. Isotropic regime of poly(ethylene oxide)-block-poly(γ-methyl-ε-caprolactone) solutions

In the isotropic regime, i.e., below a concentration of 1 wt% polymer, we expect the block copolymers to assemble into nano-sized objects such as vesicles and micelles. TEM is a powerful technique to visualize those supramolecular structures. Figure 4.1.11 shows TEM images of the four polymers at concentrations of approx. 1 mg/mL (0.1 wt%). PEO$_{23}$-*b*-PMCL$_{25}$ self-assembles into vesicular structures with radii ranging from 70 to 100 nm, and into rod-like micelles. Agglomerations of rod-like micelles are observed, some of them are shown in Figure 4.1.11 A. PEO$_{23}$-*b*-PMCL$_{32}$ forms vesicles with radii (75- 110 nm)similar to the structures formed by PEO$_{23}$-*b*-PMCL$_{25}$ and some very short rod-like micellar structures and membrane fragments. PEO$_{23}$-*b*-PMCL$_{44}$ and PEO$_{23}$-*b*-PMCL$_{54}$ self-assemble into mostly vesicular structures of slightly larger size (80-120 and 80-200 nm, respectively). However, a few worm-like micelles with diameters of 16.0 ± 2.0 nm or membrane fragments are present. All vesicles are collapsed due to drying effects during sample preparation.

41
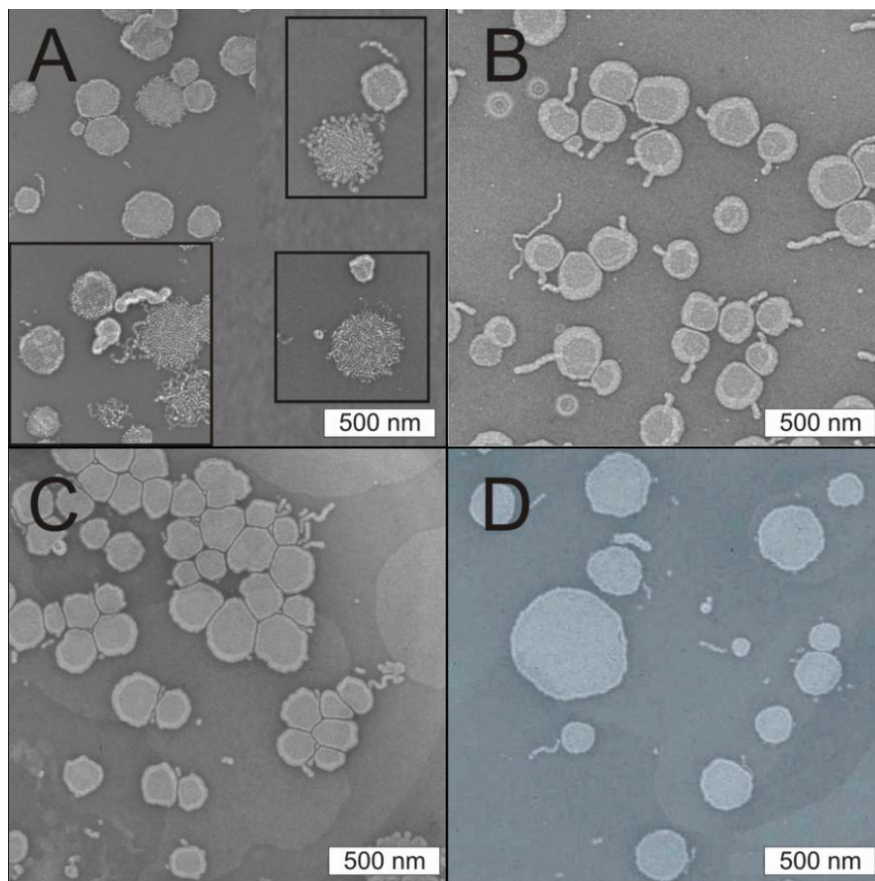
Figure 4.1.11. TEM images of 0.1 wt% block copolymer solutions of a) PEO_{23}-b-$PMCL_{25}$, b) PEO_{23}-b-$PMCL_{32,}$ c) PEO_{23}-b-$PMCL_{44}$, and d) PEO_{23}-$PMCL_{54}$. The insets show agglomerations of rod-like micelles.

Another technique to analyze supramolecular structures is light scattering. Figure 4.1.12 shows the Berry plots and apparent diffusion coefficient plots for all four polymers. The obtained radii of gyration R_G and hydrodynamic radii R_H are summarized in Table 4.1.2. Polymers that self-assemble predominantly into vesicular structures (PEO_{23}-b-$PMCL_{32-54}$) form, according to LS, larger vesicles with increasing PMCL block length (PEO_{23}-b-$PMCL_{32}$: $R_G = 106 \pm 2$ nm and $R_H = 100 \pm 2$ nm; PEO_{23}-b-$PMCL_{32}$: $R_G = 108 \pm 3$ nm and $R_H = 111 \pm 2$ nm; PEO_{23}-b-$PMCL_{32}$: $R_G = 137 \pm 2$nm and $R_H = 130 \pm 2$ nm;). Compared to the TEM images, which indicate the same trend, the radii obtained from light scattering are larger. This can be attributed to the drying process during TEM sample preparation and to the polydispersity of the systems.
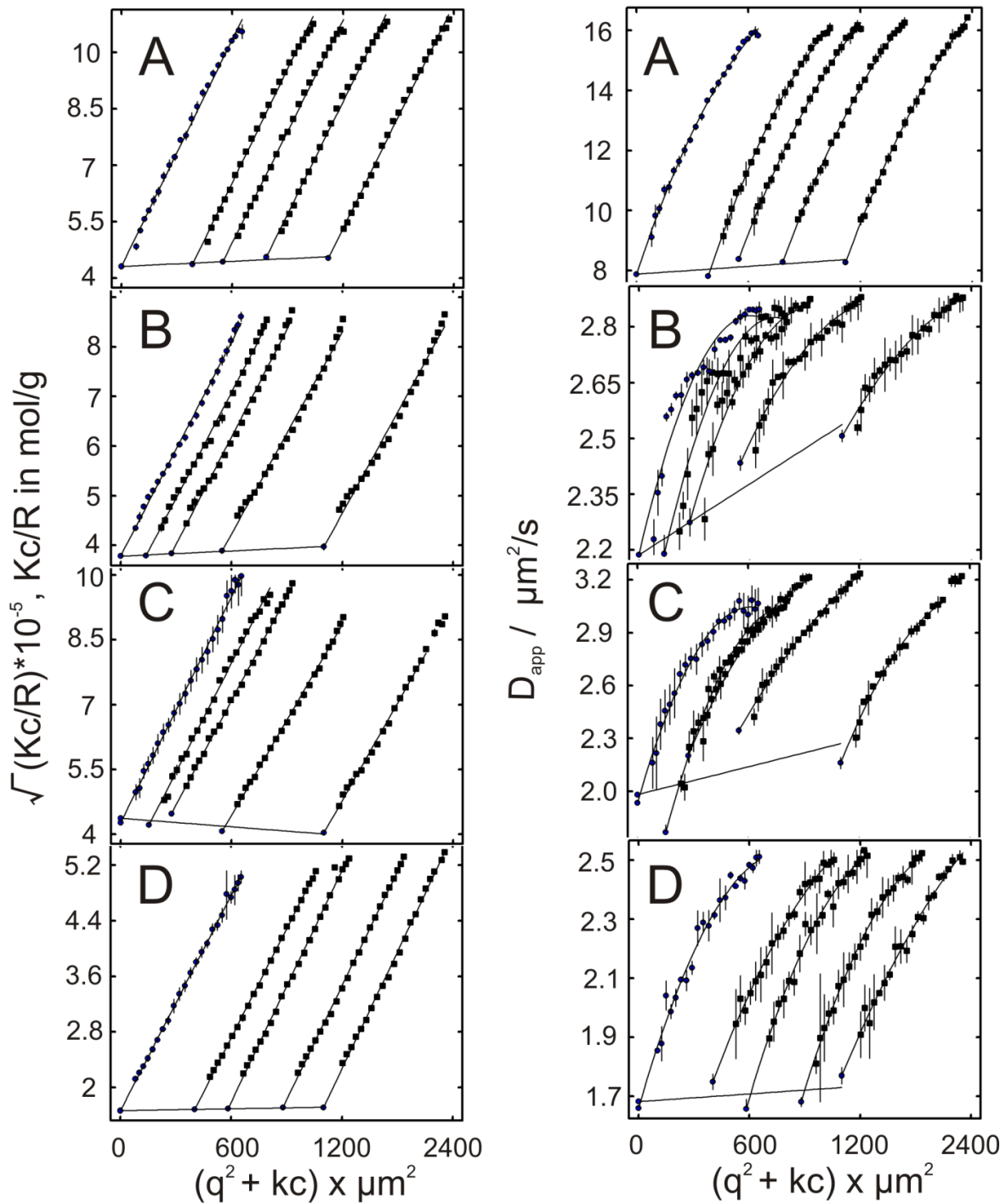
Figure 4.1.12. Light scattering data of block-copolymers a) PEO_{23}-b-$PMCL_{25}$, b) PEO_{23}-b-$PMCL_{32,}$ c) PEO_{23}-b-$PMCL_{44}$, and d) PEO_{23}-b-$PMCL_{54}$. Berry plots are shown on the left hand side. On the right side apparent diffusion coefficients are plotted versus the concentration of polymers. These plots were used to calculate R_G and R_H, respectively. Squares represent measured data, and circles are values obtained by extrapolation to zero concentration and zero angle.

RESULTS AND DISCUSSION

Table 4.1.2. Light scattering data of self-assembled PEO-*b*-PMCL.

Polymer	R_G[a] (nm)	R_H[b] (nm)	$\rho = R_G/R_H$ [c]	d*n*/dc[d] (ml/g)	Mw[e] (g/mol)	N[f]
PEO$_{23}$-*b*-PMCL$_{25}$	118 ± 2	30 ± 2	3.9 ± 0.1	0.106 ± 0.010	5.4×10^8	120 000
PEO$_{23}$-*b*-PMCL$_{32}$	106 ± 2	100 ± 2	1.06 ± 0.04	0.113 ± 0.001	7.0×10^8	137 000
PEO$_{23}$-*b*-PMCL$_{44}$	108 ± 3	111 ± 2	0.97 ± 0.03	0.124 ± 0.008	5.5×10^8	88 000
PEO$_{23}$-*b*-PMCL$_{54}$	137 ± 2	130 ± 2	1.05 ± 0.03	0.136 ± 0.007	9.9×10^8	125 000

[a] Radius of gyration obtained from SLS, [b] hydrodynamic radius obtained from DLS, [c] ratio between radius of gyration and hydrodynamic radius, [d] refractive index increment, [e] molecular mass of supramolecular structures from SLS, [f] number of polymers per supramolecular aggregate.

The presence of vesicles can be further confirmed by the LS data. For a perfect vesicle with an infinitely thin membrane, the form factor ρ, the ratio of R_G to R_H, should equal 1.[208] For the reported polymers, the light scattering form factors (Table 4.1.2) are close but not equal to 1. This can be explained by the fact that the polymers predominantly self-aggregate into vesicles, but also form some smaller structures such as rod-like micelles according to TEM (Figure 4.1.11). The presence of worm-like micelles is most probably due to the polydispersity of the block copolymers. Furthermore, the size of the vesicles is not uniform and shows an intrinsic polydispersity, even though the vesicle solutions were extruded prior to measurements. The average number N of polymer molecules in a supramolecular structure can be calculated from SLS. For PEO$_{23}$-*b*-PMCL$_{32-54}$ this value is around 100 000, which is in agreement with literature reports for vesicles. [208, 209] In contrast to the common behavior of the three polymers discussed above, the LS data for PEO$_{23}$-*b*-PMCL$_{25}$ are different. In this sample, the measured R_G agrees with the R_G of the supramolecular structures formed by the other polymers. However, R_H is almost four times smaller than the R_G of the other polymer solutions. This can be explained by the fact that PEO$_{23}$-*b*-PMCL$_{25}$ only partially self-

44

assembles into vesicles, while it also forms rod-like structures which have a $\rho \approx 2$, or more, depending on the axial ratio (Figure 8).[210] Moreover static light scattering is dominated by the higher intensity of large vesicular aggregates. Therefore the presence of rod-like aggregates does not influence the average number of polymer molecules per supramolecular structure and a similar value of N is obtained for all four polymers.

4.1.4. Conclusions and summary on the phase behavior of vesicle forming poly(ethylene oxide)-block-poly(γ-methyl-ε-caprolactone)

Figure 4.1.13 combines the findings for all four PEO-b-PMCL block-copolymers in a single phase diagram. PEO$_{23}$-b-PMCL$_{32}$, PEO$_{23}$-b-PMCL$_{44}$ and PEO$_{23}$-b-PMCL$_{54}$ self-assemble at low concentrations in aqueous solution into vesicles. PEO$_{23}$-b-PMCL$_{54}$ forms the largest vesicles. As the length of the hydrophobic block decreases, the vesicles get smaller. With increasing polymer concentration the vesicles start to pack. The packed vesicles are coexisting with lamellar structures from approximately 10 wt% polymer. This lamellar phase becomes more dominant as the polymer concentration increases. At a polymer concentration of approximately 80 wt% a transition phase occurs that leads to a disordered morphology, which is characteristic of pure polymers. PEO$_{23}$-b-PMCL$_{54}$ shows a hexagonal H$_2$ phase prior to the transition phase. The phase behavior of the shortest polymer PEO$_{23}$-b-PMCL$_{25}$ is similar to that of the larger polymers, but with some small differences: Packed rod-like micelles and a hexagonal H$_1$ phase were found.

In conclusion, the phase diagram describes the formation of vesicles when the bulk polymer is dissolved in water. The polymers undergo several phase transitions starting from disorded phase to lamellae and to packed vesicles. These findings can be used to optimize vesicle formation on the lab scale and in technical applications. We have shown that the hydrophobic PMCL block length determines the phase morphology at a given polymer concentration (Figure 4.1.6). Moreover, this block length influences the size of the vesicles and the spacing of the lamellar layers. Polymers with a higher hydrophobic-to-hydrophilic ratio form larger vesicles. Due to the biocompatibility and degradability of the polymer, vesicles formed by PEO-b-PMCL are promising candidates as nanocarriers and nanoreactors for biomedical applications.
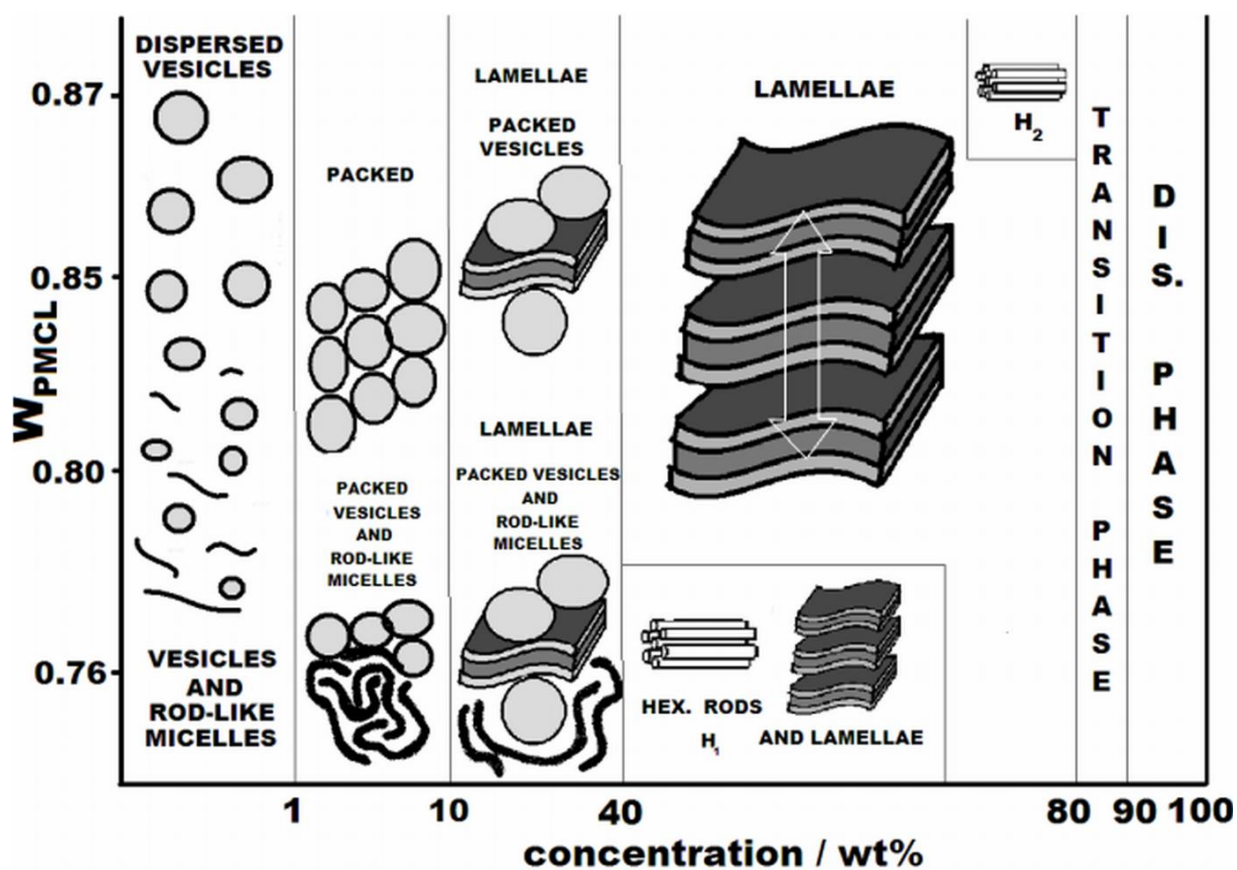
Figure 4.1.13. Schematic phase diagram of binary PEO-*b*-PMCL water mixtures.

4.2. Phase behavior of supramolecular structure forming poly(isobutylene)-block-poly(ethylene oxide)[219]

4.2.1. Synthesis of poly(isobutylene)-block-poly(ethylene oxide)

In order to understand self-assembly of block copolymers in detail it is important to control and predict their synthesis. The reactions, living cationic and anionic polymerization, are known to yield well-defined homopolymers and block-copolymers.[64 10, 140, 146]

Preparation of the macroinitiator: The homopolymer PIB-OH was synthesized by quasi-living cationic polymerization as follows: The polymerization of isobutylene was initiated with 2-chloro-2,4,4-trimethylpentane in conjunction with $TiCl_4$ in the presence of a nucleophile[184], and the polymerization was quenched with allyltrimethylsilane[185, 186], leading to allyl-terminated PIB. Hydroboration of the terminal double bonds with 9-borabicyclo[3.3.1]nonane (0.5 M in THF) and subsequent oxidative cleavage of the carbon-boron bonds with alkaline H_2O_2 resulted in a viscous PIB-OH.[187, 188] The yield was $\geq$ 90 %. ^{1}H-NMR (CDCl3): δ 3.6 (q, 1H, **H**O- CH2-CH2-), 1-72- 0.79 (m, 8H, isobutyl **H**s)..

Preparation of the diblocks: The block-copolymer PIB-*b*-PEO (5) was synthesized according to a procedure described elsewhere[189]. Briefly, to a - 5 wt% solution of PIB-OH (1) in THF was added 1.0 equivalent of the t-BuP$_4$ (1 M solution in hexane) (2) via a syringe and stirred at room temperature for 1 hour. Then, ethylene oxide (4) was added via a syringe into the reactor. The reaction mixture was stirred at that temperature for a few minutes, then slowly heated to 40 °C and stirred for 6 days under a dry argon atmosphere. After quenching the polymerization with acetic acid, the reaction solution was washed with the strongly acidic cation exchanger DOWEX Marathon to remove traces of protonated t-BuP4, filtered and concentrated *in vacuo*. The yield was $\geq$ 70 %. ^{1}H-NMR (CDCl3): δ 3.6 (m, 4 H, ethylene oxide **H**s), 1.63- 0.95 (m, 8 Hs, isobutyl **H**s).
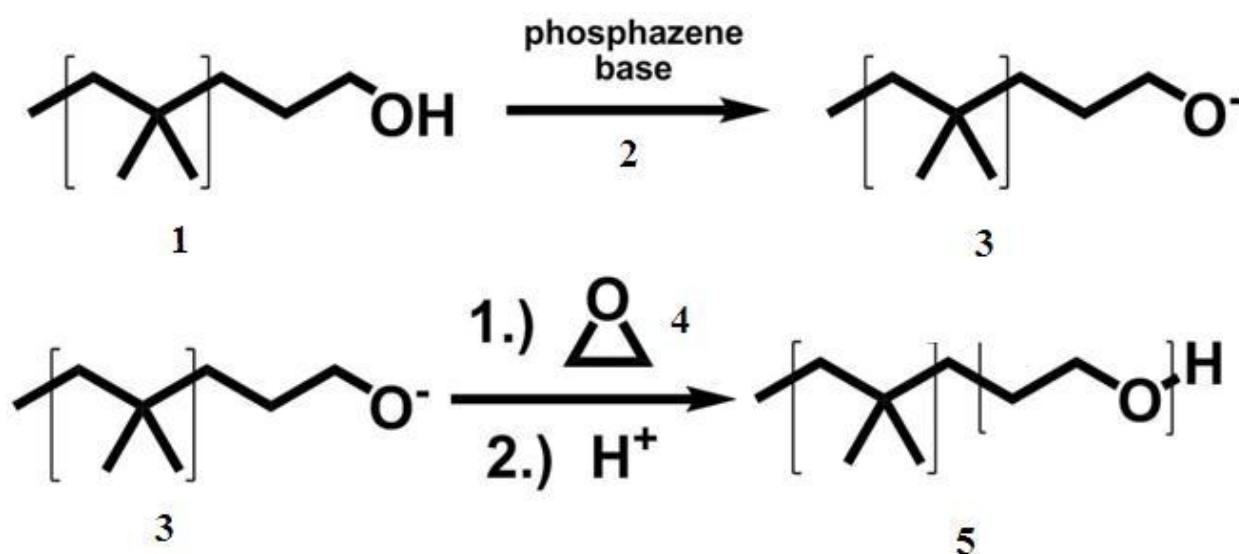
Figure 4.2.1. Anionic ring-opening polymerization of EO (3) using a hydroxyl functionalized PIB-OH macroinitiator (4) resulting in PIB-*b*-PEO (5).

Table 4.2.1 shows the molecular characteristics of the synthesized polymers. Figure 4.2.2 shows GPC elution curves of the polymers. And a ^{1}H-NMR example is also shown in Figure 4.2.2 on the right. (Figure 4.2.2 B).
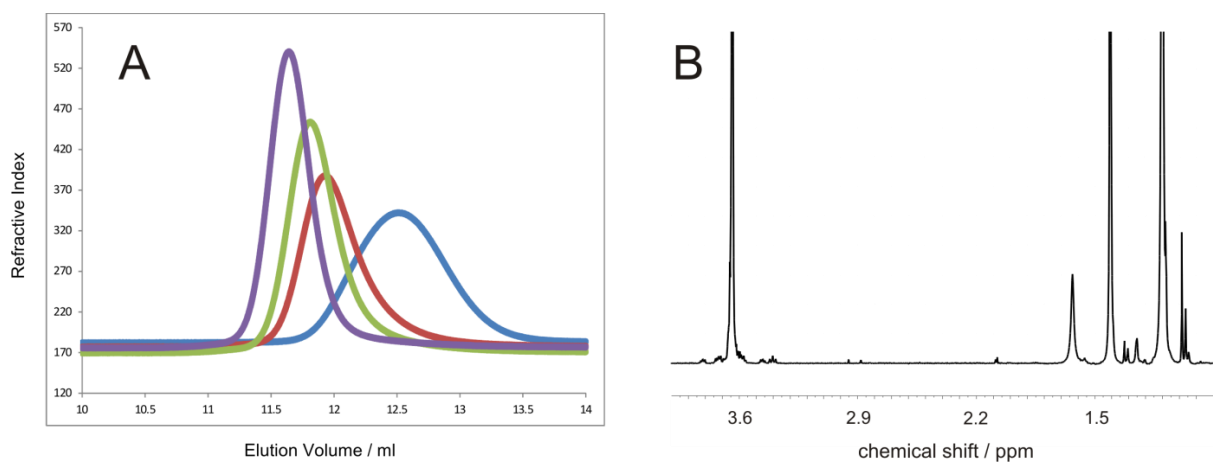
Figure 4.2.2. a) GPC elution chromatography of PIB-OH (blue), PIB$_{79}$-*b*-PEO$_{53}$ (red), PIB$_{79}$-*b*-PEO$_{68}$ (green) and PIB$_{79}$-*b*-PEO$_{106}$ (blue). b) ^{1}H-NMR spectrum of PIB$_{79}$-*b*-PEO$_{68}$ as an example .

According to ^{1}H-NMR measurements (Table XXX), the desired PMCL block lengths were obtained quite accurately. However, GPC measurements standardized with PS show slight deviations of the molecular masses. Since the molecular composition of PS differs from that

of the block-copolymers studied here, the hydrodynamic radii of the polymers in THF are also different. This explains the deviation of the molecular masses measured by GPC compared to those obtained by NMR. As expected for an anionic polymerization, the polydispersity of all polymers was measured at below 1.15.

Table 4.2.1. Molecular characteristics of synthesized block copolymers.

Polymer	$N_{PEO}(NMR)$[a]	$M_n(NMR)$ (g/mol)[b]	(M_w/M_n)[c]	W_{PIB}[d]
PIB$_{79}$-OH	-	4450	1.1	1
PIB$_{79}$-*b*-PEO$_{53}$	53	6780	1.12	0.66
PIB$_{79}$-*b*-PEO$_{68}$	68	7440	1.13	0.6
PIB$_{79}$-*b*-PEO$_{106}$	106	8910	1.14	0.5

[a] Number of monomer repeat units in PEO block as determined by ^{1}H NMR spectroscopy. [b] Number-average molecular weight of block-copolymers as determined by ^{1}H NMR spectroscopy. [c] Polydispersity index determined from GPC with polystyrene as a standard. [d] Weight fraction of the PIB block as determined by ^{1}H NMR spectroscopy.

4.2.2. .Self-assembly characterization of poly(isobutylene)-block-poly(ethylene oxide)

SAXS measurements were used to study the morphologies of the complete dilution series of PIB-*b*-PEO. In the following chapters the structure changes of the self-assembled polymers will be shown starting with the shortest polymer. In the low concentration regime, SAXS was combined with TEM and SLS/DLS experiments.

4.2.2.1 Phase diagram of self-assembled PIB$_{79}$-*b*-PEO$_{53}$

Figure 4.2.3 shows the 1-D SAXS patterns of self-assembled PIB$_{79}$-*b*-PEO$_{53}$ block-copolymer in water starting from the pure polymer down to a 5 wt% polymer concentration in water. For the pure polymer (100 wt%) the first peak has a momentum transfer of 0.22 ± 0.04 nm^{-1} and the second and third peaks are $\sqrt{3}q_1$ and $\sqrt{7}q_1$ shifted to 0.37 ± 0.05 and 0.68 ± 0.07 nm^{-1}, respectively. This is indicative for an hexagonal phase. Here, due to the absece of water it has

to be an inverse hexagonal phase (H_2). In contrast, when the polymer is mixed with small amounts of water (90 wt% PIB_{79}-b-PEO_{53}) different scattering peaks are observed. The first scattering peak q_1 is shifted towards a higher momentum transfer compared to the pure polymer and has a momentum transfer of 0.39 ± 0.02 nm^{-1}. The second and third peaks are $2q_1$ and $2.74q_1$ times shifted to 0.78 ± 0.03 and 1.07 ± 0.08 nm^{-1}, respectively. The first shift is indicative of a lamellar phase but the shift of the third peak suggests the coexistence of another phase. Since the pure polymer shows the patterns of an inverse hexagonal phase suggests that this is due to the coexistence of a lamellar and a hexagonal phase. Increasing the water concentration further (75 wt%) peaks indicative for a lamellar phase can be observed, too. Here, the first peak is appearing at 0.34 ± 0.01 nm^{-1} and such as at 90 wt% the second and third peaks are $2q_1$ and $3q_1$ times shifted to 0.68 ± 0.03 and 1.02 ± 0.04 nm^{-1}, respectively. Since a similar scattering pattern down to 30 wt% of PIB_{79}-b-PEO_{53} can be observed, this concentration range is appointed to lamellar phases, too.
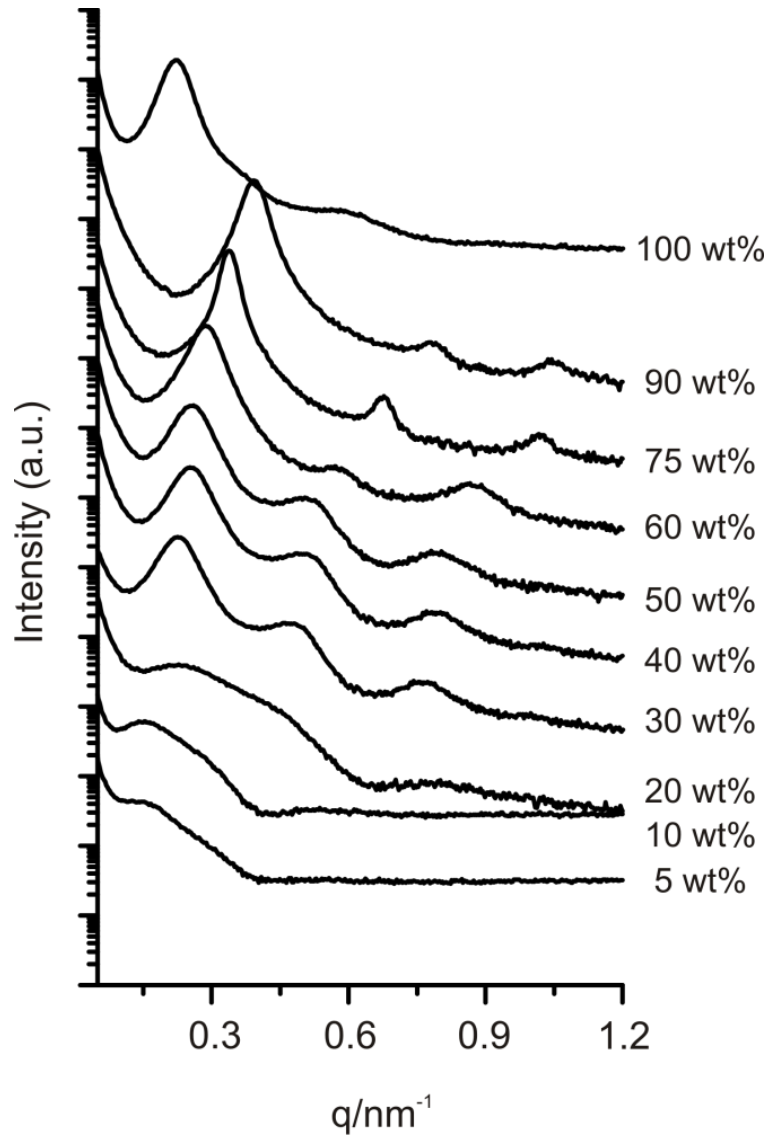
Figure 4.2.3. One-dimensional SAXS patterns of PIB_{79}-b-PEO_{53} starting from the pure polymer (100 wt%) down to a 5 wt% self-assembled polymers concentration in water.

From the positions of the first Bragg peaks q_1 in SAXS spectra the spacing d between layers in lamellar sheets can be calculated according to $d = \frac{2\pi}{q_1}$. At low water content (90 wt% polymer) the d-spacing is 16 ± 1 nm and increases linearly up to 27 ± 2 nm at higher water content (Figure 4.2.4). This phenomenon is known as lamellar swelling.[98] The lamella swell with 0.19 ± 0.01 nm/wt%. Extrapolating the linear fit ($d= 0.19$ wt% $+ 33$, where wt% is the polymer concentration) to the pure polymer a d-spacing of 14 ± 1 nm can be found. Therefore the polymers forming the lamellar layers are partially stretched. They are too long to be in a coiled conformation and too short for a fully stretched conformation.
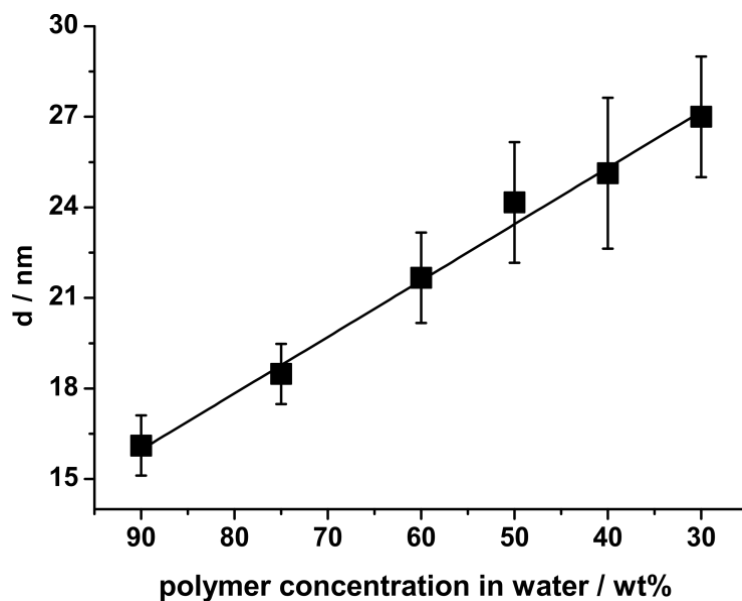
Figure 4.2.4. lamellar d-spacing *d* of self-assembled PIB$_{79}$-*b*-PEO$_{53}$. Solid line represents a linear fit (R^2= 0.99).

The number of repeating lamellar layers can be calculated knowing the correlation length $\xi = \dfrac{2\pi}{\Delta q_1}$, the ratio of the momentum transfer at the first peak (q$_1$) to the full width at half maximum (Δq$_1$) , $\dfrac{q_1}{\Delta q_1}$. At high polymer concentrations the highest number of repeating lamellar layers can be found (figure 4.2.5). But increasing the water concentration leads to a decrease of these repetitions.
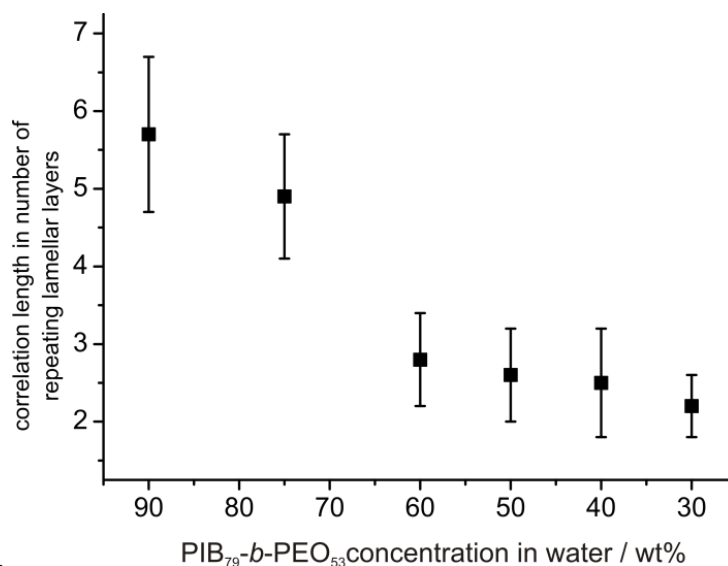
Figure 4.2.5. Number of repeating lamellae interdepending on the PIB$_{79}$-*b*-PEO$_{53}$ concentration.

Starting at 20 wt% polymer concentration the Bragg peaks vanish. But having a closer look still peaks with the same shifts as for higher concentrations are observed, indicating that there is still a lamellar phase present. Since form factors are dominating the pattern this phase is not that ordered compared to higher polymer concentrations. In addition, these form factors are typical of unilamellar and multilamellar aggregates.[99, 207] Furthermore, it is known that lamellae swell to a water concentration at which the repulsive interactions overcome the attractive interactions and the lamellar sheets start to unbind, resulting in peaks that broaden and shift their SAXS patterns[99] and result in form factors. This indicates that more than one aggregate is present and that these phases are not well-ordered.

Below a concentration of 10 wt%, TEM can be used. It was observed that at higher concentrations the electron beam could not pass through the sample, i. e. no picture could be seen. Here, at 10 wt% polymer concentration, PIB_{79}-b-PEO_{53} self-assembles still into a lamellar phase (cf. Figure 4.2.6 A indicated with a L) and into packed vesicles, too (cf. Figure 4.2.6 B). The packed deformed vesicles explain the appearance of form factors of multilamellar or unilamellar aggregates in SAXS.
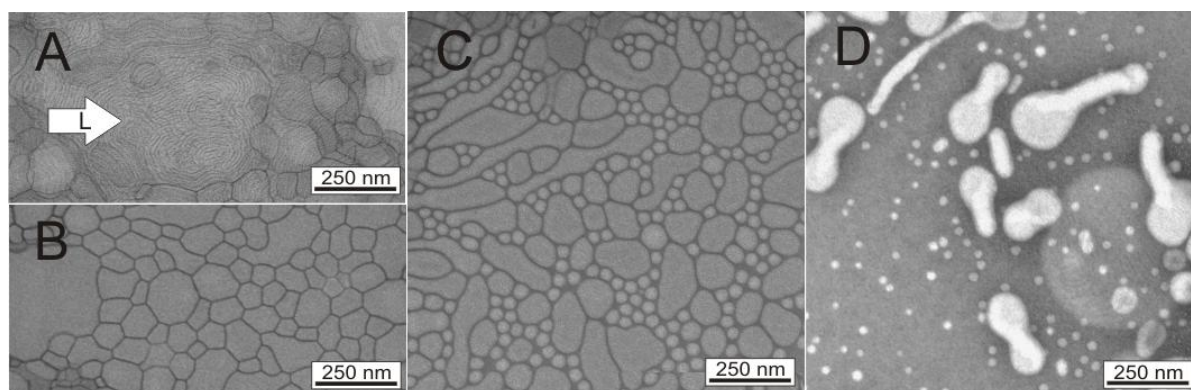
Figure 4.2.6. TEM picture $\leq$ 10 wt% PIB_{79}-b-PEO_{53}. a) and b) 10 wt% PIB_{79}-b-PEO_{53}, c) 5 wt% PIB_{79}-b-PEO_{53}, and d) 1 wt% PIB_{79}-b-PEO_{53}. Arrow points to lamellar phase (L).

For 5 % the packing of vesicles self-aggregated out of PIB_{79}-b-PEO_{53} is still observed (cf. Figure 4.2.6 C). At this concentration the polymer does not purely self-assemble into vesicles. There are some smaller aggregates – micelles - squeezed in between packed vesicles. The vesicles on the other hand do not have entirely the nice round shape, they are elongated and curved.

In the isotropic regime, i.e., below a concentration of 1 wt% polymer, we expect the block copolymer to assemble into nanozized objects like vesicles and micelles. Figure 4.2.6 D shows a TEM image of PIB_{79}-b-PEO_{53} with 1 wt% concentration. It shows three different

morphologies. On the one hand some micelles are present, which explains the micelles found at 5 wt% of polymer concentration and on the other hand a few worm/rod-like micelles with diameter of 37±7 nm can be observed. But the main fraction is composed of vesicular structures. They are not purely round objects but this phenomenon is also known from literature[211] and can be due to drying effects of the sample during sample preparation. Vesicles are - due to their fluid membrane - flexible. Another technique to analyze supramolecular structures is light scattering. For PIB_{79}-b-PEO_{53} no angle dependency of the Berry plot is observed and the data can be extrapolated to zero concentration and zero angle with a linear fitting of both momentum transfer q and concentration c. Out of the data obtained from figure 4.2.7 the calculated radii are R_G= 133 ± 2 nm and R_H= 139 ± 3 nm. For a perfect vesicle with an infinitely thin membrane, the form factor ρ from light scattering, the ratio of R_G to R_H, should equal 1.[208] Here, the ρ is 0.96 ± 0.03, which is another indication for the existence of vesicles. The deviation from 1 can be explained by the fact that besides predominance of vesicles, also some smaller structures such as worm/rod-like micelles and spherical micelles are present. Furthermore, the size of the vesicles is not uniform and shows an intrinsic polydispersity, even though the vesicle solutions were extruded prior to measurements. The average number N of polymer molecules in a supramolecular structure can be calculated (Table XXX). N is calculated to be 95 000. This number is in agreement with literature[208, 209] values obtained for vesicular structures.
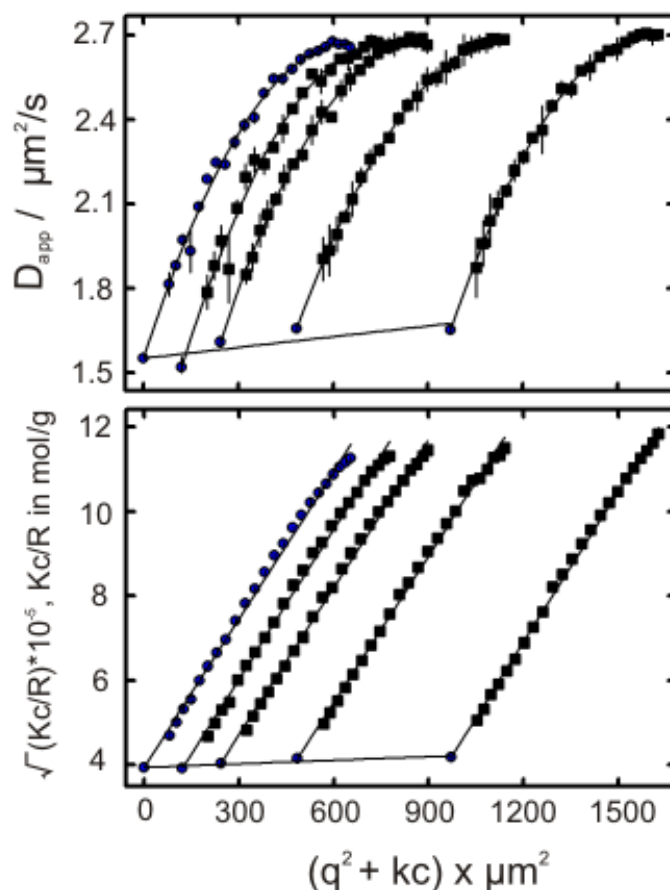
Figure 4.2.7. Light scattering data of self-assembled PIB$_{79}$-b-PEO$_{53}$ block-copolymer. The apparent diffusion coefficients are plotted versus the concentration of polymers and the Berry plot is shown. These plots were used to calculate R$_H$ and R$_G$, respectively. Squares represent measured data, and circles are values obtained by extrapolation to zero concentration and zero angle.

4.2.2.2 Phase diagram of self-assembled PIB$_{79}$-b-PEO$_{68}$

Increasing the hydrophilic block length results in a different SAXS pattern, and accordingly, into a different behavior of the self-assembly. Figure 4.2.8 shows the 1-D SAXS patterns of self-assembled PIB$_{79}$-b-PEO$_{68}$ block-copolymer in water starting from the pure polymer down to a 5 wt% polymer concentration in water. For the pure polymer (100 wt%) the peaks can be appointed to a lamellar phase. The first peak has a momentum transfer of 0.19 ± 0.05 nm^{-1} and the second peak is 2q$_1$ shifted to 0.38 ± 0.04 nm^{-1}. But the pattern is not as pronounced as the one described in the following. In contrast, when the polymer is mixed with small amounts of water (90 wt % PIB$_{79}$-b-PEO$_{68}$) a different scattering pattern is observed. Here, two superimposed scattering patterns can be observed. The scattering pattern leading to narrow and small peaks is indicative for a lamellar phase. The first peak q$_1$ of this pattern has a momentum transfer of 0.35 ± 0.02 nm^{-1} and the second and third peaks are 2q$_1$ and 3q$_1$ times

55

shifted to 0.71 ± 0.03 and 1.05 ± 0.05 nm^{-1}, respectively. In contrast, the very first peak of the whole scattering pattern is presumably a peak arising from a phase in coexistence with the lamellar phase or due to the shift of the pattern compared to the pure polymer. Increasing the water concentration further (75 wt%) only a lamellar phase can be observed. Here, the first peak appears at 0.31 ± 0.01 nm^{-1} with a $3q_1$ folds shift for the third peak (0.92 ± 0.04 nm^{-1}). The second peak is very weak but can be identified by zooming into the patterns and is assigned to 0.6 ± 0.03 nm^{-1}. The form factor, having presumably a minimum at this momentum transfer, is overlapping with the second peak and is thus vanishing. The second peak at 60 wt% is smaller than the third peak. This supports the hypothesis the minimum of the form factor and the lamellar peak overlap. At 60 and 50 wt% the scattering patterns are still indicative of a lamellar phase. For 60 wt% the first peak has a momentum transfer of 0.27 ± 0.02 nm^{-1} and the second and third peaks have a shift of $2q_1$ and $3q_1$ 0.55 ± 0.03 nm^{-1} and 0.82 ± 0.05 nm^{-1}, respectively. For 50 wt% even four peaks are observed ($q_1 = 0.26 \pm 0.03$ nm^{-1}, $q_2 = 0.52 \pm 0.04$ nm^{-1}, $q_3 = 0.78 \pm 0.03$ nm^{-1} and $q_4 = 1.04 \pm 0.05$ nm^{-1}). The peak width of the first peaks in the lamellar regime does not significantly become smaller as the water concentration increases. Accordingly the number of repeating lamellar layers is similar (approximately five repeating lamellar layers per concentration).
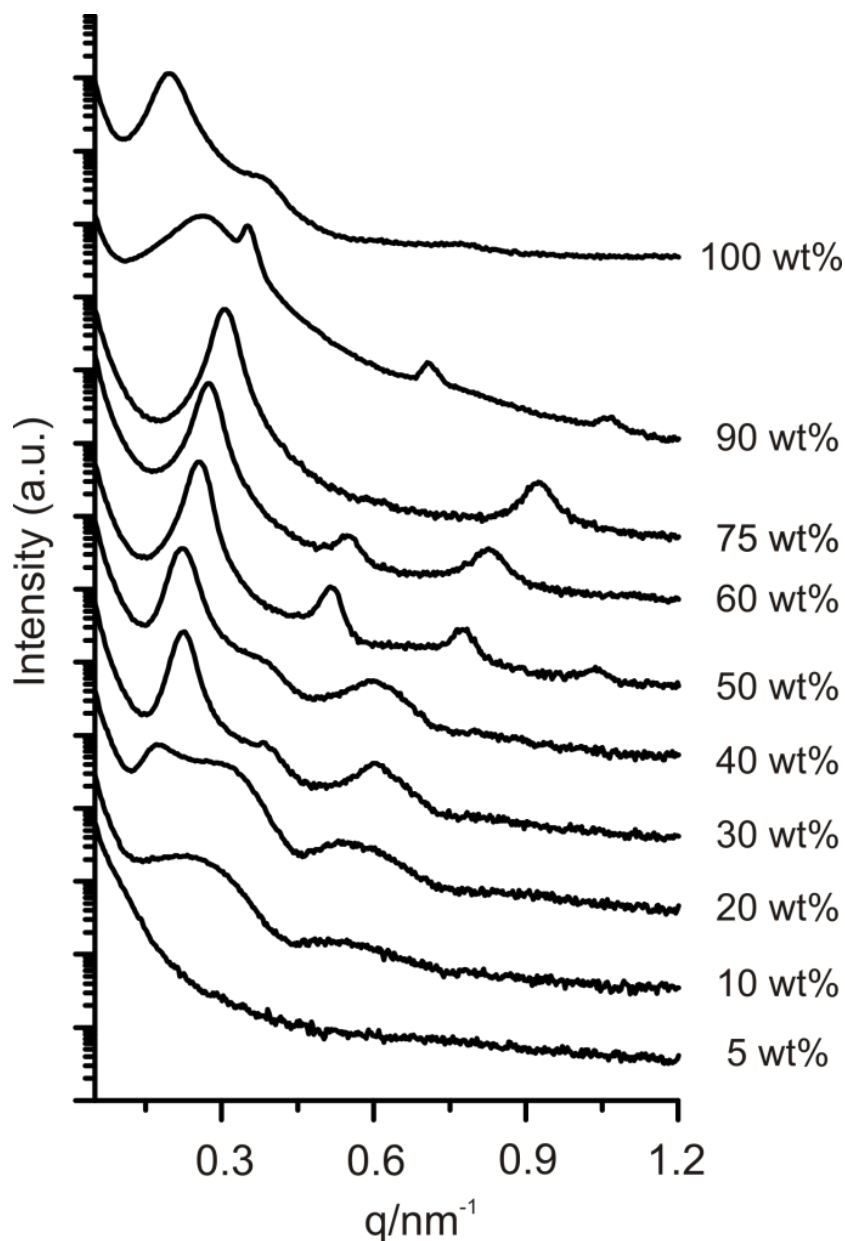
Figure 4.2.8. One-dimensional SAXS patterns of PIB_{79}-b-PEO_{68} starting from up the pure polymers (100 wt%) down to a 5 wt% of self-assembled polymers in water.

From the positions of those first Bragg peaks q_1 in SAXS spectra the spacing d between layers of the lamellar phases can be calculated such as shown for PIB_{79}-b-PEO_{53}. At low water content (90 wt% polymer) the d-spacing is 18 ± 1 nm and increases linearly up to 26 ± 3 nm at higher water content (Figure 4.2.9) due to lamellar swelling. Extrapolating the linear fit ($d = 0.17$ wt% $+ 33$) to the pure polymer a lamellar d-spacing of 16 ± 2 nm can be calculated. This is approximately 2 nm more than for the smaller vesicle forming polymer and is due to the larger size of the polymer. Again this finding agrees with the assumption that the polymers are in a partially stretched conformation.
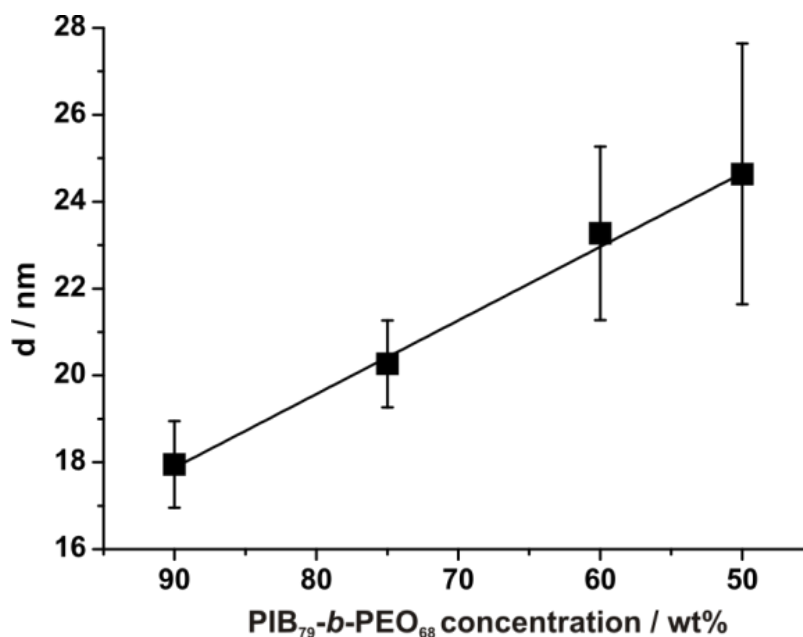
Figure 4.2.9. lamellar d-spacing d of self-assembled PIB_{79}-*b*-PEO_{68}. Solid line represents a linear fit (R^2= 0.99).

When the water concentration is even more increased (40 and 30 wt%) the first Bragg peaks at 0.23 ± 0.02 and 0.22 ± 0.01 nm^{-1} are still behaving linearly but, in contrast, the second peaks are shifted by a factor of $\sqrt{3}q_1$ (0.38 ± 0.03 and 0.37 ± 0.03 nm^{-1}, respectively). This is typical of a hexagonal phase. Here, the phase has to be a hexagonal (H_1) phase, a so-called "oil in water" phase[34] with cylinders of PIB in the PEO matrix since there is a lower polymer concentration compared to the water concentration. The third peak on the other hand is not shifted by a factor of $2q_1$ - typical for a hexagonal phase - but shifted by a factor of $\sqrt{7}q$. This shift is typically the fourth shift of a hexagonal phase. At 20 wt% two superimposing peaks and a form factor are observed. This is indicative for the coexistence of more than one phase in a less ordered system. The first peak has a momentum transfer of 0.17 ± 0.04 nm^{-1} and the second is $\sqrt{3}q_1$ (0.3 ± 0.03 nm^{-1}) shifted which is indicative for a hexagonal phase. The not well-ordered system can be directly seen when the patterns at 10 wt% and 5 wt% are examined. At 10 wt% only pure form factors from packed worm/rod-like micelles are identified. In contrast, 5 wt% shows only the small-angle x-ray scattering signal indicative for a disordered system. In contrast to the lamellar layers, the diameter of hexagonal rods in the hexagonal phase has to be calculated from the position of the first Bragg peak (q_1) in SAXS spectra according to $d_{H_1} = \dfrac{4\pi}{\sqrt{3}q_1}$. For 40 wt% a diameter of 31.5 ± 2.5 nm and for 30 wt% a diameter of 33 ± 1.5 nm is observed. These diameters are in good agreement with the

58

diameter of worm-like micelles found in the isotropic regime especially when they are packed on the TEM grid (35 ± 8 nm). The peak width does not significantly become smaller as the water concentration increases. Accordingly the number of repeating hexagonal rods is similar (approximately four repeating hexagonal rods per concentration).

At 10 wt% and lower the SAXS results were supported by TEM measurements (figure 4.2.10). At 10 wt% polymer a not clear phase was found. But at 5 wt% packing of worm/rod-like micelles and micelles was observed. In addition some round objects with radii of 60 ± 15 nm are observed. Their sizes are too large for micelles and they are presumably vesicles. Since vesicles in general self-associate out of a lamellar phase, the TEM micrograph at 10 wt% could be interpreted as a partial lamellar phase but it would not be in agreement with the SAXS results. Decreasing the polymer concentration even further the polymer forms purely worm/rod-like micelles with a diameter of 35 ± 8 nm and lengths between 200 nm up to more than 1 µm. The diameter of those worm/rod-like micelles are comparable with the diameters of the worms found with the shorter polymer but longer worms are found in here.
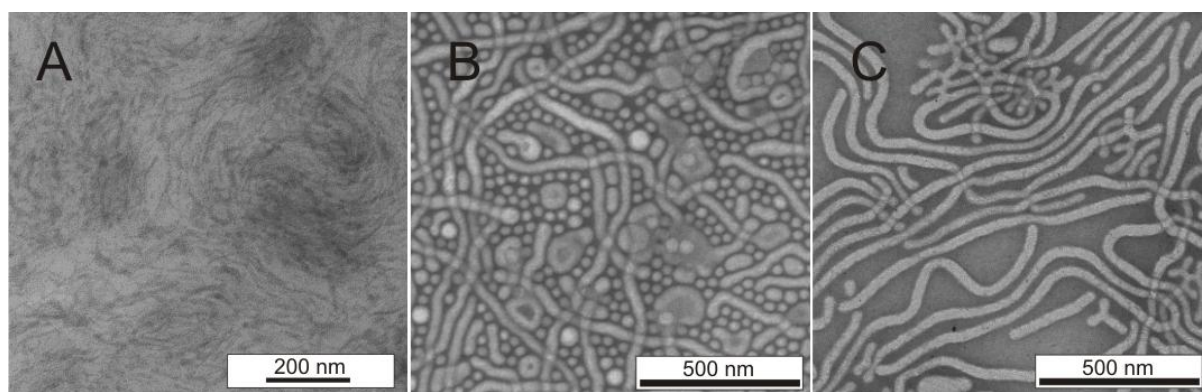
Figure 4.2.10. TEM picture of $\leq$ 10 wt% PIB$_{79}$-b-PEO$_{68}$. a) 10 wt% PIB$_{79}$-b-PEO$_{68}$, b) 5 wt% PIB$_{79}$-b-PEO$_{68}$, and c) 1 wt% PIB$_{79}$-b-PEO$_{68}$.

The TEM pictures were combined with DLS and SLS experiments. In contrast to the vesicle forming PIB$_{79}$-b-PEO$_{53}$, PIB$_{79}$-b-PEO$_{68}$ shows an angle dependency in the Berry plot. Denkinger *et. al.*[212] showed that worm/rod-like micelles show an angle-dependent scattering. Thus, and knowing that it self-assembles into worm/rod-like aggregates (Figure 4.2.11 D) the plot was extrapolated to zero concentration and zero angle with a higher order of q-fitting. But, even though higher order fits were used, the R_G/R_H yields a value of 1.52 ± 0.1. This ratio cannot explain the worm/rod-like behavior since pure rods have a ratio of 2 and higher[210]. For that the Holtzer-plot[213] XXX is used (see figure 4.2.11 C). The form-factor analysis of this plot fits very well with the worm/rod-like form-factor (full line) leading to a

length of the worm/rod-like micelles of about 400 nm. This is shorter than what is observed in TEM. In here worms/rods can be found which are longer than 1 μm. But the model used for the Holtzer-plot is for stiff rods and, in contrast, the copolymer self-assembled rods observed by TEM are flexible. The average number N of polymer molecules in a supramolecular structure (Table 4.2.2) was further estimated to 17 000. This number is in agreement with literature[208, 209208, 209] values obtained for worm/rod-like structures.[212, 213]
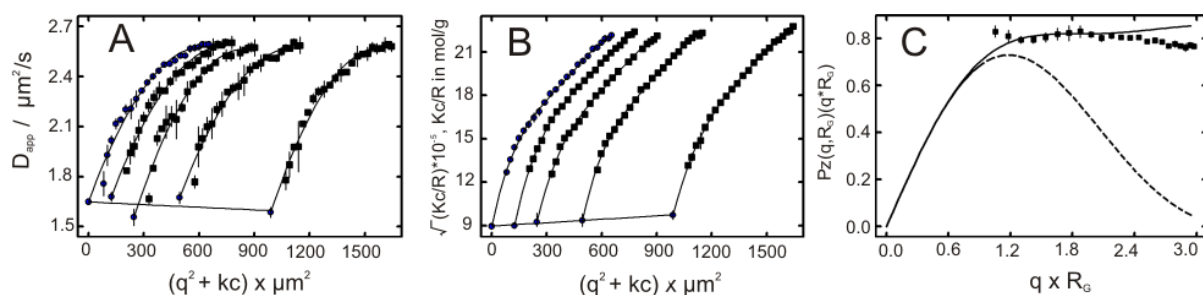
Figure 4.2.11. Light scattering by self-assembled PIB$_{79}$-b-PEO$_{68}$ block-copolymer. a) The apparent diffusion coefficients are plotted against the concentration of polymer and b) the Berry plot is shown. These plots were used to calculate R$_H$ and R$_G$, respectively. Squares represent measured data, and circles are values obtained by extrapolation to zero concentration and zero angle. c) Form factor analysis, called Holtzer-plot. Dashed line represents model form factors for hard spheres, solid line for worm/rod-like micelles, and squares are the experimental data obtained with PIB$_{79}$-b-PEO$_{68}$.

4.2.2.3 Phase diagram of self-assembled PIB$_{79}$-b-PEO$_{106}$

In order to analyze the self-assembly of PIB$_{79}$-b-PEO$_{106}$ SAXS measurements were performed with the pure polymer down to 5 wt% of PIB$_{79}$-b-PEO$_{106}$ in water. Figure 4.2.12 summarizes the 1-D SAXS patterns of self-assembled PIB$_{79}$-b-PEO$_{106}$ block-copolymers. For the pure polymer (100 wt%) SAXS patterns are observed which are indicative of a well-ordered lamellar phase. The first peak has a momentum transfer of 0.2 ± 0.03 nm^{-1} and the other peaks are 2q$_1$ 3q$_1$ and 4q$_1$ shifted (0.4 ± 0.04, 0.6 ± 0.05, and 0.8 ± 0.05 nm^{-1}, respectively). At very low water concentrations (90 wt%) a lamellar phase is still observed. In contrast, the patterns are slightly shifted towards higher momentum transfers. Here, the first Bragg peak appears at (0.25 ± 0.04) nm^{-1} and the following peaks are 2q$_1$ and 3q$_1$ folds shifted, 0.48 ± 0.06 and 0.73 ± 0.05 nm^{-1}, respectively. Increasing the water concentration further (75 wt%) a different SAXS pattern is found. The first peak can be separated into two superimposed peaks with q-values of 0.26 ± 0.04 nm^{-1} and 0.31 ± 0.05 nm^{-1}, respectively. The following peaks when they

are compared to the first of those superimposed peaks are 2 and 3 times shifted to 0.53 ± 0.03 and 0.79 ± 0.06 nm^{-1}, respectively), indicating a lamellar phase. In contrast, comparing them to the second peak of the superimposed peak at 0.31 ± 0.05 nm^{-1} they are $\sqrt{3}$, $\sqrt{6}$ and $\sqrt{9}$, respectively, shifted. This is indicative for a hexagonal phase. Accordingly at 75wt% two phases are coexisting: a hexagonal and a lamellar phase. In contrast, at 60 wt% only one phase is observed. The second and third peaks are $\sqrt{3}q_1$ and $\sqrt{7}q_1$ shifted, indicative for a hexagonal phase. The peak at $2q_1$ is presumably superimposed by the minimum of the form factor of this phase. The hexagonal phase is detected down to 20 wt%. In contrast to the worm/rod-like micelle forming PIB$_{79}$-b-PEO$_{68}$ the hexagonal phase cannot be easily assigned, i.e. at which concentrations the H$_1$ and H$_2$ phases are. Therefore we define down to 50 wt% at which the polymer-mass fraction is larger than the water fraction, the phase as a H$_2$ phase – water in oil phase - and for lower polymer concentrations a H$_1$ phase (similar to the H$_1$ phase found for PIB$_{79}$-b-PEO$_{68}$). At 20 wt% form factors from nanosized aggregates are appearing. At 10 and 5 wt % only the form factors are present.
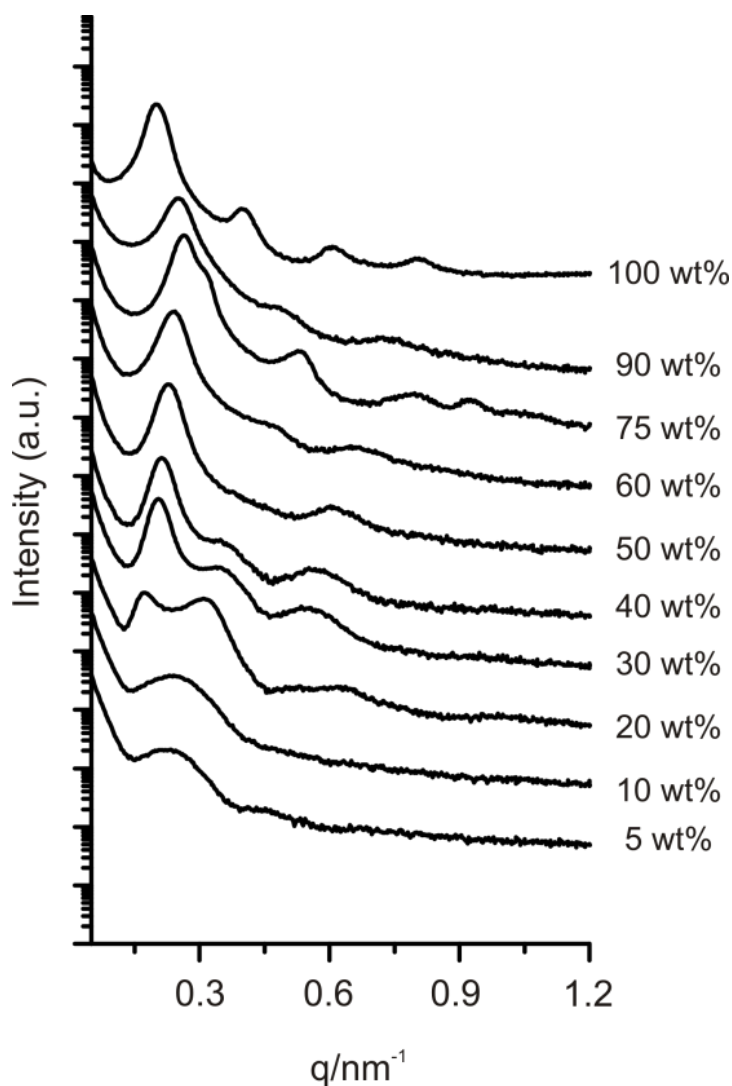
Figure 4.2.12. One-dimensional SAXS patterns of PIB$_{79}$-*b*-PEO$_{106}$ starting from the pure polymer (100 wt%) down to a 5 wt% aqueous solution of self-assembled polymers in water.

At 10 wt% and lower polymer concentrations TEM supports the findings of the SAXS measurements. At 10 wt% packed micelles and worm/rod-like micelles are observed (Figure 4.2.13 A). At 5 wt% (cf. Figure 4.2.13 B) packing of micellar and worm/rod-like micellar structures are observed. The packing of worm/rod-like structures is in good agreement with the SAXS results at higher polymer concentrations at which hexagonal phases are observed. At very low polymer concentration (< 1 wt%) mainly micelles with a diameter of 28 ± 5 nm and some worm/rod-like micelles with the same diameter are found. This finding explains the packing of both micelles and worm/rod-like micelles at higher concentrations and assignment of the hexagonal phases above 20 wt%.
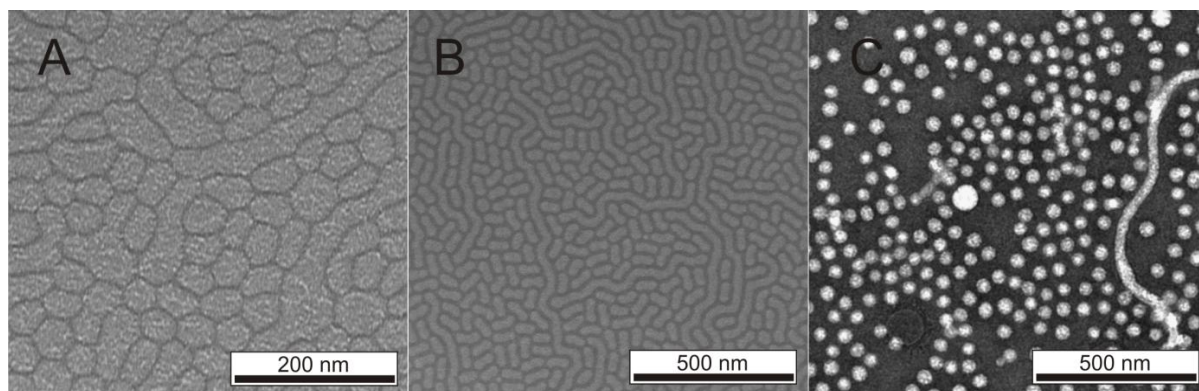
Figure 4.2.13 TEM pictures $\leq$ 10 wt% PIB_{79}-b-PEO_{106}. a) 10 wt% PIB_{79}-b-PEO_{106}, b) 5 wt% PIB_{79}-b-PEO_{106}, and c) 1 wt% PIB_{79}-b-PEO_{106}.

At polymer concentrations below 1 wt% TEM was combined with LS. Extrapolating the apparent diffusion coefficients to zero concentration and zero angle and using the Berry plot a ratio of $R_G/R_H = 0.84 \pm 0.04$ is calculated. This is close to the ratio corresponding to hard spheres ($R_G/R_H = 0.775$).[208] But the radius of gyration and the hydrodynamic radius ($R_G = 130 \pm 3$ nm and $R_H = 155 \pm 4$ nm, respectively) are too large compared to micelles observed by TEM (see above). This is due to the formation of worm/rod-like micelles which scatter due to their large size more than the smaller micelles. Therefore a number weight CONTIN fit was performed at 40°. Here, when the number weight of the aggregates was taken into account, the main radii distribution had a diameter of 26 ± 3 nm. This diameter is in good agreement with the diameter found by TEM (28 ± 5 nm). The refractive index increment (dn/dc) is 0.1242 ± 0.0087 mL/g. Knowing that and taking the average molecular weight of one polymer obtained out of ^{1}H-NMR experiments the average number of polymers (c.f. table 4.2.2) per micelle N_{MW} can be calculated to be 8 000. This number is much higher than expected[39, 214] for micellar aggregates. But this arises from the scattering by worm/rod-like micelles.
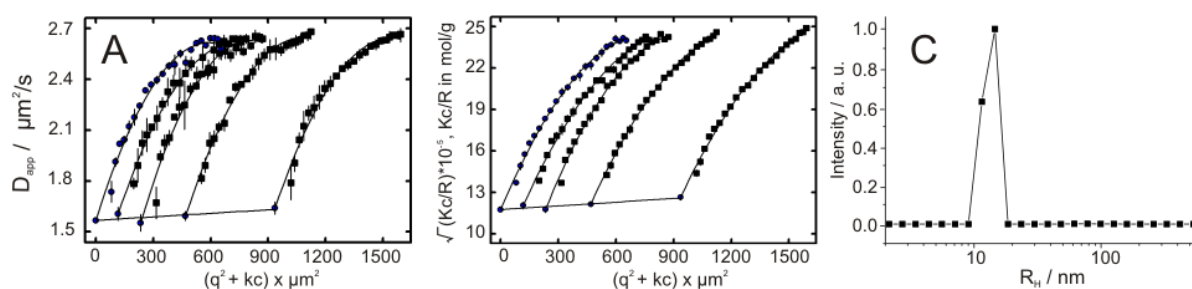
Figure 4.2.14. Light scattering data by self-assembled PIB_{79}-*b*-PEO_{106} block-copolymers. a) The apparent diffusion coefficients are plotted versus the concentration of polymers and b) the Berry plot is shown. These plots were used to calculate R_H and R_G, respectively. Squares correspond to measured data and the points on the left in the diagrams are the points extrapolated to zero concentration and zero angle. c) CONTIN fit at 40 ° at 0.1 wt% PIB_{79}-*b*-PEO_{106} concentration.

All LS results obtained with the three polymers investigated herein are summarized in table 4.2.2.

Table 4.2.2. LS data for self-assembled PIB-*b*-PEO.

Name	M_N (^{1}H -NMR) (g/mol)[a]	dn/dc (ml/g)[b]	R_G (nm)[c]	M_{WM} (g/mol)[d]	R_H (g/mol)[e]	N^f	$R_G/R_H{}^g$
PIB_{79}-*b*-PEO_{53}	6780	0.1955 ± 0.0011	133 ± 2	9.92* 10^8	139 ± 3	95000	0.96 ± 0.03
PIB_{79}-*b*-PEO_{68}	7440	0.2135 ± 0.0005	200 ± 10	1.26* 10^8	131 ± 3	17000	1.52 ± 0.1
PIB_{79}-*b*-PEO_{106}	8910	0.202 ± 0.009	130 ± 3	7.26* 10^8	155 ± 4	8100	0.84 ± 0.04

[a] Number-average molecular weight of block-copolymers as determined by ^{1}H NMR spectroscopy. [b] Refractive index increment determined with a differential refractometer. [c] radius of gyration determined by SLS. [d] Molecular weight of the analyzed nanosized morphology. [e] Hydrodynamic radius determined out of DLS. [f] Aggregate number of polymers per nanosized morphology. [g] Ratio of the radius of gyration to the hydrodynamic radius.

4.2.3 Conclusion and summary on the phase behavior of poly(isobutylene-block-poly(ethyleneoxide)

It could be shown that the hydrophobic to hydrophilic ratio of PIB-*b*-PEO does influence the nanosized morphology and the phases those morphologies have to overcome in order to form them upon dilution. Polymers have to be tailored in the right way to achieve the targeted objects. If the hydrophobic to hydrophilic ratio is only slightly changed the final morphology can vary drastically from the initial expected design. Figure 4.2.15 sums up all phases found for the three examined polymers.
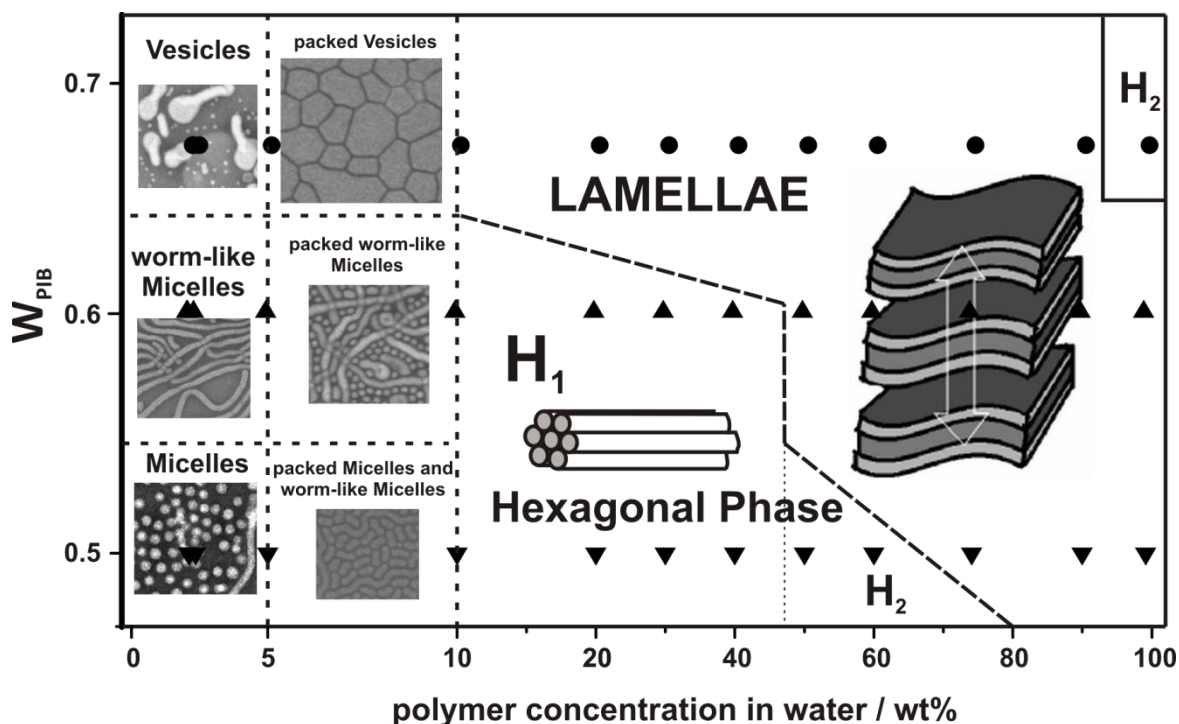
Figure 4.2.15 Schematic phase diagram of binary PIB-*b*-PMCL water mixtures.

4.3. Application of vesicle forming PEO$_{23}$-b-PMCL$_{32}$

Polymeric formulations based on vesicles have emerged as versatile for drug delivery due to their increased stability, site specificity (depending on the chemistry), blood circulation life-time and thus overall potential therapeutic effects compared to liposomes.[88] Ideally, a loaded vesicle should remain stable until it reaches the target site. Upon accumulation of the vesicle at the target, the encapsulated molecule (e.g. drug) must be released at a high enough concentration to mediate an effective therapeutic response. Consequently, drug release in response to a specific stimulus at the target site, i.e., triggered release, is a desired feature of effective targeted delivery systems. [215]

In chapter 3.1.3. the self-assembly of PEO$_{23}$-b-PMCL$_{32}$ was investigated. In contrast to the other studied polymers, it has the lowest hydrophobic to hydrophilic ratio meaning the shortest hydrophobic block, respectively. Accordingly, since shorter hydrophobic blocks favor short time scales for vesicle formation, this polymer seemed to be the most prominent polymer to study as an encapsulation and releasing system. Besides, the hydrophobic block composed of polyesters could be hydrolyzed upon proton concentration increase. The chemical principles behind hydrolyzing esters[216] have been described in review published almost decades ago by Cordes and Bull.

4.3.1. pH triggered release of fluorescein from PEO$_{23}$-b-PMCL$_{32}$

Fluorescein (figure 4.3.1) is a red crystal in the bulk. The large delocalized π-electron system makes it a very efficient energy absorbing molecule and a candidate for fluorescence.
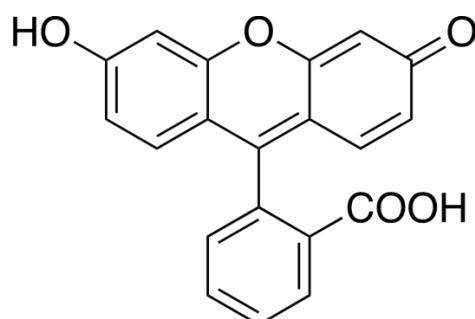
Figure 4.3.1 Molecular structure of fluorescein.

At high concentrations of fluorescein (> 20 µM) it self-quenches resulting in no fluorescence. Accordingly the dye is encapsulated at a high concentration and the resulting fluorescence signal is low. However, when the vesicle releases the fluorescein, the concentration of the fluorescent molecule in the surrounding is low and its fluorescence intensity can be detected. This is the basis for monitoring time dependent release of encapsulated fluorescent dye. Here, the starting concentration of fluorescein was for all experiments 25 mM.

Figure 4.3.2 summarizes the time dependent fluorescein release profiles when the release is triggered at different pH. At physiological pH (7.5) no fluorescence release was detected. Even after more than a month the vesicles are still stable and only 1- 3 % of fluorescence release was detected which is in the range of the detection limit of the fluorimeter. At neutral pH (pH= 7) until the 7th day almost no dye release (4 %) was observed as well. Even a few days later still a small release could be detected which did not drastically increase (6%) until the end of the time dependent measurements. A similar behavior can be also found when the pH is again slightly increased (pH= 6.5). After 36 days approximately 10 % of fluorescein were released. However, when the proton concentration is further increased the release curve changes drastically (pH= 6). Here, 3 times as much dye release after three weeks could be observed (30 %). A longer monitoring time does not yield a stronger effect. 14 days later almost the same concentration of free dye can be observed as two weeks before. Interestingly the pH profile looks the same for pH= 5.1 as for pH= 6. Here, after 21 days the maximum of free dye is observed as well. The picture changes dramatically when the proton concentration is 10 times increased (pH= 3.8). After six days 8 % of the dye is free, being the maximum concentration of free dye at neutral pH. After 16 days the released dye concentration (43 %) exceeded the maximum concentrations found at pH= 6 and 5. And finally after more than a month (36 days) almost 80 % of all encapsulated dyes were released.

In summary after three weeks the possible released dye concentration is reached depending on the pH. At high proton concentrations (pH= 3.8) and after 36 days 80 % of the encapsulated fluorescein dye is released. Since sites of inflammation and tumors are acidic this nanocarrier seems to be a promising candidate. It can keep its cargo over a long time in its interior at physiological pH and when it reaches an acidic site the vesicles release it.
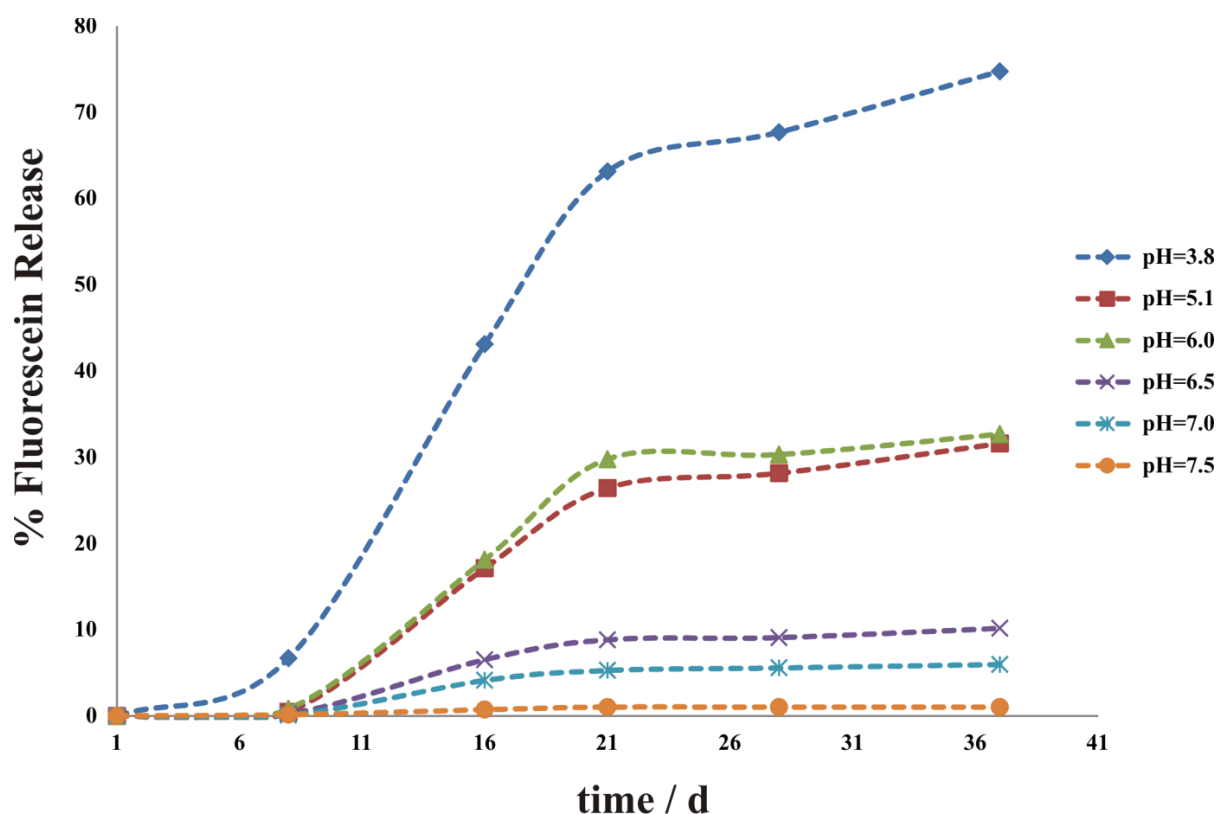
Figure 4.3.2. pH-dependent fluorescein release by PEO_{23}-$PMCL_{32}$ vesicles

4.3.2. pH triggered release of Enhanced Cyan Fluorescent Protein

Besides small molecules, polymer vesicles can encapsulate macromolecules like proteins. Delivery of proteins is important because the bioavailability limitations of proteins make them difficult to be directly delivered, particularly in diseases caused by insufficient amounts or inactive variants of those proteins. Thus, vesicles represent a new promising approach to overcome these limitations because they protect the protein in their aqueous lumen.[96] Further, polymers can be tailored in order to release the encapsulated molecules at the favored site. Thus, chemical incompatible blocks can be for instance functionalized with stimuli responsive molecules or the self-assembled blocks on their own are stimuli responsive to release their cargo by stimuli triggered by light, temperature, and chemical stimuli (ions, pH).[217, 218]

Since ECFP is able to fluoresce on its own without any further labeling this protein was chosen to demonstrate the facile encapsulation of macromolecules in polymeric vesicles. ECFP is a genetically encoded fluorophore widely used as a donor in fluorescence resonance energy transfer based cell imaging experiments. It consists of eleven β-barrels, which

surround a light active molecule in the center of the protein. A 3D representation is shown in figure 4.3.3.
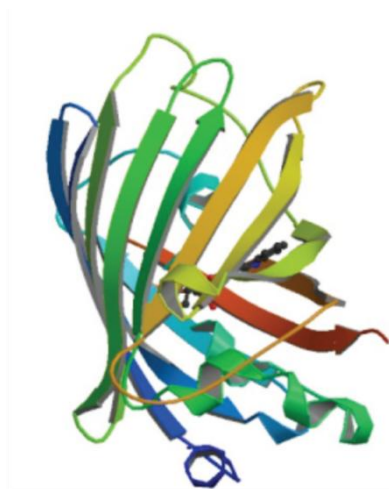
Figure 4.3.3. 3D representation of ECFP.

Three different PBS solutions were adjusted to pH 4, 5.2 and 7.4. The starting concentration of ECFP was 0.3 mg/mL (~5mmol) in all three solutions. The vesicles were prepared by bulk swelling. The encapsulation of ECFP was studied by FCS. The solution adjusted to pH= 7.4 did not contain any encapsulated ECFP. Fitting the resulting autocorrelation curves resulted in the presence of either pure, non-encapsulated ECFP or large aggregates, presumably aggregations of polymer and ECFP. At pH= 5.2, however, 10 % of the ECFP molecules were encapsulated into vesicles. Decreasing the pH further to 4 showed that 70% of the ECFP molecules were encapsulated. The favorable encapsulation of the protein at pH= 4 can be explained by considering the secondary structure of the protein (Figure 4.3.4). Here, two dominant amino acids are found: glutamic acid (E) and aspartic acid (D). The pK_A value of E and D are 4.07 and 3.90, respectively. Accordingly those amino acids are non-charged at ~pH 4. The net charge of the amino acid is zero. The secondary structure of the ECFP consists of eleven β-barrels, five small α-helices and some loops. From the convolution of the secondary structures it can be shown that most of the glutamic and aspartic acids are on the surface of the ECFP. At pH= 4 the surface of ECFP is neutral. Considering that the polymer is also not charged, the non-charged entities of ECFP at this pH favors the self-assembly of the polymer. When the pH is increased, ECFP is charged and larger aggregates are formed. These aggregates are most probable aggregations of polymers and protein. This would explain the

results at neutral pH and at pH= 5.2 where autocorrelation curves shifted towards longer relaxation times.

MVSKGEELFTGVVPILVELDGDVNGHKFSVSGEGEGDATYGKLTLKFICTTGKLPVPWPT
LVTTLTWGVQCFSRYPDHMKQHDFFKSAMPEGYVQERTIFFKDDGNYKTRAEVKFEGDTLVN
RIELKGIDFKEDGNILGHKLEYNYISHNVYITADKQKNGIKANFKIRHNIEDGSVQLADH
YQQNTPIGDGPVLLPDNHYLSTQSALSKDPNEKRDHMVLLEFVTAAGITLGMDELYK

Figure 4.3.4. The primary sequence and the secondary structure of the ECFP (yellow arrows are β-sheets, beige are α-helices and purple are turns).

Next, the pH sensitivity of the release of the polymer vesicles was studied. Two samples were stirred independently for three days at 4 °C containing the optimized conditions found previously at pH= 4. Prior to FCS measurements both samples were filtered through 400 nm filters and most of the free, non-encapsulated ECFP was separated by SEC. The difference between both solutions was the mobile phase (pH= 4 and 7.4, respectively) upon separation of the vesicles from the non-encapsulated ECFP. Though the vesicle interior had a pH= 4, the pH of the surrounding was maintained at 4 (solution 4) and 7.4 (solution 7.4), respectively. After SEC solution 4 resulted in vesicles with 70% of the initially encapsulated ECFP. In contrast solution 7.4 contained vesicles with only 50% of initial ECFP. Four days after the SEC separation and storage of the samples at 4 °C, still 60% of encapsulated ECFP was detected in solution 4. But already after 12 days most of the ECFP was released (5 % of

encapsulated ECFP). In contrast, solution 7.4 showed over the same period of time no significant difference of ECFP release.
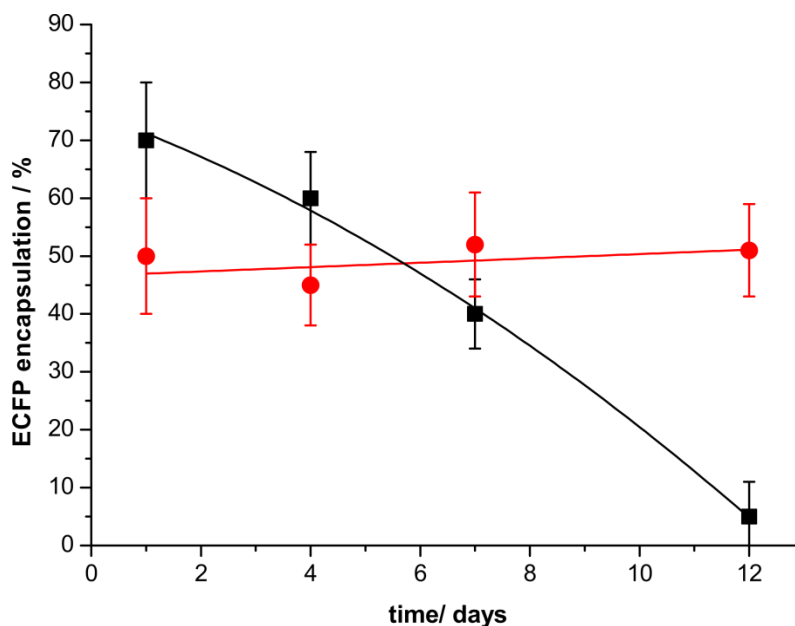
Figure 4.3.5. pH time dependent ECFP release. Red: solution 7.4 (pH= 4 inside and pH= 7.4 outside of the vesicles). Black: solution 4 (pH= 4 inside and pH= 4 outside of the vesicles). Solid lines are a guide to the eye.

Comparing the results obtained either with fluorescein or ECFP release triggered by pH shows that ECFP is interestingly released earlier than the approximately 10 times smaller molecule fluorescein. But it has to be noted that both results are not directly comparable. In the case of fluorescein the amount that was released corresponds to the real value which was encapsulated since the initial encapsulated volume was determined by chemically destroying the particles. With respect to ECFP the findings are just qualitative since FCS only enables to conclude about encapsulation happening or not. And since these are just preliminary results, it is not clear if ECFP is really encapsulated or it is on the outside of the particles.

4.3.3. Conclusion on potential applications of vesicle forming PEO$_{23}$-b-PMCL$_{32}$

It was shown that PEO$_{23}$-PMCl$_{32}$ can be used to encapsulate both small and large molecules. By adjusting the pH towards acidic conditions vesicles can be triggered to release encapsulated molecules. It was also shown that the vesicles are stable in physiological-like conditions. They are not only keeping their cargo inside they are also stable over a long period of time, making those polymer vesicles promising candidates for drug delivery. Sites of

inflammation and tumors are acidic. This favors the pH-triggerable release of the cargo, and therefore increases the efficiency of targeting drugs to desired cellular sites while protecting them from potential degradation in lysosomes. And compared to pH-sensitive liposomes those polymer vesicles are very stable. They could be still stable in the plasma, resulting in no failure to deliver their contents to their targeted sites. They could also be used in food science. Health improving food additives, that are not stable under acidic conditions, could be encapsulated. Accordingly the probability that they reach their target would be increased and subsequently the efficiency of delivery.

5. General Conclusion

It was shown that the hydrophobic to hydrophilic ratio of block copolymers is influencing the self-assembled morphologies and a fortiori the phases the macromolecules have to overcome in order to self-aggregate into their preferred structure of a given size.

The block copolymers, which are self-assembling into vesicles, PEO_{23}-b-$PMCL_{32}$, PEO_{23}-b-$PMCL_{44}$, PEO_{23}-b-$PMCL_{54}$, and PIB_{79}-b-PEO_{53}, show a similar phase behavior when they are undergoing the transition from the bulk to the diluted regime. In general, they first transform into a lamellar phase then into packed vesicles and finally into single vesicles. The exceptions are PEO_{23}-b-$PMCL_{63}$ and PIB_{79}-b-PEO_{53}. At very high polymer concentrations they self-assemble into an inverse hexagonal phase. PEO-b-PMCL block copolymers showed no long-range order in the bulk as well. In contrast to similar phase behavior of PEO-b-PMCL, it was shown that the hydrophobic PMCL block length determines the phase morphology at a given polymer concentration. Moreover, this block length influences the size of the vesicles and the spacing of the lamellar layers. Polymers with a higher hydrophobic-to-hydrophilic ratio form larger vesicles.

Block copolymers that are forming (partially) into worm/rod-like micelles (PEO_{23}-b-$PMCL_{25}$ and PIB_{79}-b-PEO_{68}, respectively) also present similarities. It has to be noted that the PEO_{23}-b-$PMCL_{25}$ dominantly forms vesicles but the worm-like micelles that are also present influence the phase diagram, which can be also compared to the PIB_{79}-b-PEO_{68} phase diagram. In both cases the block copolymers have to overcome a transition from a lamellar layer to a hexagonal phase prior to packing of those structures before they self-assemble in worm/rod-like structures. Since the dominant morphology is vesicles for PEO_{23}-b-$PMCL_{25}$ the hexagonal phase is superimposed with a lamellar phase. But similarities between those phases are definitely identified. It also has to be noted that this is the first time, to the best of our knowledge, that an experimental phase diagram displays worm/rod-like micelles self-assembled from block copolymers.

The largest polymer in this work PIB_{79}-b-PEO_{106} was the only example with which the morphology change of a micelle forming block copolymer was shown. This polymer had to undergo transitions from lamellar phases, hexagonal phases and packing of micelles prior to self-assembly into micelles.

These findings can be used to optimize vesicle/worm-like micelle/micelle formation on the lab scale and in technical applications. Due to the biocompatibility and degradability of the

polymers, morphologies self-assembled from PEO-*b*-PMCL and PIB-*b*-PEO are promising candidates as nanocarriers and nanoreactors for biomedical applications. This assumption can be strengthened since it was also possible to encapsulate both small and large molecules into PEO_{23}-$PMCl_{32}$. Furthermore, by adjusting the pH towards acidic conditions, vesicles responsiveness could be triggered to release the encapsulated molecules.

6. References

1. Painter, P. C.; Coleman, M. M., *Essentials of polymer science and engineering*. DEStech Publications: Lancaster, **2009**.
2. Hagemann, R. *Acta Hist Leopoldina* **2007**, 48, 113-58.
3. Watson, J. D.; Crick, F. H. C. *Clin Orthop Relat Res* **2007,** 462, 3-5.
4. Goettlinger, H. G.; Weissenhorn, W., Assembly and Release. In *Retroviruses: Molecular Biology, Genomics and Pathogenesis*, Caister Academic Press., **2010,**187-215.
5. Labrude, P.; Becq, C. *Rev Hist Pharm (Paris)* **2003,** 51, (337), 61-78.
6. Crespy, D.; Bozonnet, M.; Meier, M. *Angewandte Chemie-International Edition* **2008,** 47, (18), 3322-3328.
7. Duncan, R. *Nature Reviews Drug Discovery* **2003,** 2, (5), 347-360.
8. Peppas, N. A.; Bures, P.; Leobandung, W.; Ichikawa, H. *European Journal of Pharmaceutics and Biopharmaceutics* **2000,** 50, (1), 27-46.
9. Luo, D.; Saltzman, W. M. *Nature Biotechnology* **2000,** 18, (1), 33-37.
10. Aoshima, S.; Kanaoka, S. *Chemical Reviews* **2009,** 109, (11), 5245-5287.
11. Khanna, K.; Varshney, S.; Kakkar, A. *Polymer Chemistry*, **2010,** 1, (8), 1171-1185.
12. Vinogradova, L. V. *Russian Journal of Applied Chemistry*, **2010,** 83, (3), 351-378.
13. Inoue, K. *Progress in Polymer Science* **2000,** 25, (4), 453-571.
14. Ito, K.; Kawaguchi, S., Poly(macromonomers): Homo- and copolymerization. In *Branched Polymers I*, Springer-Verlag Berlin: Berlin, **1999**; 142, 129-178.
15. Yokota, K. *Progress in Polymer Science* **1999,** 24, (4), 517-563.
16. Jain, P.; Baker, G. L.; Bruening, M. L. *Annual Review of Analytical Chemistry* **2009,** 2, 387-408.
17. Kim, G.; Park, S.; Jung, J.; Heo, K.; Yoon, J.; Kim, H.; Kim, I. J.; Kim, J. R.; Lee, J. I.; Ree, M. *Advanced Functional Materials* **2009,** 19, (10), 1631-1644.
18. Edmondson, S.; Osborne, V. L.; Huck, W. T. S. *Chemical Society Reviews* **2004,** 33, (1), 14-22.
19. Kim, Y. H. *Journal of Polymer Science Part a-Polymer Chemistry* **1998,** 36, (11), 1685-1698.
20. Matthews, O. A.; Shipway, A. N.; Stoddart, J. F. *Progress in Polymer Science* **1998,** 23, (1), 1-56.
21. Lee, C. C.; MacKay, J. A.; Frechet, J. M. J.; Szoka, F. C. *Nature Biotechnology* **2005,** 23, (12), 1517-1526.
22. Ardoin, N.; Astruc, D. *Bulletin De La Societe Chimique De France* **1995,** 132, (9), 875-909.
23. Kim, J. K.; Han, C. D., Phase Behavior and Phase Transitions in AB- and ABA-type Microphase-Separated Block Copolymers. In *Polymer Materials: Block-Copolymers, Nanocomposites, Organic/Inorganic Hybrids, Polymethylenes*, Springer-Verlag Berlin: Berlin, **2010,** 231, 77-145.
24. Ellison, C. J.; Meuler, A. J.; Qin, J.; Evans, C. M.; Wolf, L. M.; Bates, F. S. *Journal of Physical Chemistry B* **2009,** 113, (12), 3726-3737.
25. Fujiwara, T.; Kimura, Y. *Macromolecular Bioscience* **2002,** 2, (1), 11-23.
26. Hamley, I. W. *Progress in Polymer Science* **2009,** 34, (11), 1161-1210.
27. Forster, S.; Berton, B.; Hentze, H. P.; Kramer, E.; Antonietti, M.; Lindner, P. *Macromolecules* **2001,** 34, (13), 4610-4623.
28. Foerster, S.; Antonietti, M. *Advanced Materials* **1998,** 10, (3), 195-217.
29. Matsen, M. W.; Schick, M. *Macromolecules* **1994,** 27, 4014.
30. Vavasour, J. D.; Whitmore, M. D. *Macromolecules* **1992,** 25, 5477.

REFERENCES

31. Matsen, M. W.; Bates, F. S. *Macromolecules* **1996,** 29, (23), 7641-7644.
32. Matsen, M. W.; Schick, M. *Macromolecules* **1994,** 27, (24), 7157-7163.
33. Matsen, M. W.; Bates, F. S. *Macromolecules* **1996,** 29, (4), 1091-1098.
34. Hajduk, D. A.; Kossuth, M. B.; Hillmyer, M. A.; Bates, F. S. *J. Phys. Chem.* **1998,** 102, 4269-4276.
35. Breunig, M.; Bauer, S.; Goefferich, A. *European Journal of Pharmaceutics and Biopharmaceutics* **2008,** 68, (1), 112-128.
36. Tanford, C. *Wiley, New York* **1973**
37. Tanford, C. *Proc. Natl Acad. Sci. USA* **1979,** 76, 4175-4176.
38. Meier, W. *Chemical Society Reviews* **2000,** 29, (5), 295-303.
39. Forster, S.; Zisenis, M.; Wenz, E.; Antonietti, M. *Journal of Chemical Physics* **1996,** 104, (24), 9956-9970.
40. Taubert, A.; Napoli, A.; Meier, W. *Current Opinion in Chemical Biology* **2004,** 8, (6), 598-603.
41. Kita-Tokarczyk, K.; Meier, W. *Chimia* **2008,** 62, (10), 820-825.
42. Kita-Tokarczyk, K.; Grumelard, J.; Haefele, T.; Meier, W. *Polymer* **2005,** 46, (11), 3540-3563.
43. Discher, D. E.; Eisenberg, A. *Science* **2002,** 297, (5583), 967-973.
44. Soo, P. L.; Eisenberg, A. *Journal of Polymer Science Part B-Polymer Physics* **2004,** 42, (6), 923-938.
45. O'Reilly, R. K.; Hawker, C. J.; Wooley, K. L. *Chemical Society Reviews* **2006,** 35, (11), 1068-1083.
46. Walker, L. M. *Current Opinion in Colloid & Interface Science* **2001,** 6, (5-6), 451-456.
47. Elias, H.-G., *Makromoleküle*. Hüthig & Wepf: Basel, **1990**; Vol. 1.
48. Forster, S.; Plantenberg, T. *Angewandte Chemie-International Edition* **2002,** 41, (5), 689-714.
49. Triolo, R.; Triolo, A.; Triolo, F.; Steytler, D. C.; Lewis, C. A.; Heenan, R. K.; Wignall, G. D.; DeSimone, J. M. *Physical Review E,* **2000,** 61, (4), 4640-4643.
50. Londono, J. D.; Dharmapurikar, R.; Cochran, H. D.; Wignall, G. D.; McClain, J. B.; Betts, D. E.; Canelas, D. A.; DeSimone, J. M.; Samulski, E. T.; Chillura-Martino, D.; Triolo, R. *Journal of Applied Crystallography* **1997,** 30, (2), 690-695.
51. ChilluraMartino, D.; Triolo, R.; McClain, J. B.; Combes, J. R.; Betts, D. E.; Canelas, D. A.; DeSimone, J. M.; Samulski, E. T.; Cochran, H. D.; Londono, J. D. *Journal of Molecular Structure* **1996,** 383, (1-3), 3-10.
52. Qin, A. W.; Tian, M. M.; Ramireddy, C.; Webber, S. E.; Munk, P.; Tuzar, Z. *Macromolecules* **1994,** 27, (1), 120-126.
53. Eckert, A. R.; Webber, S. E. *Macromolecules* **1996,** 29, (2), 560-567.
54. Voulgaris, D.; Tsitsilianis, C.; Grayer, V.; Esselink, F. J.; Hadziioannou, G. *Polymer* **1999,** 40, (21), 5879-5889.
55. Voulgaris, D.; Tsitsilianis, C. *Macromolecular Chemistry and Physics* **2001,** 202, (17), 3284-3292.
56. Gaucher, G.; Marchessault, R. H.; Leroux, J. C. *Journal of Controlled Release*, **2010,** 43, (1), 2-12.
57. Hu, X. L.; Jing, X. B. *Expert Opinion on Drug Delivery* **2009,** 6, (10), 1079-1090.
58. Qiu, L. Y.; Zheng, C.; Jin, Y.; Zhu, K. J. E. *Expert Opinion on Therapeutic Patents* **2007,** 17, (7), 819-830.
59. Osada, K.; Christie, R. J.; Kataoka, K. *Journal of the Royal Society Interface* **2009,** 6, S325-S339.

60. Talelli, M.; Rijcken, C. J. F.; van Nostrum, C. F.; Storm, G.; Hennink, W. E. *Advanced Drug Delivery Reviews* 62, **2010,** (2), 231-239.
61. Mondon, K.; Gurny, R.; Moller, M. *Chimia* **2008,** 62, (10), 832-840.
62. Tirrell, M., Serie E: applied sciences. In *Serie E: applied sciencesNATO ASI series*, S.E. Webber, P. M. a. Z. T., Ed. Dordrecht: **1996**; Vol. 327, pp 281–308.
63. Hamley, I. W., *The physics of block copolymers, chapter 3 and 4*. **1998**; Vol. 4, p 131-265.
64. G. Riess; Hurtrez, G.; Bahadur, P., *Encyclopedia of Polymer Science and Engineering*. Wiley: New York, **1985**.
65. Nace, V. M., *Surfactant science series*. Marcel Dekker: New York, **1996**.
66. Alexandridis, P.; Yang, L. *Macromolecules* **2000,** 33, (9), 3382-3391.
67. Torchilin, V. P. *Journal of Controlled Release* **2001,** 73, (2-3), 137-172.
68. Kabanov, A. V.; Batrakova, E. V.; Alakhov, V. Y. *Journal of Controlled Release* **2002,** 82, (2-3), 189-212.
69. Otsuka, H.; Nagasaki, Y.; Kataoka, K. *Advanced Drug Delivery Reviews* **2003,** 55, (3), 403-419.
70. Alarcon, C. D. H.; Pennadam, S.; Alexander, C. *Chemical Society Reviews* **2005,** 34, (3), 276-285.
71. Geng, Y.; Dalhaimer, P.; Cai, S. S.; Tsai, R.; Tewari, M.; Minko, T.; Discher, D. E. *Nature Nanotechnology* **2007,** 2, (4), 249-255.
72. Fox, M. E.; Szoka, F. C.; Frechet, J. M. J. *Accounts of Chemical Research* **2009,** 42, (8), 1141-1151.
73. Frechet, J. M. J. *Journal of Polymer Science Part a-Polymer Chemistry* **2003,** 41, (23), 3713-3725.
74. Cai, S. S.; Vijayan, K.; Cheng, D.; Lima, E. M.; Discher, D. E. *Pharmaceutical Research* **2007,** 24, (11), 2099-2109.
75. Christian, D. A.; Cai, S.; Garbuzenko, O. B.; Harada, T.; Zajac, A. L.; Minko, T.; Discher, D. E. *Molecular Pharmaceutics* **2009,** 6, (5), 1343-1352.
76. Bagshaw, S. A.; Prouzet, E.; Pinnavaia, T. J. *Science* **1995,** 269, (5228), 1242-1244.
77. Taylor, K. C.; Nasr-El-Din, H. A. *Journal of Petroleum Science and Engineering* **1998,** 19, (3-4), 265-280.
78. Antonietti, M.; Forster, S. *Advanced Materials* **2003,** 15, (16), 1323-1333.
79. Lasic, D. D.; Joannic, R.; Keller, B. C.; Frederik, P. M.; Auvray, L. *Advances in Colloid and Interface Science* **2001,** 89, 337-349.
80. Hyde, S. T. *Journal De Physique* **1990,** 51, (23), C7209-C7228.
81. Israelachvili, J. N.; Mitchell, D. J.; Ninham, B. W. *Journal of the Chemical Society-Faraday Transactions Ii* **1976,** 72, 1525-1568.
82. Israelachvili, J. N., *Intermolecular and Surface Forces*. **1991**, p 291 pp.
83. Zhang, L. F.; Eisenberg, A. *Journal of the American Chemical Society* **1996,** 118, (13), 3168-3181.
84. Discher, B. M.; Won, Y. Y.; Ege, D. S.; Lee, J. C. M.; Bates, F. S.; Discher, D. E.; Hammer, D. A. *Science* **1999,** 284, (5417), 1143-1146.
85. Zupancich, J. A.; Bates, F. S.; Hillmyer, M. A. *Macromolecules* **2006,** 39, 486-4288
86. Nardin, C.; Hirt, T.; Leukel, J.; Meier, W. *Langmuir* **2000,** 16, (3), 1035-1041.
87. Lee, J. C. M.; Bermudez, H.; Discher, B. M.; Sheehan, M. A.; Won, Y. Y.; Bates, F. S.; Discher, D. E. *Biotechnology and Bioengineering* **2001,** 73, (2), 135-145.
88. Onaca, O.; Enea, R.; Hughes, D. W.; Meier, W. *Macromolecular Bioscience* **2009,** 9, (2), 129-139.
89. Ben-Haim, N.; Broz, P.; Marsch, S.; Meier, W.; Hunziker, P. *Nano Letters* **2008,** 8, (5), 1368-1373.

REFERENCES

90. Grzelakowski, M.; Onaca, O.; Rigler, P.; Kumar, M.; Meier, W. *Small* **2009,** 5, (22), 2545-2548.
91. Balasubramanian, V.; Onaca, O.; Enea, R.; Hughes, D. W.; Palivan, C. G. *Expert Opinion on Drug Delivery* 7, **2010,** (1), 63-78.
92. Levine, D. H.; Ghoroghchian, P. P.; Freudenberg, J.; Zhang, G.; Therien, M. J.; Greene, M. I.; Hammer, D. A.; Murali, R. *Methods* **2008,** 46, (1), 25-32.
93. Castellana, E. T.; Cremer, P. S. *Surface Science Reports* **2006,** 61, (10), 429-444.
94. Brown, L.; McArthur, S. L.; Wright, P. C.; Lewis, A.; Battaglia, G. *Lab on a Chip* 10, **2010,** (15), 1922-1928.
95. Shum, H. C.; Kim, J. W.; Weitz, D. A. *Journal of the American Chemical Society* **2008,** 130, (29), 9543-9549.
96. Onaca, O.; Hughes, D. W.; Balasubramanian, V.; Grzelakowski, M.; Meier, W.; Palivan, C. G. *Macromolecular Bioscience*, **2010,** 10, (5), 531-538.
97. del Barrio, J.; Oriol, L.; Sanchez, C.; Serrano, J. L.; Di Cicco, A.; Keller, P.; Li, M. H. *Journal of the American Chemical Society*, **2010,** 132, (11), 3762-3769.
98. Battaglia, G.; Ryan, A. *J. Nat. Mater.* **2005,** 4, 869-876.
99. Battaglia, G.; Ryan, A. *Macromolecules* **2006,** 39, 869-876
100. Derici, L.; Ledger, S.; Mai, S. M.; Booth, C.; Hamley, I. W.; Pedersen, J. S. *Physical Chemistry Chemical Physics* **1999,** 1, (11), 2773-2785.
101. Pople, J. A.; Hamley, I. W.; Fairclough, J. P. A.; Ryan, A. J.; Komanschek, B. U.; Gleeson, A. J.; Yu, G. E.; Booth, C. *Macromolecules,* **1997,** 30, (19), 5721-5728.
102. Hamley, I. W.; Pople, J. A.; Fairclough, J. P. A.; Terrill, N. J.; Ryan, A. J.; Booth, C.; Yu, G. E.; Diat, O.; Almdal, K.; Mortensen, K.; Vigild, M. *Journal of Chemical Physics* **1998,** 108, (16), 6929-6936.
103. Braun, J.; Bruns, N.; Pfohl, T.; Meier, W, *Macromol. Chem. Phys.,* **2011**, *212*, 1245–1254 .
104. Matthews, F. E.; Strange, E. H. Caoutchouc-like substances. 1910.
105. Harries, C. *Liebigs Ann. Chem.* **1911,** 383.
106. Schlenk, W.; Thal, A. *Ber Dtsch Chem Ges* **1913,** 46, 2480 pp.
107. Schlenk, W.; Thal, A. *Ber Dtsch Chem Ges* **1914,** 47, 473 pp.
108. Ziegler, K.; Colonius, H.; Schäfer, O. *Liebigs Ann. Chem.* **1929,** 473, 36.
109. Ziegler, K.; Schäfer, O. *Liebigs Ann. Chem.* **1930,** 479, 150.
110. Ziegler, K.; Jacob, L.; Wollthan, H.; Wenz, A. *Liebigs Ann Chem* **1934,** 511, 64.
111. Ziegler, K. *Angewandte Chemie* **1936,** 49, 499.
112. Ziegler, K.; Bähr, K. *Chem Ber* **1928,** 61, 253.
113. Ziegler, K.; Eimers, E.; Hechelhammer, W.; Wilms, M. *Liebigs Ann. Chem.* **1945,** 567, 43.
114. Ziegler, K.; Crössmann, F.; Kleiner, H.; Schäfer, O. *Liebigs Ann. Chem.* **1929,** 473, 1929.
115. Schlenk, W.; Bergmann, E.; Benedikt, B.; Blum, O.; Bresiewicz, C.; I.Rodloff; al., e. *Liebigs Ann. Chem.* **1928,** 463, 1-97.
116. Schlenk, W.; Bergmann, E.; Blum-Bergmann, O. *Liebigs Ann. Chem.* **1930,** 479, 78.
117. Scott, N. D.; Walker, J. F.; Hansley, V. L. *Journal of american Chemical Society* **1936,** 58, 2442.
118. Lipkin, D.; Paul, D. E.; Townsend, J.; Weissman, S. I. *Science* **1953,** 117, (3046), 534-535.
119. Paul, D. E.; Lipkin, D.; Weissman, S. I. *Journal of the American Chemical Society* **1956,** 78, (1), 116-120.
120. Scott, N. Method of polymerization of styrene. 1939.

121. Blomquist, A. T.; Tapp, W. J.; Johnson, J. R. *Journal of the American Chemical Society* **1945,** 67, (9), 1519-1524.
122. Beaman, R. G. *Journal of the American Chemical Society* **1948,** 70, (9), 3115-3118.
123. Robertson, R. E.; Marion, L. *Canadian Journal of Research Section B-Chemical Sciences* **1948,** 26, (9), 657-667.
124. Szwarc, M.; Levy, M.; Milkovich, R. *Journal of the American Chemical Society* **1956,** 78, (11), 2656-2657.
125. Szwarc, M. *Nature* **1956,** 178, (4543), 1168-1169.
126. Baskaran, D.; Muller, A. H. E. *Progress in Polymer Science* **2007,** 32, (2), 173-219.
127. Szwarc, M., *living polymers and electron transfer process*. Wiley Interscience: New York, 1968.
128. Bochmann, M. *Journal of the Chemical Society-Dalton Transactions* **1996**, (3), 255-270.
129. Schubert, U. *Chemistry of Materials* **2001,** 13, (10), 3487-3494.
130. Bellas, V.; Rehahn, M. *Angewandte Chemie-International Edition* **2007,** 46, (27), 5082-5104.
131. Platel, R. H.; Hodgson, L. M.; Williams, C. K. *Polymer Reviews* **2008,** 48, (1), 11-63.
132. Bolton, P. D.; Mountford, P. *Advanced Synthesis & Catalysis* **2005,** 347, (2-3), 355-366.
133. Dubois, P.; Ropson, N.; Jerome, R.; Teyssie, P. *Macromolecules* **1996,** 29, (6), 1965-1975.
134. Wachhold, M.; Rangan, K. K.; Lei, M.; Thorpe, M. F.; Billinge, S. J. L.; Petkov, V.; Heising, J.; Kanatzidis, M. G. *Journal of Solid State Chemistry* **2000,** 152, (1), 21-36.
135. Minsker, K. S.; Babkin, V. A.; Zaikov, G. E. *Uspekhi Khimii* **1994,** 63, (3), 289-298.
136. Mauritz, K. A.; Hassan, M. K. *Polymer Reviews* **2007,** 47, (4), 543-565.
137. Bates, F. S.; Fredrickson, G. H. *Annual Review of Physical Chemistry* **1990,** 41, 525-557.
138. Jerome, R.; Tong, J. D. *Current Opinion in Solid State & Materials Science* **1998,** 3, (6), 573-578.
139. Keul, H.; Moller, M. *Journal of Polymer Science Part a-Polymer Chemistry* **2009,** 47, (13), 3209-3231.
140. Levy, M. *Polymers for Advanced Technologies* **2007,** 18, (9), 681-684.
141. Sakurai, H. *Proceedings of the Japan Academy Series B-Physical and Biological Sciences* **2006,** 82, (8), 257-269.
142. Kloninger, C.; Knecht, D.; Rehahn, M. *Polymer* **2004,** 45, (25), 8323-8332.
143. Ludwigs, S.; Boker, A.; Abetz, V.; Muller, A. H. E.; Krausch, G. *Polymer* **2003,** 44, (22), 6815-6823.
144. Lutz, J. F. *Journal of Polymer Science Part a-Polymer Chemistry* **2008,** 46, (11), 3459-3470.
145. Patten, T. E.; Matyjaszewski, K. *Advanced Materials* **1998,** 10, (12), 901-+.
146. Zheltonozhskaya, T. B.; Fedorchuk, S. V.; Syromyatnikov, V. G. *Uspekhi Khimii* **2007,** 76, (8), 784-820.
147. Spain, S. G.; Gibson, M. I.; Cameron, N. R. *Journal of Polymer Science Part a-Polymer Chemistry* **2007,** 45, (11), 2059-2072.
148. Ladmiral, V.; Melia, E.; Haddleton, D. M. *European Polymer Journal* **2004,** 40, (3), 431-449.
149. Percec, V.; Tomazos, D. *Advanced Materials* **1992,** 4, (9), 548-561.
150. Erussalimsky, B. L. *Uspekhi Khimii* **1992,** 61, (1), 139-160.

PHASE DIAGRAMS AND APPLICATIONS OF AMPHIPHILIC

BLOCK COPOLYMERS IN AQUEOUS SOLUTIONS

REFERENCES

151. Evans, A. C.; Skey, J.; Wright, M.; Qu, W. J.; Ondeck, C.; Longbottom, D. A.; O'Reilly, R. K. *Journal of Polymer Science Part a-Polymer Chemistry* **2009,** 47, (24), 6814-6826.
152. Dove, A. P. *Chemical Communications* **2008**, (48), 6446-6470.
153. Grishin, I. D.; Grishin, D. F. *Uspekhi Khimii* **2008,** 77, (7), 672-689.
154. Pyun, J.; Matyjaszewski, K. *Chemistry of Materials* **2001,** 13, (10), 3436-3448.
155. Moad, G.; Rizzardo, E.; Thang, S. H. *Polymer* **2008,** 49, (5), 1079-1131.
156. Korolev, G. V.; Marchenko, A. P. *Uspekhi Khimii* **2000,** 69, (5), 447-475.
157. Kyung-Youl, B. *Molecular Crystals and Liquid Crystals* 520, 256-261.
158. Grishin, D. F.; Semyonycheva, L. L. *Uspekhi Khimii* **2001,** 70, (5), 486-510.
159. Ali, M.; Brocchini, S. *Advanced Drug Delivery Reviews* **2006,** 58, (15), 1671-1687.
160. McLeary, J. B.; Klumperman, B. *Soft Matter* **2006,** 2, (1), 45-53.
161. Limer, A.; Haddleton, D. M. *Progress in Reaction Kinetics and Mechanism* **2004,** 29, (3), 187-241.
162. Hudson, R. D. A. *Journal of Organometallic Chemistry* **2001,** 637, 47-69.
163. Khan, J. H.; Schue, F.; George, G. A. *Polymer International* **2009,** 58, (3), 296-301.
164. Hirao, A.; Sugiyama, K.; Matsuo, A.; Tsunoda, Y.; Watanabe, T. *Polymer International* **2008,** 57, (4), 554-570.
165. Butun, V.; Armes, S. P.; Billingham, N. C. *Polymer* **2001,** 42, (14), 5993-6008.
166. Bywater, S.; Worsfold, D. J.; Johnson, A. F. *Canadian Journal of Chemistry-Revue Canadienne De Chimie* **1964,** 42, (6), 1255-&.
167. Claesson, P. *Colloids Surf. A* **1993,** 77, 109.
168. Ghoroghchian, P. P.; Frail, P. R.; Li, G.; Zupancich, J. A.; Bates, F. S.; Hammer, D. A.; Therien, M. J. *Chem. Mater.* **2007,** 19, 1309-1318.
169. Chen, D.; Kennedy, J. P.; Kory, M. M.; Ely, D. L. *Journal of Biomedical Materials Research* **1989,** 23, (11), 1327-1342.
170. Keszler, B.; Kennedy, J. P.; Ziats, N. P.; Brunstedt, M. R.; Stack, S.; Yun, J. K.; Anderson, J. M. *Polymer Bulletin* **1992,** 29, (6), 681-688.
171. Kennedy, J. P. *Journal of Macromolecular Science-Pure and Applied Chemistry* **1994,** A31, (11), 1771-1790.
172. Plazek, D. J.; Zheng, X. D.; Ngai, K. L. *Macromolecules* **1992,** 25, (19), 4920-4924.
173. Boyd, R. H.; Pant, P. V. K. *Macromolecules* **1991,** 24, (23), 6325-6331.
174. delRio, C.; MartinAlvarez, P. J.; Acosta, J. L. *Polymer Bulletin* **1997,** 38, (3), 353-357.
175. Kunal, K.; Paluch, M.; Roland, C. M.; Puskas, J. E.; Chen, Y.; Sokolov, A. P. *Journal of Polymer Science Part B-Polymer Physics* **2008,** 46, (13), 1390-1399.
176. Trollsas, M.; Kelly, M. A.; Claesson, H.; Siemens, R.; Hedrick, J. L. *Macromolecules* **1999,** 32, (15), 4917-4924.
177. Ghoroghchian, P. P.; Frail, P. R.; Susumu, K.; Blessington, D.; Brannan, A. K.; Bates, F. S.; Chance, B.; Hammer, D. A.; Therien, M. J. *Proceedings of the National Academy of Sciences of the United States of America* **2005,** 102, (8), 2922-2927.
178. Uchegbu, I. F. *Expert Opin Drug Deliv* **2006,** 3, (5), 629-40.
179. Yow, H. N.; Routh, A. F. *Soft Matter* **2006,** 2, (11), 940-949.
180. Zupancich, J. A.; Bates, F. S.; Hillmyer, M. A. *Macromolecules* **2006,** 39, (13), 4286-4288.
181. Binder, W. H.; Sachsenhofer, R. *Macromolecular Rapid Communications* **2008,** 29, (12-13), 1097-1103.
182. Vangeyte, P.; Leyh, B.; Heinrich, M.; Grandjean, J.; Bourgaux, C.; Jerome, R. *Langmuir* **2004,** 20, (20), 8442-8451.
183. Vangeyte, P.; Gautier, S.; Jerome, R. *Colloids and Surfaces a-Physicochemical and Engineering Aspects* **2004,** 242, (1-3), 203-211.

184. Kennedy, J. P.; Iván, B. *Hanser-Gardner, Cincinnati, OH* **1992**.

185. Iván, B.; Kennedy, J. P.; Chang, V. S. C. *J. Polym. Sci., Polym. Chem. Ed.* **1980,** 18, (11), 3177-3191.

186. Ivan, B.; Kennedy, J. P. *Journal of Polymer Science Part a-Polymer Chemistry* **1990,** 28, (1), 89-104.

187. Erdodi, G.; Ivan, B. *Chemistry of Materials* **2004,** 16, (6), 959-962.

188. Bae, Y. C.; Faust, R. *Macromolecules* **1998,** 31, (8), 2480-2487.

189. Schlaad, H.; Kukula, H.; Rudloff, J.; Below, I. *Macromolecules* **2001,** 34, (13), 4302-4304.

190. Schärtl, W., *Light scattering from polymer solutions and nanoparticle dispersions*. 2007; p 191.

191. S. Schmitz, K., *An introduction to dynamic light scattering by macromolecules*. 1990; p 449.

192. Brown, W., *Dynamic light scattering: the method and some applications*. 1993; p 735.

193. Burchard, W., *In Physical techniques for the study of food biopolymers*. Blackie Academics and Professional: New York, 1994.

194. Maulucci, G.; De Spirito, M.; Arcovito, G.; Boffi, F.; Castellano, A. C.; Briganti, G. *Biophysical Journal* **2005,** 88, (5), 3545-3550.

195. Tuzar, Z.; Kratochvil, P., *In Surface and colloid science*. Ed. Plenum Press: New York, 1993; Vol. 15.

196. Ruska, E.; Knoll, M. *Zeitschrift fur Technische Physik* **1931,** 12; 12, (8), 389; 448-399; 448.

197. Knoll, M.; Ruska, E. *Zeitschrift fur Physik* **1932,** 78, (5-6), 318-339.

198. Knoll, M.; Ruska, E. *Annalen Der Physik* **1932,** 12, (6), 641-661.

199. Knoll, M.; Ruska, E. *Annalen Der Physik* **1932,** 12, (5), 607-640.

200. Meunier, J.; Belenguer, P.; Boeuf, J. P. *Journal of Applied Physics* **1995,** 78, (2), 731-745.

201. Helmreich, E. J. M. *Biophysical Chemistry* **2003,** 100, (1-3), 519-534.

202. Cockcroft, S. *Cellular and Molecular Life Sciences* **2001,** 58, (11), 1674-1687.

203. Magde, D.; Webb, W. W.; Elson, E. *Physical Review Letters* **1972,** 29, (11), 705-&.

204. Haustein, E.; Schwille, P. *Annual Review of Biophysics and Biomolecular Structure* **2007,** 36, 151-169.

205. Vangeyte, P.; Jerome, R. *Journal of Polymer Science Part a-Polymer Chemistry* **2004,** 42, (5), 1132-1142.

206. Glatter, O.; Kratky, O., *Small Angle X-Ray scattering*. Academic Press: London, 1982.

207. Battaglia, G.; Ryan, A. J. *Macromolecules* **2006,** 39, (2), 798-805.

208. Stauch, O.; Schubert, R.; Savin, G.; Burchard, W. *Biomacromolecules* **2002,** 3, (3), 565-578.

209. Gao, W. P.; Bai, Y.; Chen, E. Q.; Li, Z. C.; Han, B. Y.; Yang, W. T.; Zhou, Q. F. *Macromolecules* **2006,** 39, (14), 4894-4898.

210. Santos, N. C.; Castanho, M. *Biophysical Journal* **1996,** 71, (3), 1641-1650.

211. Mui, B. L. S.; Dobereiner, H. G.; Madden, T. D.; Cullis, P. R. *Biophysical Journal* **1995,** 69, (3), 930-941.

212. Denkinger, P.; Kunz, M.; Burchard, W. *Colloid and Polymer Science* **1990,** 268, (6), 513-527.

213. Fuetterer, T.; Nordskog, A.; Hellweg, T.; Findenegg, G. H.; Foerster, S.; Dewhurst, C. D. *Phys Rev E Stat Nonlin Soft Matter Phys* **2004,** 70, (4 Pt 1), 041408.

214. Yao, J. H.; Mya, K. Y.; Li, X.; Parameswaran, M.; Xu, Q. H.; Loh, K. P.; Chen, Z. K. *Journal of Physical Chemistry B* **2008,** 112, (3), 749-755.

REFERENCES

215. Drummond, D. C.; Meyer, O.; Hong, K. L.; Kirpotin, D. B.; Papahadjopoulos, D. *Pharmacological Reviews* **1999,** 51, (4), 691-743.
216. Cordes, E. H.; Bull, H. G. *Chemical Reviews* **1974,** 74, (5), 581-603.
217. Cabane, E.; Malinova, V.; Meier, W. *Macromolecular Chemistry and Physics*, **2010,** 211, (17), 1847-1856.
218. Stuart, M. A. C.; Huck, W. T. S.; Genzer, J.; Muller, M.; Ober, C.; Stamm, M.; Sukhorukov, G. B.; Szleifer, I.; Tsukruk, V. V.; Urban, M.; Winnik, F.; Zauscher, S.; Luzinov, I.; Minko, S. *Nature Materials* **2010***, 9, (2), 101-113.
219. J.Braun, A. Szabo, N. Bruns, T. Pfohl, B. Ivan, and W. Meier, in progress.

7. Abbreviations

a	interfacial area of the hydrophobic volume
A	surface area occupied by the surfactant head group
A_i	ith virial coefficient
ATRP	Atom-Transfer Radical Polymerization
C	hexagonally packed cylinders
C	concentration
CPS	closed packed spheres
D	double diamond surfaces
D	aspartic acid
d	spacing
DIS	disordered phase
DLS	dynamic light scattering
D_m	translatory diffusion coefficient
DNA	deoxyribonucleic acid
E	glutamic acid
EB	poly(oxyethylene)-*block*-poly(oxybutylene)
ECFP	Enhanced Cyan Fluorescent Protein
EO	ethylene oxide
f	volume fraction of one of the blocks (V_A/V_B)
fcc	face-centered cubic
FCS	fluoresence correlation spectroscopy
G, G_1, G_2	bicontinuous gyroid
GPC	gel permeation chromatography

GTP	Chain Transfer Polymerization, Group Transfer Polymerization
^{1}H-NMR	proton nuclear magnetic resonance spectroscopy
H	area-averaged mean curvature
H(EX), H_1, H_2	hexagonal phase
HCl	hydrochloric acid
K	optical contrast factor
KCl	potassium chloride
k_d	diffusion virial coefficient
K_G	Gaussian curvature
KH_2PO_4	potassium dihydrogenphosphate
L or Lam	lamellae
l	extended length of the hydrophobic portion
LS	light scattering
MCL	γ-methyl-ε-caprolactone
mCPBA	*m*-chloroperbenzoic acid
M_N weights	average- number molecular
M_W	average-weight molecular weights
M_w/M_n, PDI	polydispersity index
N (N_A, N_B)	total number of statistical segments (whole polymer or block A and B)
n_0	refractive index
Na_2HPO_4	disodium hydrogenphosphate

83

ABBREVIATIONS

NaCl	sodium chloride	RNA	ribonucleic acid
p	packing parameter	ROP	ring opening polymerization
$P(q)$	particle scattering factor	S	spheres
PBS	phosphate buffer	S_0	ground state
PEE-*b*-PEO	poly(ethylene)-*block*-poly(ethylene oxide)	S_1	relaxed singlet exited state
PEO	poly(ethylene oxide)	S_1`	excited electronic singlet state
PEO-*b*-PMCL	poly(ethylene oxide)-*block*-poly(γ-methyl-ε-caprolactone)	SAXS	small-angle X-ray scattering
		SEC	size exclusion chromatography
PET	,polyethylenterephthalat	SLS	static light scattering
PIB	poly(isobutylene)	T	temperature
PIB-*b*-PEO	poly(isobutylene)-*block*-poly(ethylene oxide)	tax	Paclitaxel®
PIB-OH	ω-Hydroxy-poly(isobutylene)	t-BuP$_4$	phosphazene base
PL	perforated lamellae	TEM	transmission electron microscopy
PMCL	poly(γ-methyl-ε-caprolactone)	T_g	glass transition temperature
PS	polystyrene	THF	tetrahydrofuran
q (LS)	scattering vector	TMS	tetramethylsilane
q (SAXS)	wave number	$V_{A(B)}$	volume of block A or B
q^2	zero momentum transfer	w_{PMCL}	Weight fraction of the PMCL block
R	curvature	X	semicrystalline lamellae
$R(q)$	Rayleigh ratio	Z	number of block copolymers in a micelle
RAFT	Reversible Addition Fragmentation	ε	differences in the conformational properties of the polymer chains
R_g	radius of gyration	λ	wavelength
R_h	hydrodynamic radius	χ	interaction parameter

PHASE DIAGRAMS AND APPLICATIONS OF AMPHIPHILIC
BLOCK COPOLYMERS IN AQUEOUS SOLUTIONS

Curriculum vitae

Personal Data

Name	Jörg Braun
Date and place of birth	21.01.1983 in Lörrach (Germany)
Nationality	German

Education

02/2008 -
04/2011

PhD studies supervised by Prof. Dr. Wolfgang Meier
(University of Basel, Switzerland)

11/2006 -
01/2008

master studies in chemistry
(University of Basel, Switzerland)
master thesis supervised by Prof. Dr. Markus Meuwly

10/2003 -
10/2006

bachelor studies
(University of Basel, Switzerland)

10/2002 -
07/2003

military service
(Grundwehrdienst)

07/2002

A-levels ("Abitur")
(Theodor-Heuss-Gymnasium Schopfheim, Germany)

The following lecturers participated in the educational training during the PhD studies:
Nico Bruns, Edwin Constable, Katarzyna Kita-Tokarzyk, WolfgangMeier, Markus Meuwly,
Cornelia Palivan, Thomas Pfohl, Marek Tulej, Stefan Willitsch, Erich Windhab.

Impact of the work

Publications

J. Braun, A. Fouqueau, R. J. Bemish and M. Meuwly *Solvent Structures of MixedWater/Acetonitrile Mixtures at Chromatographic Interfaces from Computer Simulations,* PCCP, **2008**, *10*, 4765-4777.

H. Li, P. Jiang, C. Yi, C. Li, S.-X. Liu, S. Tan, B. Zhao, **J. Braun**, W. Meier, T. Wandlowski, and S. Decurtins, *Benzodifuran-Based π- Conjugated Copolymers for Bulk Heterojunction Solar Cells,* Macromolecules, **2010**, *43*, 8058-8062.

J. Braun, N. Bruns, T. Pfohl, and W. Meier *Phase behavior of vesicle forming block-copolymers in aqueous solutions*, *Macromol. Chem. Phys.,* **2011**, *212*, 1245–1254.

J. Braun, A. Szabo, N. Bruns, T. Pfohl, B. Ivan, and W. Meier, *Nanophasic self-assembly of PIB-b-PEO block copolymers in aqueous media: a phase diagram from lamellae to micelles and vesicles*, in progress.

J. Montenegro, **J. Braun**, O. Fischer-Onaca, W. Meier, and S. Matile, *Synthetic polyion-counterion transport systems in polymersomes and gels*, *Org. and Biomol. Chem.*, **2011**, DOI: DOI: 10.1039/c1ob05835e.

Patents

A. Bohm, J. Lisner, **J. Braun**, H. Engel, E. Windhab, W. Meier, ***Verfahren und Vorrichtungen zur Vesikelbildung, insbesondere unter Verwendung von Block copolymeren,*** Eur. Pat. Appl. (2010)

Book chapter

J. Braun, K. Renggli, J. Razumovitch and C. Vebert, *Supramolecular Materials Chemistry and Dynamic Light Scattering*, accepted.

Conference Posters

J. Braun, W. Meier, *From Bulk Polymer to Polymer Vesicles,* PILS Meeting, Basel (Switzerland)*, 2009*

H. Engel, **J. Braun**, W. Meier, and E. J. Windhab, *Electric field assisted formation of giant polymer vesicle,* 1st Swiss FoodTec Day, Schlieren, Switzerland, *2009*

H. Engel, **J. Braun**, W. Meier, P. Fischer, and E. J. Windhab, *Stability and release properties of food grade polymer vesicles*, Delivery of functionality in complex food systems, Wageningen, Netherlands, *2009*

J. Braun, W. Meier, *From Polymer Vesicles to Bulk Polymer*, Swiss Soft days (Fribourg, Switzerland), 2010

PHASE DIAGRAMS AND APPLICATIONS OF AMPHIPHILIC
BLOCK COPOLYMERS IN AQUEOUS SOLUTIONS